The Alpha-Activator Complex, Cellular Maturation, and Catalytic Mechanism of Iron-Type Nitrile Hydratase

Wasantha Lankathilaka Karunagala Pathiranage
Marquette University

THE ALPHA-ACTIVATOR COMPLEX, CELLULAR MATURATION, AND CATALYTIC MECHANISM OF IRON-TYPE NITRILE HYDRATASE

by

Wasantha Lankathilaka Karunagala Pathiranage, B.Sc., M.Sc.
University of Colombo, Sri Lanka

A Dissertation submitted to Faculty of the Graduate School,
Marquette University,
in Partial Fulfillment of the Requirements for
the Degree of Doctor of Philosophy

Milwaukee, Wisconsin

August 2019

ABSTRACT

THE ALPHA-ACTIVATOR COMPLEX, CELLULAR MATURATION, AND CATALYTIC MECHANISM OF IRON-TYPE NITRILE HYDRATASE

Wasantha Lankathilaka Karunagala Pathiranage, B.Sc., M.Sc.

Marquette University, 2019

In industry, chemicals are typically synthesized through catalytically accelerated chemical processes. The use of biocatalysts is an increasingly important trend in achieving environmentally friendly chemical production processes. Nitrile Hydratases (NHases) are well-known biocatalysts that are used by several manufacturers such as Mitsubishi Rayon Corporation and Lonza for the conversion of acrylonitrile to acrylamide and 3-cyanopyridine to nicotinamide, respectively. Amides, in general, are used in polymer preparation, adhesive manufacturing, and the paper industry.

Refrigeration is needed in the enzymatic hydration process on the industrial scale to maintain a low reaction temperature to stabilize the NHase enzyme. The use of whole cells instead of purified enzyme is one way to overcome this stability issue. However, the permeability of nitriles across the bacterial plasma membrane and cell wall is an important issue in order to get nitrile substrates into the cell and amide products excreted. The presence of unwanted enzymes in whole cells that can interfere with NHase activity, raw material, or product inhibition are also important considerations. Despite these issues, NHase shows great promise as a biocatalyst and, as a more detailed understanding of their catalytic mechanism and biological assembly processes emerge, improved biocatalyst designs that are more efficient, stable, and selective will advance their industrial use.

The goal of the dissertation is to: study the formation of Fe-Type $\alpha(\varepsilon)$ protein complex, investigate the cellular maturation of Fe-Type nitrile hydratase, and discover intermediates along the catalytic cycle of NHases in-order to gain additional insight into the bio-assembly and catalytic mechanism of NHase enzymes.

ACKNOWLEDGMENTS

Wasantha Lankathilaka Karunagala Pathiranage, B.Sc., M.Sc.

I would like to express my sincere gratitude, first and foremost, to my academic advisor Dr. Richard C. Holz for accepting me into his lab, for his constructive guidance and continuous support as I work on research projects. Also, it's a pleasure to express my sincere thanks to our EPR collaborator, Dr. Brian Bennett for his massive support in planning and understanding EPR experiments.

I would also like to thank Dr. Martinez and Dr. Gumataotao for their patience and for letting me learn from them the basic concepts I needed in order to work on my projects. I would also like to thank my group members Irene and Xinhang for their support and encouragement in my work.

I am grateful to Dr. James R. Gardinier, Dr. Evgueni Kovriguine, Dr. Martin St. Maurice and Dr. Nicholas Reiter for agreeing to be Committee members and helping me as I work on my projects. I am so grateful to Dr. St. Maurice and Dr. Edwin Antony for kindly offering the ITC instrument and the stopped-flow instrument for my research. Also, I would like to thank Dr. Stein for her support and advice.

I would like to express my heartfelt thanks to my father Mr. Thilakasiri, mother Mrs. Mili Magret, brother Mr. Sampath Lankathilaka and aunt Suneetha for their unconditional support and help for my academic success. Last but not least, I would like to express my heartful thanks to my loving wife Nilmini and my little son Thusindu for being with me in Milwaukee and encouraging me continuously.

TABLE OF CONTENTS

LIST OF TABLES

LIST OF FIGURES

CHAPTER 1

INTRODUCTION

1.1 General introduction

1.1.1. Overview

Nitrile Hydratases (NHase) are produced by numerous plants, bacteria and fungi [1]. They catalyze the hydration of nitrile compounds to their corresponding amides under mild reaction conditions such as ambient temperatures (~20-22 ˚C), physiological pH (~7.4), and use of aqueous medium. Because of these properties, there is a growing interest in using NHases in industrial applications [2]. Annual production of acrylamide and nicotinamide *via* NHases at Mitsubishi Rayan Corporation and Lonza group is more than 100,000 tons and 3500 tons respectively [2]. NHases also represent a new type of "green chemistry" as they can degrade environmentally harmful nitriles such as bromoxynil [2-4].

NHases consist of two types of subunits (α and β) with almost the same molecular mass of ~23 kDa [5]. Structural studies on NHase enzymes revealed the formation of a heterotetramer ($\alpha_2\beta_2$) where both α-subunits contains either a low-spin non-corrin Co^{3+} (Co-type) or low-spin non-heme Fe^{3+} (Fe-type) metal ion [1, 3, 6]. The active site metal ion is coordinated by three cysteine sulfur atoms, two amide nitrogen atoms (from the backbone of the amino acid chain) and a water molecule (Figure 1) [1, 3]. Mass spectrometric and X-ray crystallography studies revealed the post-translational modifications of two active site cysteine ligands to cysteine sulfinic acid (Cys-SO_2H) and

cysteine sulfenic acid (Cys-SOH) [5, 7]. NHase was the first metalloprotein to be identified with post-translationally modified cysteine ligands [5].

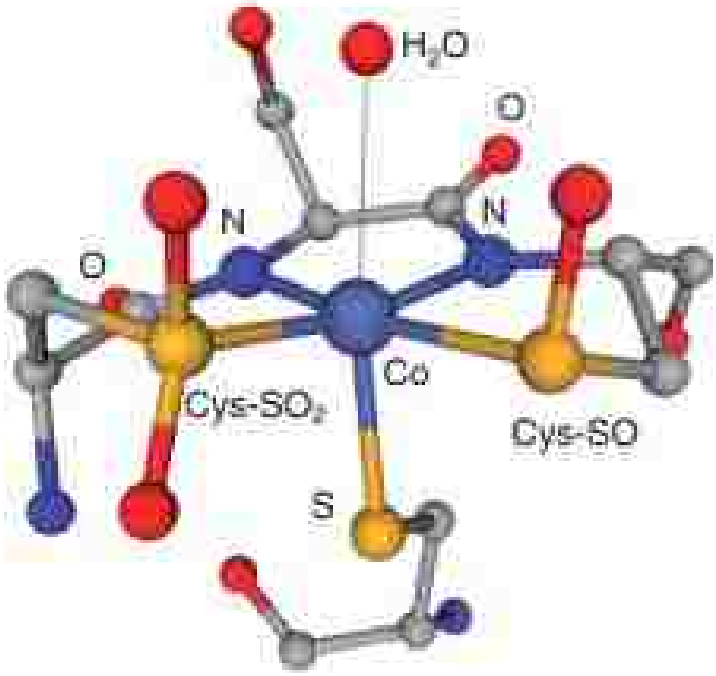

Figure 1. Active site structure of Co-type NHase from *Pseudonocardia thermophilia* JCM 3095 [8]

Studies on NHase gene operons have demonstrated the requirement of an accessory protein encoded by a downstream gene for the efficient synthesis of NHase enzymes [6, 7]. This accessory protein was termed the "activator protein" (ε). Both Co-type and Fe-type NHases are known to require the co-expression of the activator protein for expression as a fully functional enzyme [6, 7]. Co-type activator proteins are small ~15 kDa and have significant sequence identity with the NHase β-subunit. It was proposed that two Co-type NHase activator proteins (*e.g*. *Rhodococcus rhodochrous* J1) interact with one α-subunit ($\alpha\varepsilon_2$) [7, 9]. Furthermore, insertion of the metal ion into the apo-$\alpha_2\beta_2$ complex through the holo-$\alpha\varepsilon_2$ complex was proposed to occur *via* a "self-

subunit swapping" mechanism [7, 9]. On the other hand, Fe-type NHase activator proteins (*e.g. Rhodococcus sp.* N-771) are ~45 kDa and contain a conserved CXCC amino acid sequence [6]. No molecular level evidence exists that demonstrates the role of the Fe-type NHase activator in the biosynthesis of NHase.

Gaining insight into; the role of the activator protein, cellular maturation of nitrile hydratase enzymes, and catalytic intermediates of the reaction cycle will provide evidence for the important steps in the bio-assembly and the reaction cycle of NHase enzymes. Ultimately, an improved biocatalyst design that is more efficient, stable, and selective will be discovered and it will advance the industrial use of NHase enzyme.

1.1.2. Nitrile compounds

Organic compounds that contain "-CN (Cyano)" groups are called "Nitriles" [10, 11]. Nitriles are widespread in the natural environment as more than 2,000 plant species have the ability to synthesize nitriles [10]. Nitriles are found not only in plants but also in insects and due to the toxic nature of nitriles, they are widely used in self-defense mechanisms for both plants and insects [10].

Nitriles do not occur in large concentrations in plants or in insects [12]. So nitriles used industrially within the pharmaceutical, agrochemical, and automotive businesses have to synthesized [9]. As an example, ~90% of the world's acrylonitrile demand is supplied by propylene ammoxidation in the presence of ammonia and oxide-metal catalysts [13]. Different manufacturers use differing compositions of catalysts such as Co, Fe, Ni, Bi, K, or Mo [13]. The catalytic production of nitriles is relatively expensive due to the cost of propylene (Figure 2), hence there is an increasing interest in using propane as the starting material for acrylonitrile production to reduce the costs.

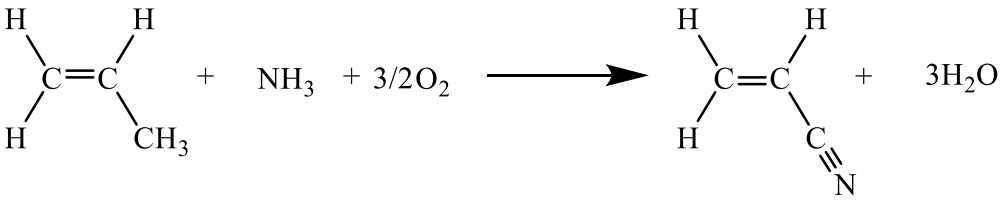

Figure 2. Chemical synthesis of acrylonitrile from propylene [13]

Another industrial example involves the production of 3-cyanopyridine using pyridine-3-carboxylic acid (Figure 3) [14]. Reaction time and yield is dependent upon the solvent with the maximum yield observed when CS_2 is used as the solvent [9, 14]. Purified 3-cyanopyridine molecules are used in the production of Vitamin B_3 [2, 3].

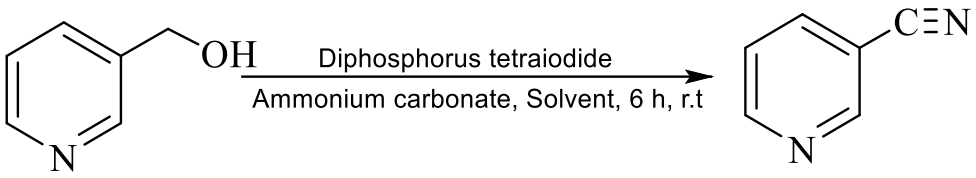

Figure 3. Chemical synthesis of 3-Cyanopyridine from pyridine-3-carboxylic acid [9, 14]

Knowledge about the formation and degradation of nitrile compounds in the environment is important as nitriles are used in many large scale industrial processes [4]. Amino acids are the precursors for the biological synthesis of nitriles. The biotransformation of nitriles to organic acids follows two routes (Figure 4). In the first, nitrilase directly converts nitriles to organic acids while in the second nitrile hydratase and amidase participate in a two consecutive steps to transform nitriles to organic acids (Figure 4). The involvement of nitrile hydratase in the conversion of nitriles to their corresponding amides is the step of primary interest for industries preparing economically important amides.

1.1.3. Bio-formation and bio-degradation of nitriles

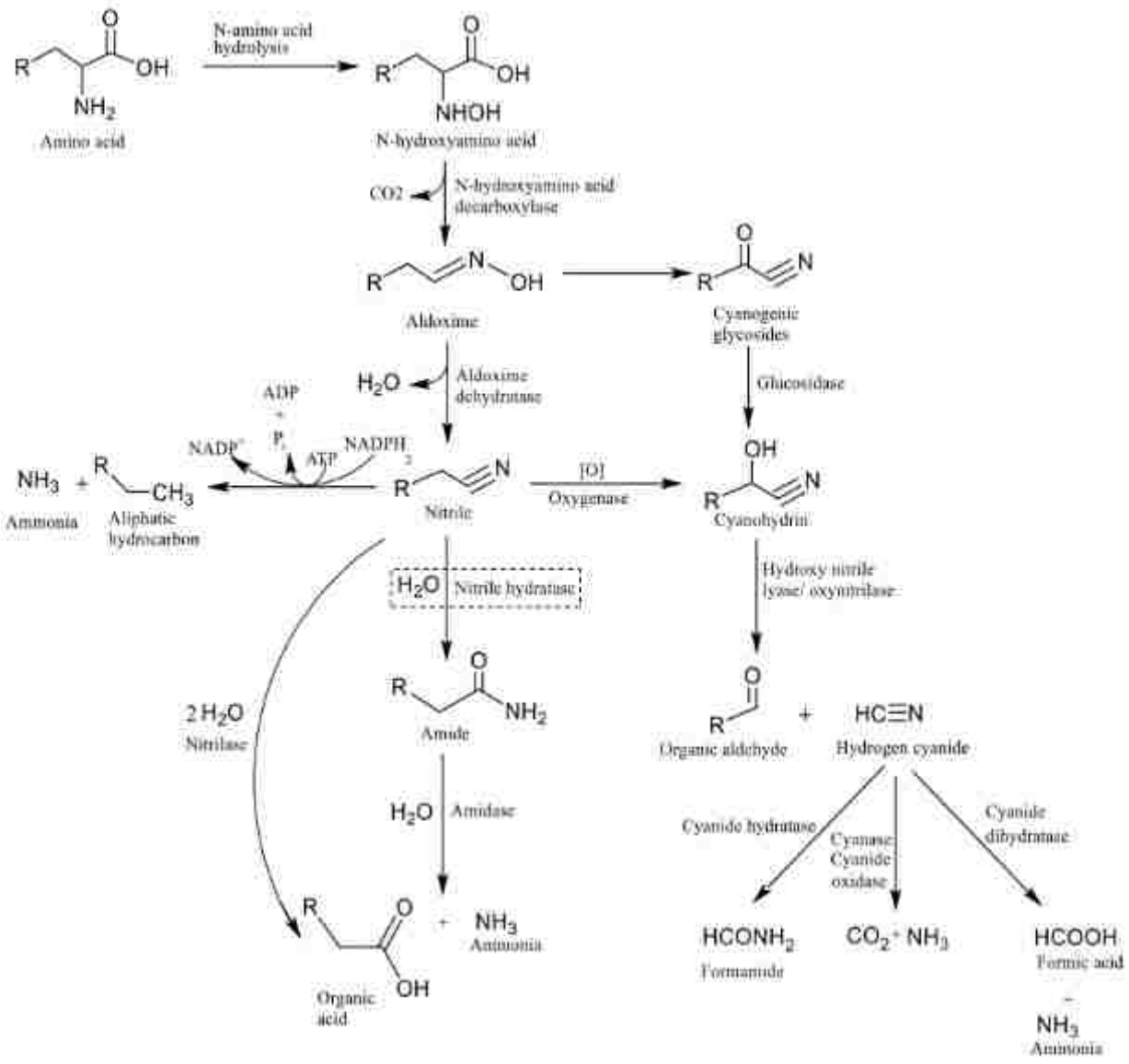

Figure 4. Metabolic pathways of nitrile synthesis and degradation in microorganisms [4]

1.1.4. Industrial importance of NHases

In industry, chemicals are typically synthesized through catalytically accelerated chemical processes [9, 15]. The use of biocatalysts is an increasingly important trend to achieving environmentally safe chemical production processes. NHases are well-known biocatalysts that are used by several manufactures such as Mitsubishi Rayon Corporation in Japan, and Lonza chemical company in Switzerland for the conversion of acrylonitrile to acrylamide and 3-cyano pyridine to nicotinamide respectively [2, 16]. Amides in general are used in polymer preparation, adhesive manufacturing, and the paper industry [17].

Initially, acrylamide was produced from acrylonitrile *via* two main chemical synthetic processes by Mitsubishi Rayon Corporation [15]. One is sulfuric acid hydrolysis and the other is copper-catalyzed hydrolysis. Since 1985 they have been commercially producing acrylamide *via* an enzymatic process using NHases as biocatalysts (Figure 5) [15]. Over the years, NHase has been shown to be an efficient catalyst for the industrial production of acrylamide from acrylonitrile by not only eliminating the formation of acrylic acid, but also performing the reaction in a single step as opposed to the multi-step reactions required in traditional amide synthesis [4]. Also, the high selectivity NHases exhibit towards nitriles is significant, compared to traditional amide synthesis methods. Annual production of acrylamide at Mitsubishi Rayon Corporation is ~100,000 tons.

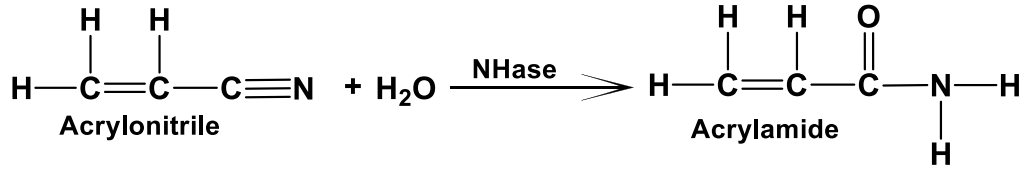

Figure 5. Conversion of acrylonitrile to acrylamide

Experiments conducted by Mitsubishi Rayon Corporation revealed that, the hydration of nitriles by NHase is both cost effective and produces a high purity product [15]. Table 1 shows the comparison of their enzymatic process versus their copper based catalytic process.

Table 1. Comparison of chemical nitrile hydration and enzymatic nitrile hydration of acrylonitrile which was performed by Mitsubishi Rayon Corporation [15]

Fact	**Chemically catalyzed hydration**	**Enzymatic hydration**
Reaction temperature	343 K	273 - 288 K
One-pass reaction yield	70-80%	~100%
Acrylamide	~30%	48 - 50%
Concentration	Required	Not required
Purification	Catalyst removal	Protein removal

Several other experiments have been performed to investigate the environmental impacts of NHase mediated acrylamide production [15]. Energy consumption and carbon dioxide production during the industrial process were the most significant factors. These studies concluded that the enzymatic process is more environmentally friendly than the chemical catalytic process. Energy consumptions for the copper based catalytic process *vs*. the new NHase biocatalytic process were 5.0 MJ/kg acrylamide and 3.5 MJ/kg

acrylamide, respectively. Generation of CO_2 from the copper based catalytic process *vs*. NHase was 3.8 kg CO_2/kg acrylamide and 2.6 kg CO_2/kg acrylamide, respectively.

Lonza chemical company produces ~3,500 tons of nicotinamide per year using NHase biocatalysts (Figure 6), which is used primarily in the production of vitamin B_3 [2, 3]. Conversion of 3-cyanopyridine to nicotinamide was originally carried out by caustic hydrolysis at Lonza [18]. Copious amounts of salt water and nicotinic acid were the byproducts. By using whole cells immobilized in a polyacrylamide gel that contains the NHase from *Rhodococcus rhodochrous* JI, Lonza can produce nicotinamide under mild reaction conditions [18]. This biocatalytic process boasts high conversion (~100%) rates and excellent selectivity (>99.3%) [18].

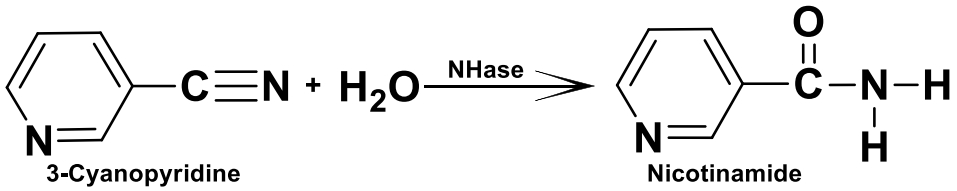

Figure 6. Conversion of 3-cyanopyridine to nicotinamide

1.1.5. Limitations in the use of NHases for the conversion of nitriles to their corresponding amides

Refrigeration is needed in the enzymatic hydration process on the industrial scale to maintain a low reaction temperature to stabilize the NHase enzyme [15]. The use of whole cells instead of purified enzyme is one way to overcome this stability issue. However, permeability of nitriles across the bacterial plasma membrane and cell wall is an important issue in order to get nitrile into the cell. The presence of unwanted enzymes in whole cells that can interfere with NHase activity, raw material, or product is also an

important consideration [15]. Despite these issues, NHase shows great promise as a biocatalyst and, as a greater understanding of the catalytic mechanism emerges, improved biocatalyst designs that are more efficient, stable, and selective will advance their industrial use.

1.2. Nitrile Hydratase enzyme, structure, active site, and catalytic reaction

1.2.1. Nitrile Hydratase enzyme

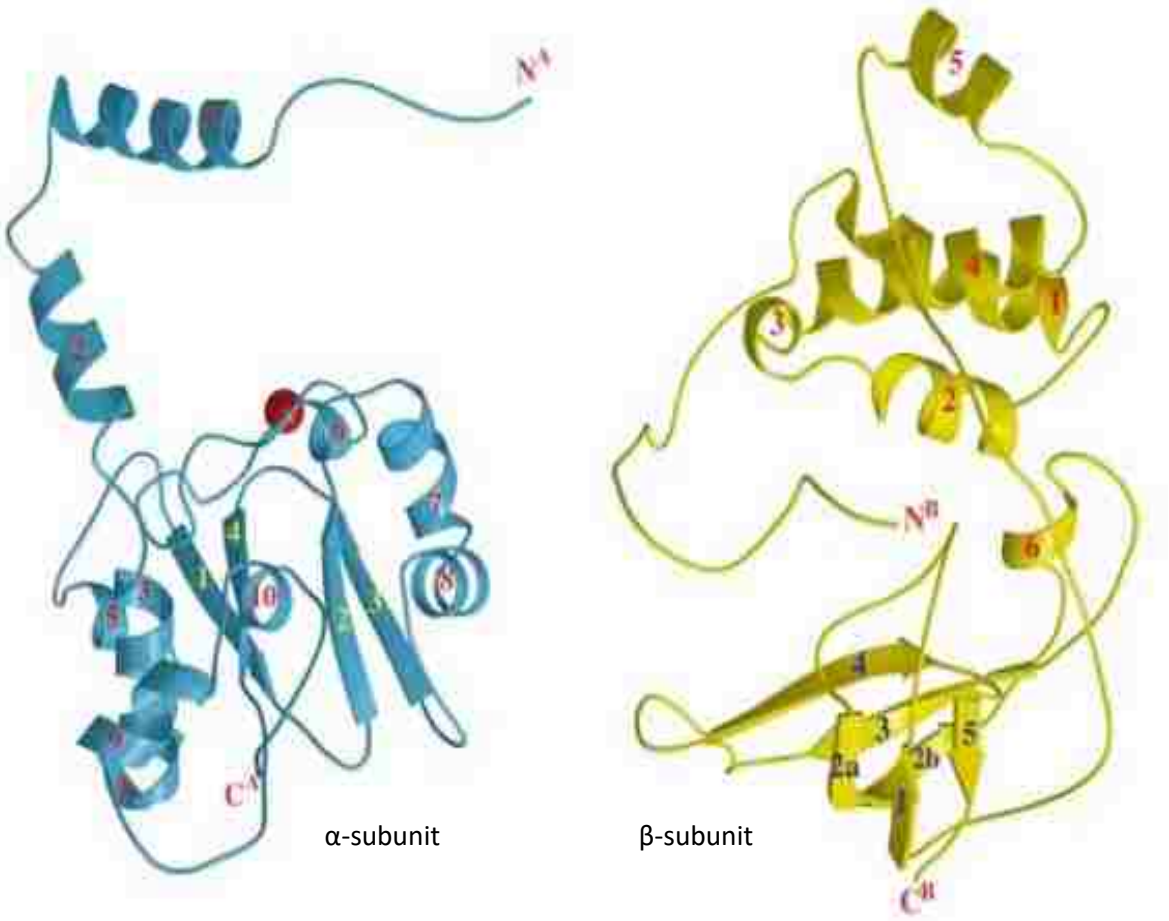

Figure 7. Crystal structures of *Rhodococcus* sp. R312 NHase α-subunit and β-subunit [3]

The active site low-spin non-corrin Co^{3+} or low-spin non-heme Fe^{3+} metal ion is located in the α-subunit where it interfaces with the β-subunit [3, 6]. Both the α- and β-subunits are similar in size (~23 kDa). The α-subunit consists of long extended N-terminal helices and a globular C-terminal domain while the β-subunit has a long N-terminal loop and a C-terminus that consists of beta sheets and α-helices (Figure 9) [3]. A long loop on the β-subunit is intertwined within the α subunit to form an αβ heterodimer. There is a large open cavity at the interface of the two subunits and the metal center is located in this cavity, bound to the α-subunit [3]. Two of these αβ heterodimers form the $\alpha_2\beta_2$ heterotetramer that is typical for NHase enzymes. A conserved domain in the N-terminus of the β-subunit is involved in the interaction between two dimers [1, 3].

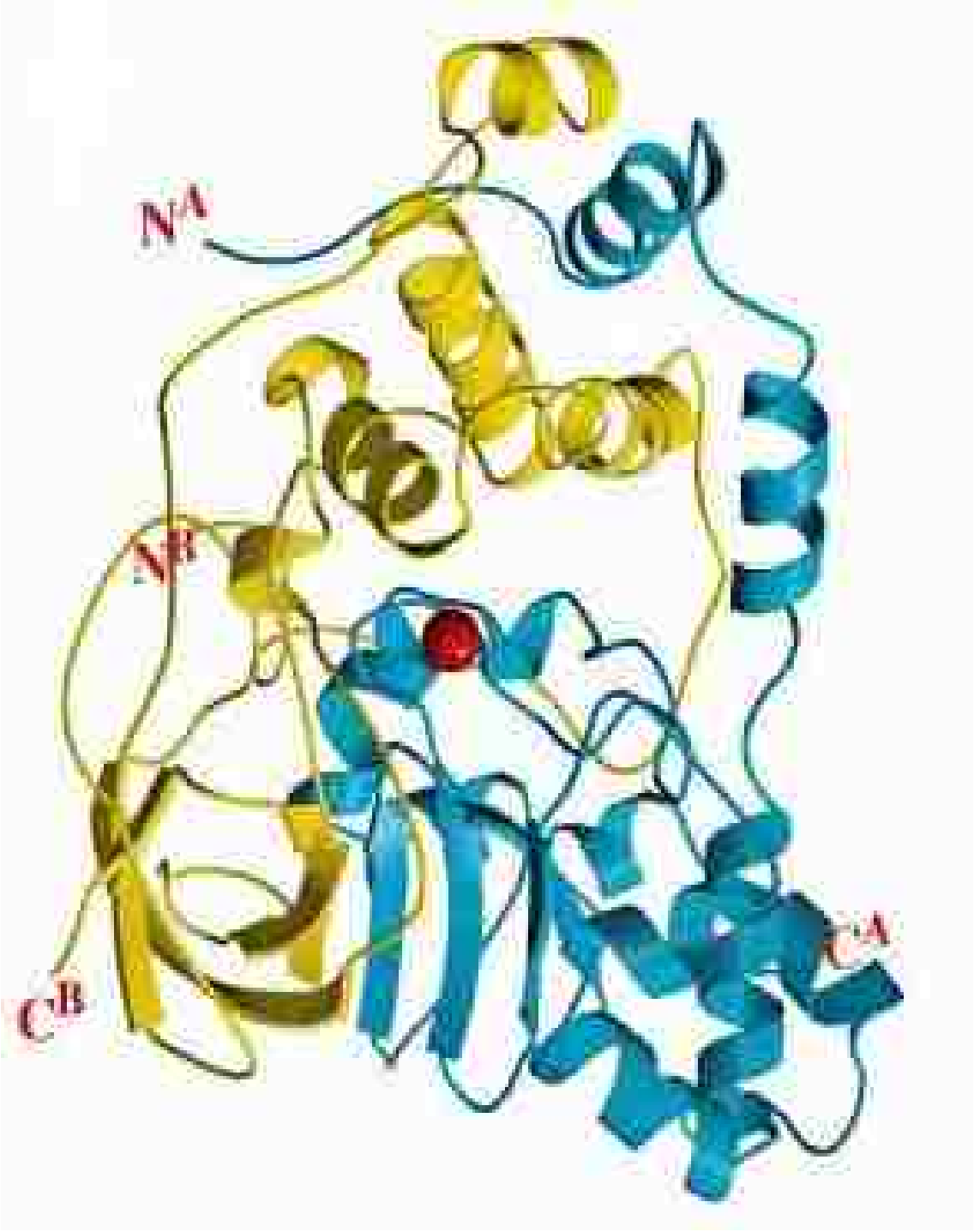

Figure 8. Crystal structure of *Rhodococcus* sp. R312 NHase αβ- heterodimer [3]

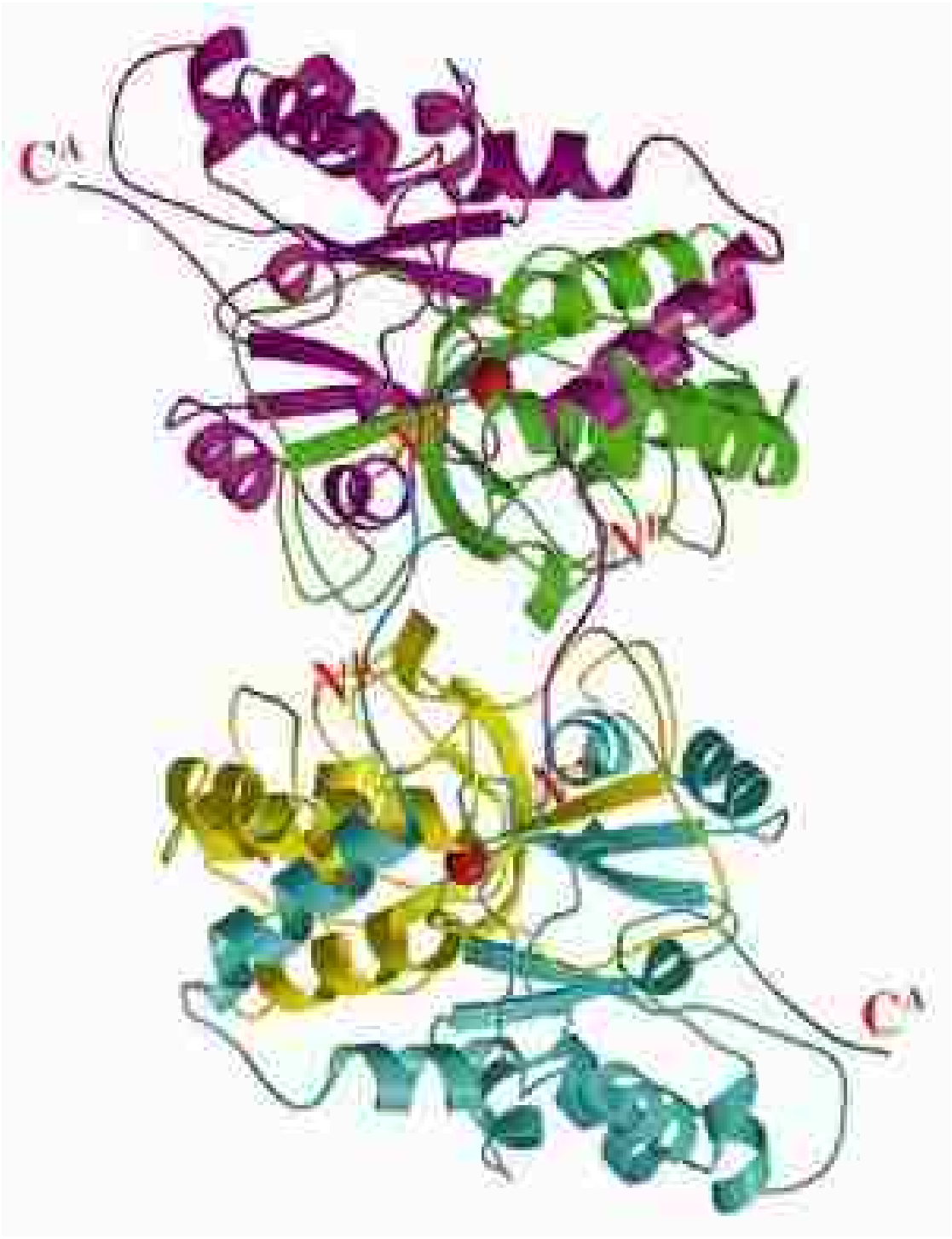

Figure 9. Crystal structure of *Rhodococcus sp.* R312 NHase $\alpha_2\beta_2$- heterotetramer [3]

1.2.2. Structure of the active site of NHase enzyme

The active site metal ions in NHases are coordinated by three sulfur atoms from cysteine residues, two amide backbone nitrogen atoms, and one water molecule (Figure 1) [6, 8, 16]. Two of the cysteine sulfur atoms along with the two backbone nitrogen atoms reside in the same plane with the metal ion. The third sulfur atom and water molecule are coordinated in the axial positions, forming an octahedral geometry. Recent NHase crystal structures revealed the post-translational modifications of the two equatorial cysteine sulfur atoms [16]. One of these cysteine sulfur atoms is oxidized to a cysteine sulfinic acid (Cys-SO_2H) while the other is a cysteine sulfenic acid (Cys-SOH) [16].

1.2.3. Catalytic reaction mechanism

Though a detailed reaction mechanism for NHase enzymes has remained elusive, X-ray crystal structure analysis, studies on substrate- and transition-state analog inhibitors, computational studies, mutational studies, and spectroscopic studies have allowed several possible reaction steps to be proposed [2, 16, 19-21]. The NHase reaction mechanisms that have been proposed are termed the “activated substrate” mechanism (Figure 10), the “directly activated nucleophile” mechanism (Figure 11), the “indirectly activated nucleophile” mechanism (Figure 12), and the “activated sulfenate” mechanism (Figure 13). Nucleophilic attack on the substrate carbon atom is a common feature in all four proposed reaction mechanisms; however, the source of nucleophile is still enigmatic.

1.2.3.1. Activated substrate mechanism

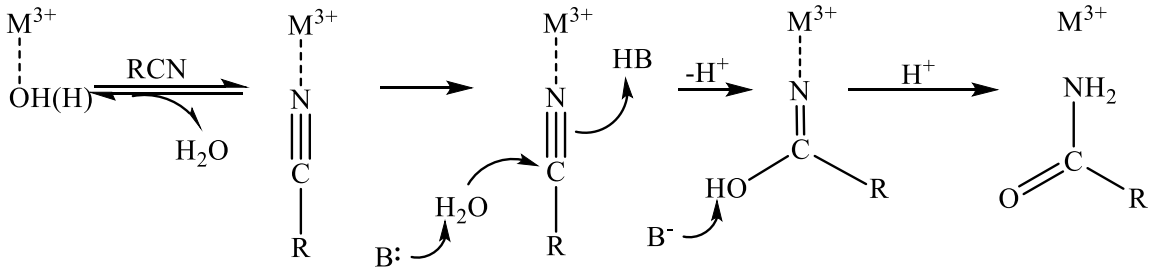

Figure 10. "Activated substrate" catalytic mechanism of NHase

The "Activated substrate" mechanism is one of the most accepted catalytic mechanisms for nitrile hydration by NHases [20]. In this mechanism, nitrile substrate directly binds to the low-spin metal ion at the sixth coordination site by replacing the water molecule [20]. This mechanism suggests that the nitrile group of the substrate molecule is bound to the metal ion through the nitrogen atom. Nitrile binding to the metal ion results in increased electrophilicity on the nitrile carbon atom making it susceptible to nucleophilic attack by a base activated water molecule. Though the source of the active site base was unconfirmed, αSer113, αCys114, or βTyr72 residues were suggested as the possible sources [20, 21].

1.2.3.2 Directly activated neucleophile mechanism

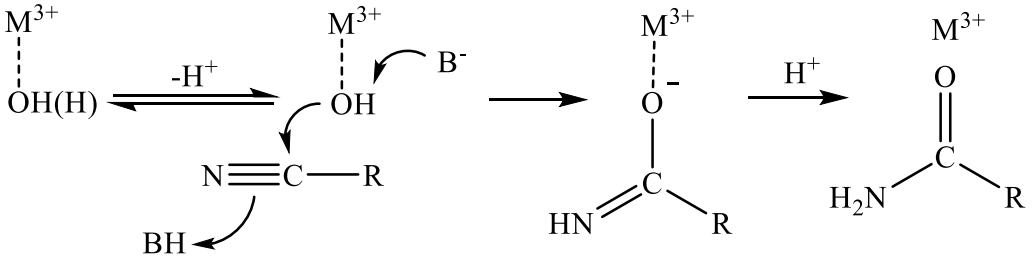

Figure 11. "Directly activated nucleophile" catalytic mechanism of NHase

In the directly activated nucleophile proposed mechanism, the substrate molecule is not directly bound to the metal ion [3]. A metal bound hydroxyl group acts as the nucleophile and attacks the carbon atom of nitrile group. Once nucleophilic attack occurs, an imidate intermediate is formed resulting in the oxygen atom of the imidate bound to the metal ion [3, 4]. Amide product is released upon rearrangement of the imidate to an amide.

1.2.3.3. Indirectly activated nucleophile mechanism

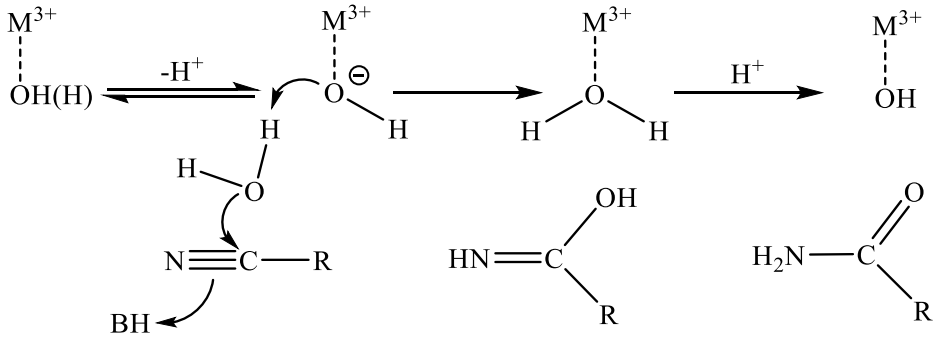

Figure 12. "Indirectly activated nucleophile" catalytic mechanism of NHase

In the indirectly activated nucleophile catalytic mechanism, a water molecule plays the role of the nucleophile and the substrate is not bound to the metal ion [3, 4]. A metal bound hydroxyl group is activated by a base and in turn, a water molecule is activated by the metal bound hydroxide group. The newly formed hydroxyl group can carry out the hydrolysis of the nitrile substrate through nucleophilic attack of the carbon atom of the nitrile group [3, 4].

1.2.3.4. Activated sulfenate mechanism

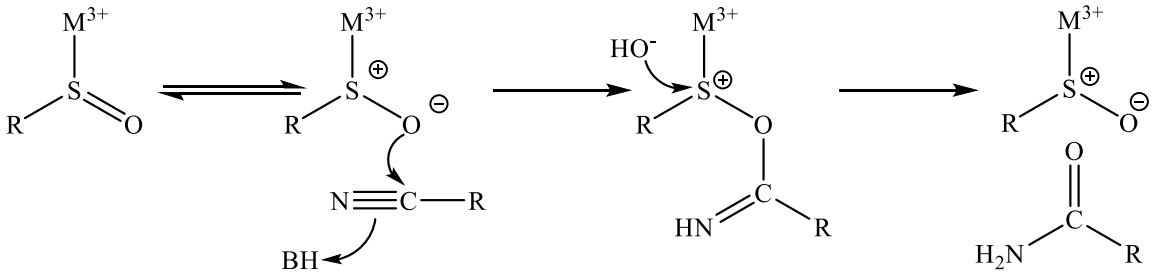

Figure 13. "Activated sulfenate" catalytic mechanism of NHase

In the last proposed catalytic mechanism for NHase enzymes, the activated sulfenate mechanism, the active site metal ion has no direct coordination with the substrate molecule. The cysteine sulfenic (SO^-) ligand plays the role of the nucleophile by attacking the nitrile carbon atom of the substrate [22].

1.2.3.5. Proposed reaction mechanism of NHase

Recent studies on NHase enzymes has provided insight into the catalytic mechanism resulting in a new reaction mechanism being proposed [23]. Replacement of the coordinated water molecule from the metal center by an incoming nitrile substrate is a common step for these mechanisms [16, 24, 25]. Holz and co-workers found evidence for the possible source of the initial nucleophilic attack on the substrate molecule [16]. Combination of stopped-flow and X-ray crystallography data has revealed a possible full reaction mechanism for nitrile hydration by NHase enzyme (Figure 14) [2, 16]. Initially, the axial water molecule is replaced by the incoming substrate molecule and coordinates to the active site metal ion [2, 16]. After that, the cysteine sulfenic ligand (Cys113-SOH) attacks the carbon atom of nitrile group to form a cyclic intermediate [16]. At the same time one proton transfer occurs between the Cys113-SOH group and nitrile N atom [16].

Then, two possible paths have been proposed. In path A, the cyclic intermediate is nuleophilically attacked by a water molecule, breaking the S-O bond of the cyclic intermediate resulting the metal bound imidate.

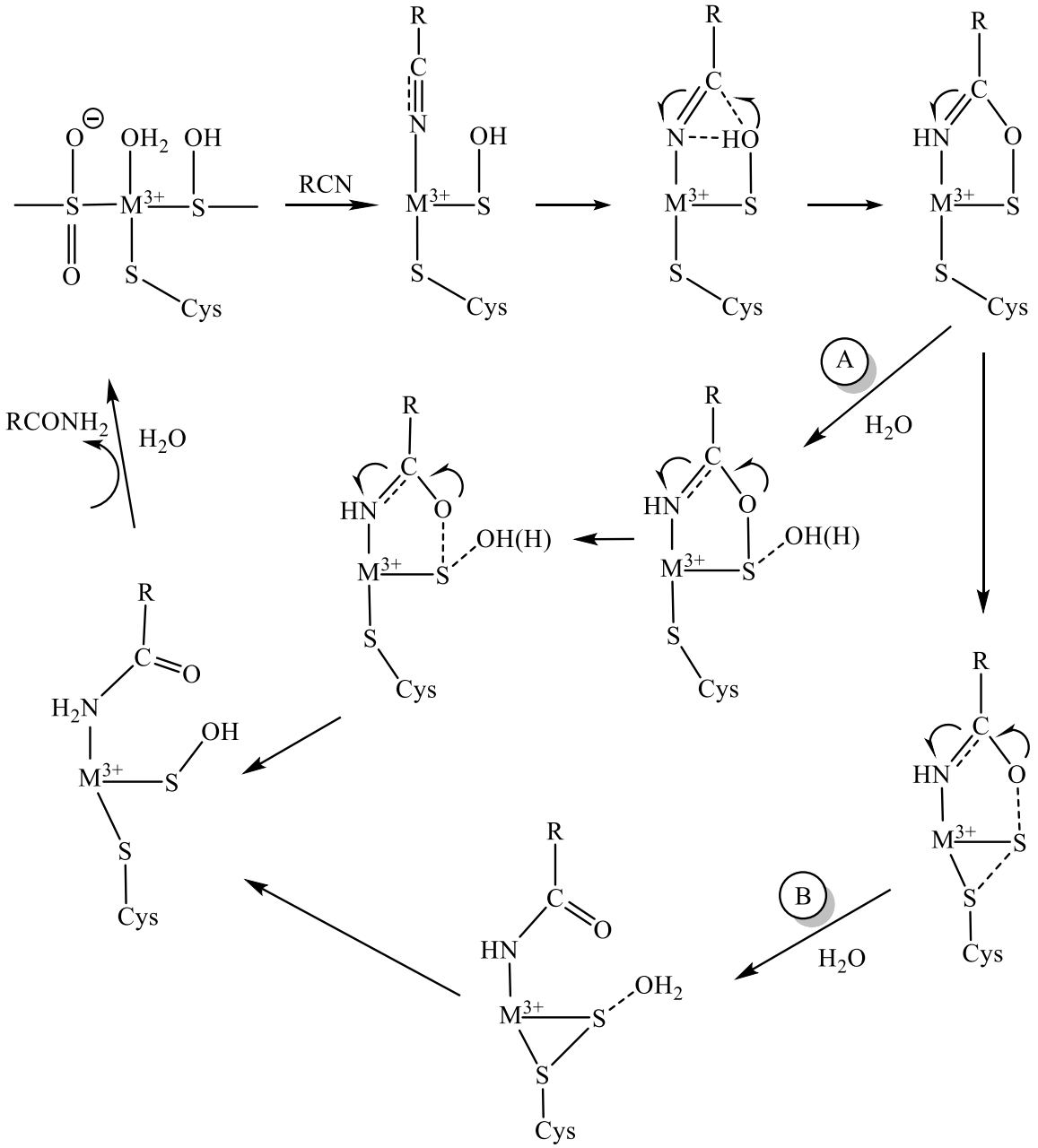

Figure 14. Full reaction mechanism of NHase proposed by Holz et al. Path; (A) S-O bond is cleaved by nucleophilic attack of a water molecule on the S atom of the cyclic intermediate, (B) S-O bond is cleaved by nucleophilic attack of the thiolate ligand on the S atom of the cyclic intermediate [23]

At the same time the second proton transfer occurs between Cys113S bound H_2O molecule and imidate N atom. In path B, the cyclic intermediate is nuleophilically attacked by the thiolate sulfur of the axial αCys108S^- ligand, forming a disulfide intermediate which assists in breaking the S-O bond of the cyclic intermediate resulting a metal bound amide. The second proton transfer occurs between a Cys113S coordinated H_2O molecule and N atom of the metal bound amide. Finally, coordination of a new water molecule to the metal center at sixth ligand position displaces the product and regenerates the active site [16, 23].

Odaka and co-workers have verified this reaction mechanism based on time-resolved X-ray crystallographic studies (Figure 15). Initially, the axial water molecule is replaced by the incoming substrate and coordinates to the active site metal ion. Then the cysteine sulfenic ligand (Cys114-SO^-) attacks the nitrile carbon atom to form a cyclic intermediate [19]. Next, the nitrogen atom of cyclic intermediate obtains a proton from oxygen atom on the sulfur atom of Cys114. Finally, the nitrogen atom of the imidate intermediate extracts a proton from the regenerated Cys114-sulfenic acid (Cys114-SOH) [19]. Coordination of a new water molecule to the metal center at sixth ligand position completes the reaction cycle [19].

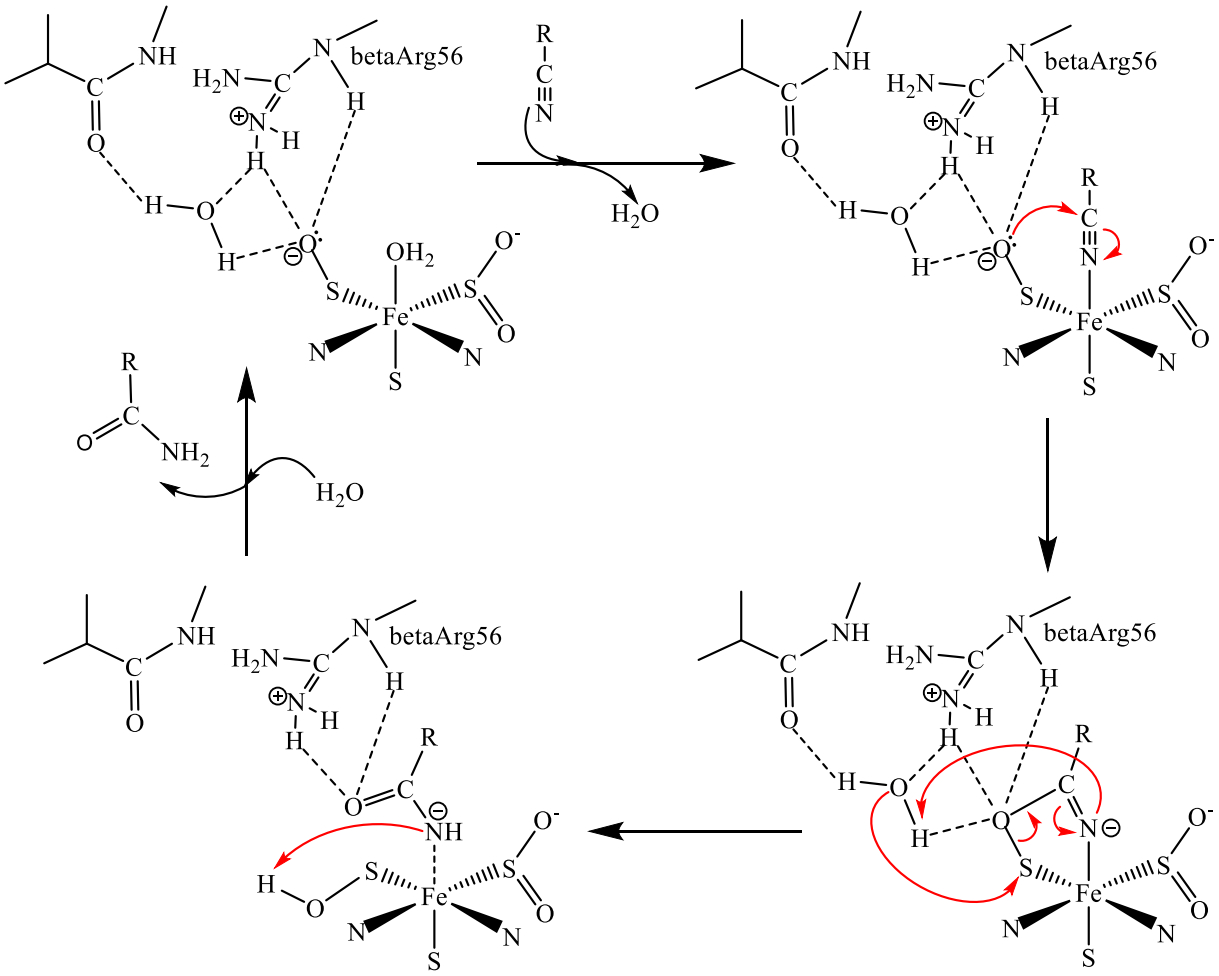

Figure 15. Full reaction mechanism of NHase proposed by Odaka [19]

1.3. Activator protein of NHase

1.3.1. Overview

Almost half of all known enzymes require a metal ion in order to perform their biological activities in living organisms, including structural stabilization, substrate activation, enzymatic catalysis, and electron transfer [26, 27]. Unregulated concentrations of transition metal ions in the cellular system may cause irreversible damage to the cell [27]. Therefore, continuous regulation of cellular metal ion concentrations is required in order to avoid cellular toxicity including harmful redox reactions, competition for inappropriate metal binding sites, and the formation of insoluble aggregates [27]. Due to the bioavailability of various metals ions in the cytoplasm, a key question that arises is how are specific metal co-factors transported to diverse locations and subsequently inserted into the correct enzyme [28]?

Interestingly, cellular metallochaperones have been identified that function in a "chaperone-like" manner, guiding and protecting the metal ion while facilitating appropriate partnerships [28]. Metallochaperones act as metal ion regulators and contribute to the metal homeostasis process by engaging the following functions.

- Metal ion selectivity [27].
- Safe transport of metal ions in biological environments (*i.e*. inhibit unwanted metal dependent reactions) [27].
- Deliver metal ions to their respective target site *via* direct protein-protein interactions [27].

There are well-known metallochaperones for the transportation of Cu^{2+}, Zn^{2+}, Cd^{2+} and Hg^{2+} [27, 28]. These contain the conserved amino acid sequence "MXCXXC" and the ability to act as an ATPase [27].

Fe^{2+} is considered as the second most abundant transition metal ion in the cytoplasm and is available in high micromolar levels [29]. On the other hand, concentrations of Co^{2+} in the cytoplasm is in the low micromolar level [29]. The concentration difference between Fe^{2+} and Co^{2+} in the cytoplasm suggests the existence of two different metal insertion mechanisms for Fe-type and Co-type NHases, otherwise, it seems, all NHases would be activated by inserting the more abundant Fe^{2+} ion. In 2000, Nojiri and co-workers expressed the Fe-type nitrile hydratase from *Rhodococcus sp.* N-771 in *E. coli* and supplemented the medium with Co^{2+} in the absence of the NHase activator gene [30]. Although, a Co-type NHase was obtained, activity levels were ~6% of the wild-type enzyme [30]. Miyanaga and co-workers performed a similar experiment on the Co-type NHase obtained from *Pseudonocardia thermophila* JCM 3095 [31]. They obtained apo-NHase after expression in the absence of Co^{2+} or in the presence of Fe^{2+} supplemented media [31].

Nojiri's and Miyanaga's experiments suggest that metal insertion into the active site of NHase is a closely regulated cellular process. Therefore, it was hypothesized that the specificity of NHase for Co^{2+} or Fe^{2+} is dependent on the type of activator protein present. Moreover, post-translational active site cysteine oxidation of the equatorial cysteine residues into cysteine sulfenic acid (Cys-SOH) and cysteine sulfinic acid (Cys-SO_2H), was also hypothesized as a role for NHase activator proteins [6, 32].

Interestingly, there is no sequence similarity between Fe-type activator proteins and Co-type activator proteins [33, 34]. Molecular biological studies on NHase enzymes have revealed that the NHase gene operon consists of six genes [6]. The first two genes belong to the NHase regulator 2 and NHase regulator 1 proteins. The third gene encodes for an amidase while the fourth and fifth genes encode for the NHase α-subunit and β-subunit, respectively. The sixth gene, which is downstream from the NHase α- and β-subunit genes, is recognized as the NHase activator gene [6].

Interestingly, the NHase gene operon for Fe-type NHase enzymes is different from the Co-type NHase gene operon (Figure 16) [34, 35]. The order of the genes in Fe-type NHase operon has the gene encoding for the α-subunit upstream from the gene encoding the β-subunit followed by the activator gene. On the other hand, the Co-type gene operon reveals that the gene encoding for the β-subunit is upstream from the gene encoding the α-subunit followed by the activator gene. However, Holz and co-workers showed that the Fe-type NHase from *Comamonas testosteroni* Ni1 does not require an activator protein for expression of a fully metalated and active NHase enzyme [32]. This is the only known NHase at this time that does not require an activator protein for metal insertion into active site.

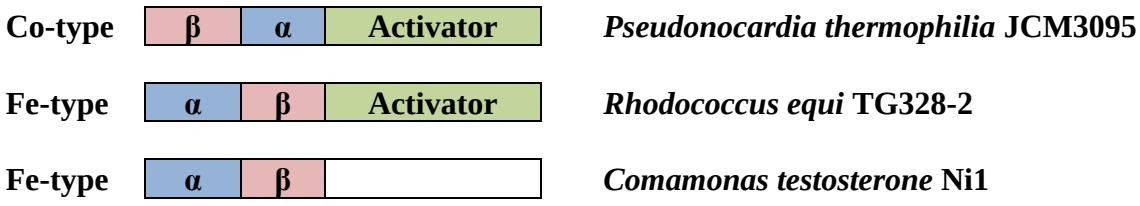

Figure 16. Arrangement of α, β , and activator genes in Fe-type and Co-type NHases [6, 32]

1.3.2. Co-type activator protein

Recent studies by Zhou and co-workers revealed that Co-type activators from *Rhodococcus rhodochrous* J1 utilize a "self-subunit swapping" mechanism to insert a metal ion into the α subunit of Co-type NHases (Figure 17) [7, 9].

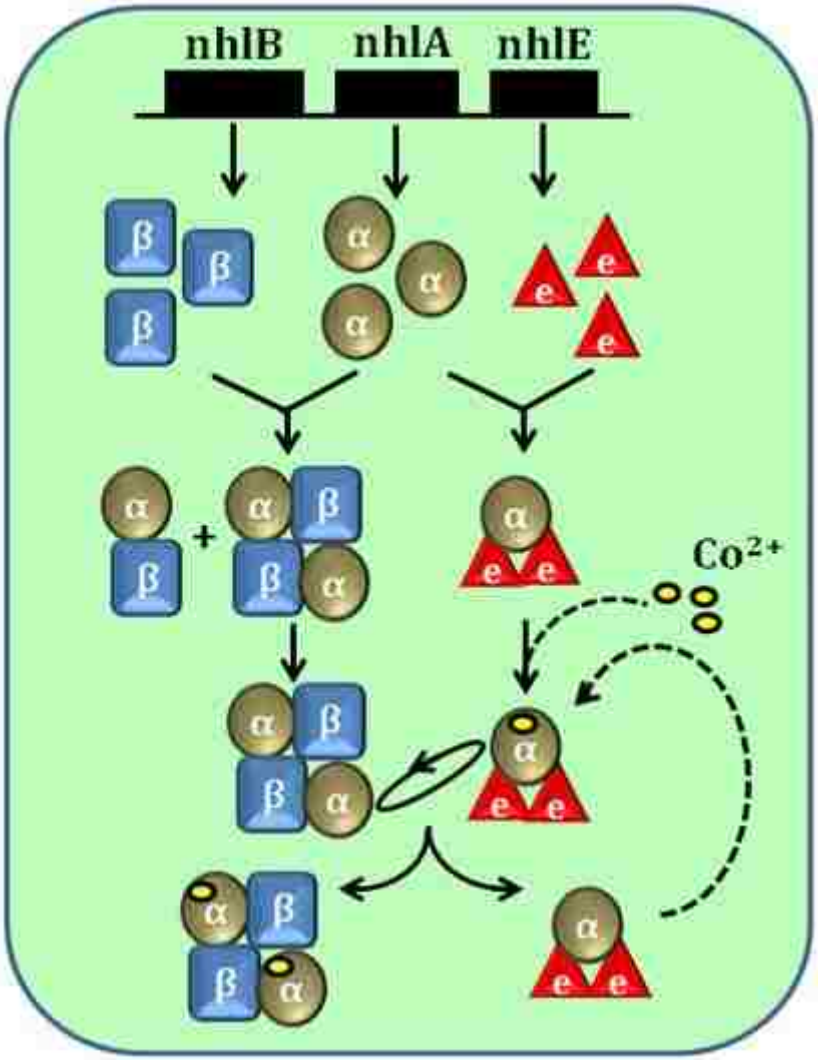

Figure 17. Proposed self-subunit swapping mechanism in Co-type NHase from *Rhodococcus rhodochrous* J1 [9]

According to the proposed self-subunit swapping mechanism, the α-subunit can interact with both the β-subunit and the activator protein (ε). Initially, both the $\alpha_2\beta_2$ and $\alpha\varepsilon_2$ complexes are apo. The apo-$\alpha\varepsilon_2$ complex scavenges a Co^{2+} ion which coordinates into the α-subunit with the assistance of the activator protein. Next, the α-subunit is exchanged between a holo-$\alpha\varepsilon_2$ complex and an apo-$\alpha_2\beta_2$ complex to form the holo-$\alpha_2\beta_2$ protein complex and used apo-$\alpha\varepsilon_2$ is recycled [7, 9]. The interaction between apo-$\alpha_2\beta_2$ and holo-$\alpha\varepsilon_2$ suggests that the Co-type activator acts as a subunit-swapping chaperone. Significant sequence homology between the activator protein and the β-subunit also strengthens the hypothesis of the subunit swapping mechanism.

Requirement of the activator protein for the post-translational oxidation of the two equatorial cysteine residues has been investigated by mass spectroscopy [7]. MALDI spectroscopic analysis revealed that the non-oxidized cysteine residues within the apo-α-subunit of *Rhodococcus rhodochrous* J1, were modified after the activator mediated Co^{2+} insertion step [7]. Therefore, the availability of metal ion in the active site appears to be crucial for the post translational oxidation process [7, 9]. The Co-type NHase activator protein from *Pseudomonas putida* NRRL-18668 also shows similar behavior to the NHase activator of *Rhodococcus rhodochrous* J1 [36]. Together, these data illustrate the function of Co-type activator protein is a self-subunit swapping chaperone and also as a metallochaperone [36].

1.3.3. Fe-type activator

Fe-type NHase activators have no sequence or structural similarity to the Co-type NHase activators [33, 34]. Amino acid sequence comparisons and the proposed metal ion trafficking role of the Fe-type NHase activator from *Rhodococcus sp.* N-771 suggests

that it resides in the COG0523 protein sub-group [37]. However structural information for proteins within the COG0523 sub-group is limited to the YjiA protein, which resides in the COG0523 sub-group-9 [37]. The COG0523 sub-group is a member of the G3E NTPase family as it contains a phosphate-binding loop (P-loop) [33, 37]. As such, one role for COG0523 proteins is hydrolyzing GTP [37]. The mononucleotide binding site is composed of a conserved nucleotide-binding motif that is a common feature for all known P-loop NTPases. NTPase enzymes within the COG0523 family are typically made up of a central, mostly parallel β-sheet that is surrounded by α-helices [37, 38]. The P-loop (Walker A motif), Walker B motif, and another region known as "switch I" are the three conserved elements in NTPase structures [37].

Metal binding affinities of the YjiA protein have been obtained using UV absorption spectroscopy [37]. It has been demonstrated that the YjiA protein can bind one equivalent of Co^{2+}, two equivalents of Ni^{2+} or four Zn^{2+} ions. The apparent K_d value for Co^{2+} binding is ~20 μM whereas YjiA binds two Ni^{2+} ions with K_d values of ~3.7 μM. Two binding sites for Zn^{2+} exhibited K_d values < 10 μM while the other two exhibited K_d values of ~10 μM [37].

The crystal structure of the aaTHEP1 protein from *Aquifex aeolicus* was also shown to be a member of the G3E NTPase family (Figure 18). Within the aaTHEP1 protein is a putative metal binding site in between the Walker A and Walker B motifs, which is common among G3E GTPases. The suggested role of the "Walker A" motif is to position the triphosphate group of GTP [38]. Magnesium binding, which is necessary for GTP hydrolysis, is proposed to bind to the "Walker B motif".

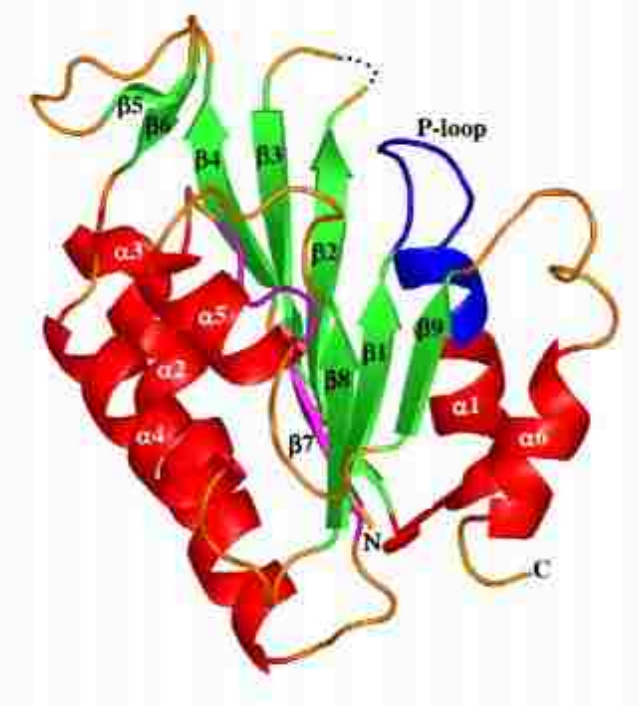

Figure 18. Ribbon representation of the crystal structure of aaTHEP1 (Walker A and Walker B motifs are in blue and magenta respectively) [39]

Fe-type NHase activator proteins contain a conserved CXCC motif (Table 2). Cysteine rich regions in proteins play important roles such as, protein-protein interactions, binding and transportation of metals, and also redox reaction regulations [6, 40]. As an example, there are at least three copper chaperones with cysteine-rich motifs that are involved in copper trafficking in *Saccharomyces cerevisiae*.[40] COX17 is responsible for transporting copper to mitochondrial cytochrome oxidase using a CXCC metal binding motif [6, 28]. Copper is delivered to CCC2 by Atx1, which contains an MTCXXC motif, [27, 28] whereas a CXC motif is used to transport copper to cytisolic SOD1 [6, 28]. However, molecular level evidence to describe the contribution of the activator protein CXCC motif in NHase metallocenter biosynthesis is lacking. Odaka and co-workers studied the effect of cysteine to serine mutations on the CXCC motif in the Fe-type activator from *Rhodococcus sp*. N-771 on the specific activity of the resulting

NHase enzyme. The specific activity of the expressed NHase was dramatically decreased suggesting that the CXCC motif in the NHase activator protein is critical for the functional expression of NHase enzymes [6].

Table 2. Conserved CXCC motifs in Fe-type NHase activators from different species [6]

Name	**Species**	**Region containing putative binding motif**
NHase Activator	*Rhodococcus sp*. N-771	69MTNG**CICC**TLR79
P44K protein	*Rhodococcus sp*. AJ270-6	68MTNG**CICC**TLR78
P47K	*Pseudomonas chloraphis* B23	72MTNG**CICC**TLR82
KB15K	*Rhodococcus equi* TG328-2	68MTNG**CICC**TLR78

Interestingly, the NHase activator from *Rhodococcus equi* TG328-2, which is of interest in this study, also contains a Walker A motif 13GFLGAGK21, a Walker B motif 97LIIESSG104, and the previously described metal binding motif at 72CICC75 [37]. Sequence analysis and homology modeling have also suggested that it is a G3E P-loop guanosine triphosphatase (GTPase) within the COG0523 subfamily [41]. Kinetic studies revealed that the Fe-type activator protein is capable of hydrolyzing GTP to GDP with a k_{cat}value of $1.2 \times 10^{-3}\,s^{-1}$ and a K_m value of 40 μM [41]. The addition of divalent metal ions, such as Co(II), which binds to the *Re*NHase TG328-2 activator protein with a K_d of 2.9 μM, accelerated the rate of GTP hydrolysis, suggesting that GTP hydrolysis is potentially connected to the proposed metal chaperone function of the *Rhodococcus equi* Nitrile Hydratase TG328-2 (*Re*NHase) activator protein [41].

1.4. Scope of the study

In this study, the Fe-type NHase and its corresponding activator protein from *Rhodococcus equi* TG328-2 were studied under three different projects to understand the enzyme and the catalytic cycle. Those projects were; **Chapter 2.** The Fe-type NHase form *Rhodococcus equi* TG328-2 forms an alpha-activator protein complex, **Chapter 3.** Cellular Maturation of an Fe-Type Nitrile Hydratase using EPR Spectroscopy, **Chapter 4.** Identification of an intermediate species along the Nitrile Hydratase reaction pathway by EPR.

Chapter 2. According to structural studies, NHases are heterotetramers that consist of two types of subunits ($\alpha_2\beta_2$) [5]. While Co- and Fe-type NHases have high α- and β-subunit sequence similarity, their respective (**ε**) proteins differ in size and share little to no sequence identity, suggesting that the mechanism of metallocenter assembly is possibly different [42-44]. Co-type NHase (**ε**) proteins are small (~15 kDa) and have significant sequence identity with the NHase β-subunit [9, 45]. The Co-type (**ε**) protein from *Rhodococcus rhodochrous* J1 was shown to form an $\alpha(\boldsymbol{\varepsilon})_2$ complex, which was proposed to bind Co(II) and insert it into apo-$\alpha_2\beta_2$ NHase *via* a "self-subunit swapping" mechanism [27, 44]. Interestingly, Fe-type NHase (**ε**) proteins are larger (~45 kDa) and contain a highly conserved cysteine-rich (CXCC) motif that is a known metal binding site in other metallochaperones such as COX17 (copper) and the Hyp proteins (nickel) [46, 47]. In our study we have seen the first known α(**ε**) complex of Fe-type NHase of *Re*NHase TG328-2, and analyzed via SDS-PAGE and MALDI-TOF. Further, the condition for the in-vitro activation of α(**ε**) complex were also studied.

Chapter 3. Fe-type NHases are more susceptible to inactivation by the oxidation of active site sulfenic groups into sulfinic groups [23, 48]. So, purified *Re*NHase-TG328-2 is a mixture of active and inactive enzyme molecules. Multiple species make it difficult to distinguish Electron Paramagnetic Resonance (EPR) signals. It was important to understand whether these multiple states are solely the consequence of how the enzyme is purified (anerobic vs aerobic) or whether they arise in intact cells during NHase expression. Hence, the cellular maturation of *Re*NHase-TG328-2 was studied using EPR spectroscopy to understand the initiation and the progression of the observed NHase EPR signals.

Chapter 4. *Re*NHase-TG328-2 is EPR active due to the low spin Fe(III) ion in the active center. EPR spectra of the resting state of *Re*NHase-TG328-2 has shown multiple overlapped rhombic EPR signals around $\sim g = 2$. The addition of nitrile substrates or inhibitors results in new species being observed in the EPR spectrum with different g values. Electronic and structural studies on intermediates will provide information about the steps in the reaction cycle. Hence, intermediates were trapped using cryoenzymological methods and analyzed by EPR spectroscopy.

CHAPTER 2

THE FE-TYPE NITRILE HYDRATASE FROM *RHODOCOCCUS EQUI* TG328-2 FORMS AN ALPHA-ACTIVATOR PROTEIN COMPLEX

2.1. Introduction

Nitrile hydratases (NHases, EC 4.2.1.84) are metalloenzymes that catalyze the hydration of nitriles to their corresponding higher value amides under mild conditions (room temperature and physiological pH) [49, 50]. X-ray crystallographic studies indicate that they are $\alpha_2\beta_2$ heterotetramers with an active site consisting of three cysteine residues, two amide nitrogens, a water molecule, and either a low-spin, non-heme Fe(III) ion (Fe-type) or a low-spin, non-corrin Co(III) ion (Co-type) [51, 52]. Two of the active site cysteine residues are post-translationally modified to cysteine-sulfinic acid ($–SO_2H$) and cysteine-sulfenic acid (–SOH) yielding an unusual metal coordination geometry, termed a "claw-setting." The protonation states of the active site equatorial sulfenic and sulfinic acids were suggested to be Cys-SOH and Cys-SO_2^- based on sulfur K-edge XAS and geometry-optimized DFT calculations [53]; oxidation of the equatorial Cys residues is essential for catalysis [6]. While the X-ray crystal structures of Fe- and Co-type NHases are very similar, interestingly, Fe-type NHases are specific for Fe(III) while Co-type NHases are specific for Co(III) [51].

Several open reading frames (ORFs) have been identified just downstream from the structural α- and β-subunit genes in both Co- and Fe-type NHases, and one of these genes has been proposed to function as an activator (**ε**) protein [54-56]. Current data indicate that both Co- and Fe-type NHase enzymes typically require the co-expression of an (**ε**) protein to be fully metallated, post-translationally modified, and functional [54-56].

While Co- and Fe-type NHases have high α- and β-subunit sequence similarity, their respective (**ε**) proteins differ in size and share little to no sequence identity, suggesting that the mechanism of metallocenter assembly is different [42-44]. Co-type NHase (**ε**) proteins are small (~15 kDa) and have significant sequence identity with the NHase β-subunit [9, 45]. The Co-type (**ε**) protein from *Rhodococcus rhodochrous* J1 was shown to form an $\alpha(\boldsymbol{\varepsilon})_2$ complex, which was proposed to bind Co(II) and insert it into apo-$\alpha_2\beta_2$ NHase *via* a "self-subunit swapping" mechanism [44]. The Co-type (**ε**) protein was also proposed to facilitate oxidation of two active site Cys-residues. On the other hand, Fe-type NHase (**ε**) proteins are large (~45 kDa) and contain a highly conserved cysteine-rich (CXCC) motif that is a known metal binding site in other metallochaperones such as COX17 (copper) and the Hyp (nickel) proteins [6, 46]. While Fe-type NHase (**ε**) proteins may form an $\alpha(\boldsymbol{\varepsilon})_x$ complex and insert Fe(II) into the α-subunit, similar to Co-type (**ε**) proteins, no data exists to support this hypothesis.

Recently, an Fe-type NHase (**ε**) protein was expressed and characterized revealing that it is a member of the COG0523 subfamily of G3E P-loop GTPases and that GTPase activity is regulated by metal binding [37, 57]. Since the role of the Fe-type (**ε**) protein in NHase metallocenter assembly is directly related to NHase structure and function, investigating this process will identify aspects of the metallocenter assembly that are essential for catalysis. Herein we describe the formation of an α(**ε**) protein complex for the Fe-type (**ε**) protein from *Rhodococcus equi* TG328-2 (*Re*NHase TG328-2). Kinetic data reveal that the addition of GTP and the *Re*NHase TG328-2 β-subunit under reducing conditions, results in NHase activity establishing for the first time the involvement of both the Fe-type (**ε**) protein and GTP in the maturation of Fe-type NHase enzymes.

2.2. Materials and methods

2.2.1. Materials

Guanosine triphosphate (GTP), isopropyl-β-D-1-thiogalactopyranoside (IPTG), tris(2-carboxyethyl)phosphine (TCEP), N-2-hydroxyethylpiperazine-N-2-ethane sulfonic acid (HEPES**),** 2-amino-2-(hydroxymethyl)-1,3-propanediol hydrochloride (Tris-HCl), and acrylamide were purchased from Sigma-Aldrich or Fisher scientific as the highest purity available. NEB and BL21(DE3) competent *E. coli* cells were obtained from Agilent Technologies and plasmid preparation kits were purchased from Promega. All other reagents were purchased commercially and were the highest purity available.

2.2.2. Plasmid construction

The plasmid expressing the Fe-type nitrile hydratase from *Rhodococcus equi* TG328-2 (*Re*NHase TG328-2) was kindly provided by Professor Uwe Bornscheuer [58]. The original plasmid had the NHase α, β, and activator genes in tandem. Therefore, separate pET-28a$^+$ plasmids containing only the His_6-tagged *Re*NHase TG328-2 α-subunit and the His_6-tagged *Re*NHase TG328-2 β-subunit genes were synthesized by Genscript, while the pMCSG9 plasmid containing the *Re*NHase TG328-2 (**ε**)-MBP-His_6 protein with a Tobacco Etch Virus (TEV) protease cleavage site between MBP and the *Re*NHase TG328-2 (**ε**) protein, as previously described, was used to express the *Re*NHase TG328-2 (**ε**) protein [57]. All plasmid sequences were confirmed using automated DNA sequencing at the Functional Biosciences DNA sequencing facility.

2.2.3. Expression of recombinant *Re*NHase TG328-2 α, β and (ε) proteins

The pMCSG9 plasmid containing the *Re*NHase TG328-2 (**ε**)-MBP-His_6 gene was transformed into BL21 magic cells for the soluble expression of the *Re*NHase TG328-2 (**ε**) protein. Similarly, individual expression systems for the *Re*NHase TG328-2 α- and β-subunits were prepared by transforming the pET-21a$^+$ plasmids containing the His_6-*Re*NHase TG328-2 α-subunit gene and the His_6-*Re*NHase TG328-2 β-subunit gene into BL21(DE3) cells. A single colony of each transformation was typically used to inoculate separate 50 mL flasks of LB Miller culture containing 50 μg/mL of kanamycin and allowed to grow at 37 °C with constant shaking overnight. These cultures were used to inoculate 6 L of LB Miller culture containing kanamycin (50 μg/mL) and ampicillin (100 μg/mL). Cells were allowed to grow at 37 °C with constant shaking until an optical density of ~0.8-1.0 at 600 nm was reached. In each case, the culture was cooled to 18 °C and induced with 0.1 mM Isopropyl-β-D-1- thiogalactopyranoside (IPTG) and shaken for an additional 16 hrs at 18 °C. Cells were pelleted by centrifugation at 5000 × *g* for 10 minutes and resuspended in 50 mM phosphate buffer at pH 7.5 (500 mM NaCl, 50 mM imidazole, and 10% glycerol) for *Re*NHase TG328-2 α- and β-proteins and 50 mM Tris buffer at pH 7.4 (200 mM NaCl) for the *Re*NHase TG328-2 (**ε**) protein. All cell paste was stored at -80 ^oC until needed.

2.2.4. Purification of recombinant *Re*NHase TG328-2 (ε) protein

Cells containing the *Re*NHase TG328-2 (**ε**) plasmid (His_6-MBP-TEV-**ε**) were lysed by ultrasonication (Misonix Sonicator 3000) in 30 second increments for 4 minutes at 21 W. Cell lysate was separated from cell debris by centrifugation for 40 min. at

10,000 × *g*. The supernatant was loaded onto two, pre-equilibrated 5 mL MBP-Trap columns (GE Healthcare) and washed with 20 column volumes of 20 mM Tris-HCl buffer at pH 7.5 containing 200 mM NaCl. *Re*NHase TG328-2 (**ε**) protein was eluted with a 10 mM maltose gradient in 20 mM Tris-HCl buffer at pH 7.5 containing 200 mM NaCl. Fractions containing *Re*NHase TG328-2 (**ε**)-MBP-TEV-His_6 were pooled and the buffer exchanged into 50 mM Tris-HCl buffer at pH 7.5 containing 10% glycerol (0.5 mg/mL). His_6-TEV protease (total protein: TEV (w/w) = 50:1) and 10 mM tris(2-carboxyethyl)phosphine (TCEP) was added to the protein sample and stirred gently for ~36 hours at 4 ˚C. The sample containing cleaved *Re*NHase TG328-2 (**ε**) protein was concentrated to 5 mL and loaded onto two 5 mL MBP-Trap columns (GE Healthcare) connected to an ÄKTA Prime Plus FPLC system that was previously equilibrated with 20 mM Tris-HCl buffer at pH 7.5 containing 10% glycerol and 5 mM TCEP. The cleaved *Re*NHase TG328-2 (**ε**) protein was collected in the flow through and concentrated. The protein was then buffer exchanged into 50 mM sodium phosphate buffer at pH 7.5 containing 10% glycerol and 5 mM TCEP to a total volume of 5 mL and loaded onto a pre-packed 5 mL immobilized-metal affinity chromatography (IMAC) nickel-nitrilotriacetic acid (Ni-NTA) column (QIAGEN) connected to an ÄKTA Prime Plus FPLC system that was previously equilibrated with 50 mM sodium phosphate buffer at pH 7.5 containing 10% glycerol, 5 mM TCEP. The *Re*NHase TG328-2 (**ε**) protein was collected in the flow through and shown to be pure via SDS-PAGE (12.5%).

2.2.5. EDTA treatment of recombinant *Re*NHase TG328-2 (ε) protein

Purified *Re*NHase TG328-2 (**ε**) protein was treated with 10 mM EDTA in 50 mM HEPES buffer, pH 7.5 containing 20 mM TCEP and incubated overnight under nitrogen at 4 ˚C. The EDTA and TCEP were removed by dialysis against Chelexed 50 mM HEPES buffer, pH 7.5. The metal-free *Re*NHase TG328-2 (**ε**) protein was concentrated and the protein concentration determined using a Bradford assay. Samples were frozen at -80 ˚C until needed.

2.2.6. Purification of the *Re*NHase TG328-2 α- and β-proteins

Cells were lysed by ultra-sonication using a microtip (30 seconds on and 45 seconds off) over 8 minutes at 21 W. The supernatant was separated from the cell debris by centrifugation at 4 ˚C for 40 min. at 10,000 × *g*. Based on SDS-PAGE (12.5%) analysis, both the α- and β-proteins expressed as inclusion bodies. Therefore, the pellet proteins were re-suspended in 4 M urea and centrifuged at 4 ˚C and 10,000 × *g* for 40 minutes. The supernatant was dialyzed at 4 ˚C against 50 mM HEPES buffer, pH 7.5 containing 2 M urea using a 10 kDa cutoff dialysis bag. Successive dialysis steps were undertaken at 4 ˚C against 50 mM HEPES buffer, pH 7.5 containing 1 M, 0.5 M urea and no urea, respectively, with the dialysis buffer exchanged at least three times every three hours.

The solubilized α- and β-proteins were loaded individually onto pre-equilibrated 5 mL IMAC-Ni-NTA columns. The columns were washed with 10 column volumes of 50 mM sodium phosphate buffer at pH 7.5 (300 mM NaCl, and 10 mM imidazole). Both the His_6-tagged α- and β-proteins were eluted with a linear gradient (0-100%) of a high

imidazole content buffer (50 mM NaH_2PO_4 pH 7.5, 300 mM NaCl, 10% glycerol, 200 mM imidazole) at a flow rate of 1 mL/min. The fractions containing protein were concentrated and shown to be soluble and pure by SDS-PAGE (12.5%). Samples were frozen at -80 ^oC until needed.

2.2.7. Purification of an *Re*NHase TG328-2 $\alpha(\varepsilon)_x$ complex

Cells were lysed by ultra-sonication using a microtip (30 seconds on and 45 seconds off) over 4 minutes at 21 W. Cell lysate was separated from cell debris through centrifugation at 4 ˚C for 40 min. at 10,000 × *g*. Protein was purified from the re-suspended pellet using 4 M urea as the target protein was found with the cell debris. The resulting solution was centrifuged at 4 ˚C for 40 min. at 10,000 × *g*. The supernatant was dialyzed using a 10 kDa cutoff dialysis bag at 4 ˚C. The first dialysis step was done in 50 mM HEPES buffer at pH 7.5 containing 2 M urea. The second and third steps were done with 1 M and 0.5 M urea in 50 mM HEPES buffer at pH 7.5, respectively. The supernatant was dialyzed an additional three times in urea free 50 mM HEPES buffer at pH 7.5. The sample to buffer ratio was 100:1 at each dialysis step and the dialysis buffer was changed every 16 hours.

Dialyzed supernatant was loaded onto a pre-equilibrated 5 mL IMAC-Ni-NTA column. The column was washed with 10 column volumes of 50 mM sodium phosphate buffer at pH 7.5 (300 mM NaCl, 40 mM butyric acid, and 10 mM imidazole). His_6-tagged protein was eluted using 10 column volumes of 50 mM sodium phosphate buffer at pH 7.5 (300 mM NaCl, 40 mM butyric acid, and 200 mM imidazole). The eluted sample was concentrated and analyzed by SDS-PAGE (12.5%).

Another sample was purified under denaturing conditions by loading solubilized protein onto a pre-packed 5 mL IMAC-Ni-NTA column that had been equilibrated with 4 M urea and 50 mM HEPES buffer at pH 7.5. Purification was performed using an AKTA Prime Plus FPLC system. The column was washed with 10 column volumes of 50 mM HEPES buffer at pH 7.5 containing 4 M urea. The urea concentration was gradually decreased to 0% by increasing the percentage of urea free 50 mM HEPES buffer at pH 7.5 over 5 column volumes. The column was then washed with 5 column volumes of 50 mM HEPES buffer at pH 7.5. His_6-tagged protein was eluted using 50 mM sodium phosphate buffer at pH 7.5 containing 300 mM NaCl, 40 mM butyric acid, and 200 mM imidazole. Fractions were collected and analyzed by SDS-PAGE (12.5%).

2.2.8. MALDI TOF analysis of the *Re*NHase TG328-2 $\alpha(\varepsilon)_x$ complex

Matrix-assisted laser desorption/ionization time of flight (MALDI TOF) mass spectroscopy (MS) was utilized to examine the *Re*NHase TG328-2 $\alpha(\boldsymbol{\varepsilon})_x$ complex in 50 mM HEPES, pH 7.5 (1 mg/mL). The matrix consisted of α-cyano-4-hydroxycinnamic acid (α-CHCA) dissolved in a minimal amount of acetone, which was applied to the MALDI target (0.5 µL). Once dried, 0.5 µL of a 1 mg/mL *Re*NHase TG328-2 $\alpha(\boldsymbol{\varepsilon})_x$ complex protein solution was applied along with a calibrant spot containing albumin followed by another 0.5 µL of α-CHCA matrix solution. Samples were dried under air and then MALDI TOF MS spectra were recorded on a Voyager-DE^{TM} PRO BioSpectrometer (EVISA).

2.2.9. In vitro activation of *Re*NHase TG328-2

The purified *Re*NHase TG328-2 α-subunit in 50 mM HEPES buffer, pH 7.5 was mixed with Fe(II), Fe(II) + activator, or Fe(II) + activator + GTP in the absence and presence of TCEP anaerobically (Table 5). Each of the previous combinations was also mixed with purified β-subunit (Table 5). Samples prepared in the presence of TCEP were incubated for ~36 hours at 4 ˚C, after which TCEP, GTP, and unbound Fe(II) was removed by buffer exchange using a 10 kDa amicon ultra centrifugal filtration unit. The enzymatic activity of each combination towards acrylonitrile (acrylamide; $\Delta\varepsilon_{225}$ = 2.9 mM^{-1} cm^{-1}) was measured using a Shimadzu UV-2450 spectrophotometer. A 1 mL reaction consisted of 50 mM HEPES buffer, pH 7.5 at 25 °C, 80 mM acrylonitrile and 1 μM *Re*NHase TG328-2 α-subunit. Data analysis was performed using OriginPro 9.0 (OriginLab, Northampton, MA). The kinetic constants V_{max} and K_m were calculated by fitting the data to the Michaelis and Menten equation. One unit of enzyme activity was defined as the amount of enzyme that catalyzed the production of 1 μmol of the amide per minute at 25 °C.

2.2.10. Metal content

The metal content of each purified protein was determined by inductively-coupled plasma mass spectrometry (ICP-MS). Each protein (1 mg) was incubated overnight in 8 M urea followed by digestion with a mixture of 2% HNO_3 and 0.5% HCl. After 24 hours, the digested protein samples were filtered using 0.2 μM syringe filters and submitted, along with a control of buffer containing no protein, for analysis at the Water

Quality Center in the College of Engineering at Marquette University (Milwaukee, WI, USA).

2.2.11. Electronic absorption spectra

All electronic absorption spectra were recorded on a Shimadzu UV-2600 spectrophotometer equipped with a TCC-240A temperature-controlled cell holder. Spectra were obtained at 25 °C in a 1 cm quartz cuvette in 50 mM HEPES buffer, pH 7.5.

2.3. Results and Discussion

The prevailing dogma is that both Co- and Fe-type NHase enzymes require the co-expression of the α- and β-subunits with an (**ε**) protein to be fully metallated, post-translationally modified, and functional [59-61]. While (**ε**) proteins may indeed dictate the identity of the metal ion in NHases and participate in the controlled oxidation of the two equatorial Cys residues, no biochemical or structural data exist to support this hypothesis in Fe-type NHases. Recently, the Fe-type *Re*NHase (**ε**) protein was heterologously over-expressed and purified [57]. These data established, for the first time, that the *Re*NHase (**ε**) protein is a member of the COG0523 subfamily of G3E P-loop GTPases and that GTPase activity is regulated by metal binding. However, two significant questions remain unanswered: i) does an $\alpha(\boldsymbol{\varepsilon})_x$ complex form for Fe-type NHases? and ii) is GTP hydrolysis connected to iron insertion into the NHase α-subunit?

To determine if an Fe-type (**ε**) protein α-subunit complex can form, a plasmid that contains only the His_6-tagged α-subunit of *Re*NHase was prepared and co-expressed with untagged WT *Re*NHase (**ε**) protein. In the absence of the β-subunit, the $\alpha(\boldsymbol{\varepsilon})_x$ complex is found as inclusion bodies (Figure 19A). The complex was solubilized in 4 M urea followed by its step-wise removal *via* dialysis and purification by IMAC [62]. The resulting, soluble $\alpha(\boldsymbol{\varepsilon})_x$ complex was shown to be pure *via* SDS-PAGE and contain both the α-subunit at ~23 kDa and the (**ε**) protein at ~46 kDa (Figure 19A). Since only the α-protein is His-tagged but both proteins purify together on the IMAC column, these data suggest the formation of a soluble $\alpha(\boldsymbol{\varepsilon})_x$ complex. The solubilized $\alpha(\boldsymbol{\varepsilon})_x$ complex was also applied to an IMAC column without removing the 4 M urea, resulting in the separation of the (**ε**) protein from the His_6-tagged α-subunit. As the (**ε**) protein does not contain a His_6-

tag, it was eluted in the wash buffer while the His_6-taged α-subunit remained bound to the column (Figure 19B). As the WT *Re*NHase (**ε**) protein has no His_6-tag, it has no specific affinity towards the IMAC column when denatured and can only remain bound to the column due to complex formation with the α-subunit in the absence of urea. These data establish, for the first time, that an Fe-type α-subunit can bind to an Fe-type (**ε**) protein forming an $\alpha(\boldsymbol{\varepsilon})_x$ complex.

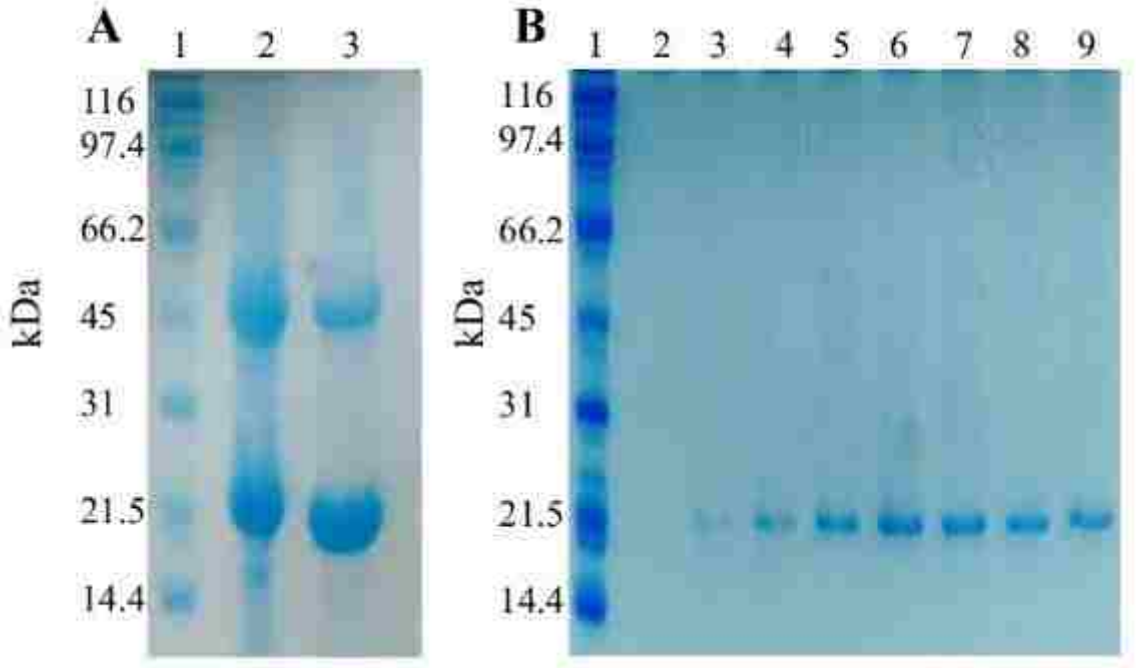

Figure 19. SDS-PAGE analysis of (A) re-folded protein sample before and after Ni-NTA column purification (Lane 1-Protein marker, Lane 2-Re-folded protein before purification, Lane 3-Re-folded protein after the purification), (B) the eluted α-subunit protein fractions when purified under denaturation conditions (Lane 1-Protein marker, Lane 2 to 9-Eluted fractions at 200 mM imidazole concentration).

The Co-type (**ε**) protein from *Rhodococcus rhodochrous* J1 was shown to form an $\alpha(\boldsymbol{\varepsilon})_2$ complex, but Co-type NHase (**ε**) proteins are small (~15 kDa), which is less than half the size of Fe-type (**ε**) proteins (~47 kDa) [9, 44, 45]. To determine the molar ratio of the *Re*NHase $\alpha(\boldsymbol{\varepsilon})_x$ complex, MALDI-TOF MS data were obtained (Figure 20). Masses were observed at 23,865 Da and 47,769 Da, which are in a good agreement with the theoretical masses of the α-subunit (23,904 Da) and the (**ε**) protein (47,756 Da). A mass was also observed at 71,593 Da, which is in good agreement with the theoretical mass (71,660 Da) of an α(**ε**) complex with a 1:1 molar ratio. Given the large size of the *Re*NHase (**ε**) protein, these data support the existence of 1:1 α(**ε**) protein complex that can be dissociated into the α-subunit and the (**ε**) protein.

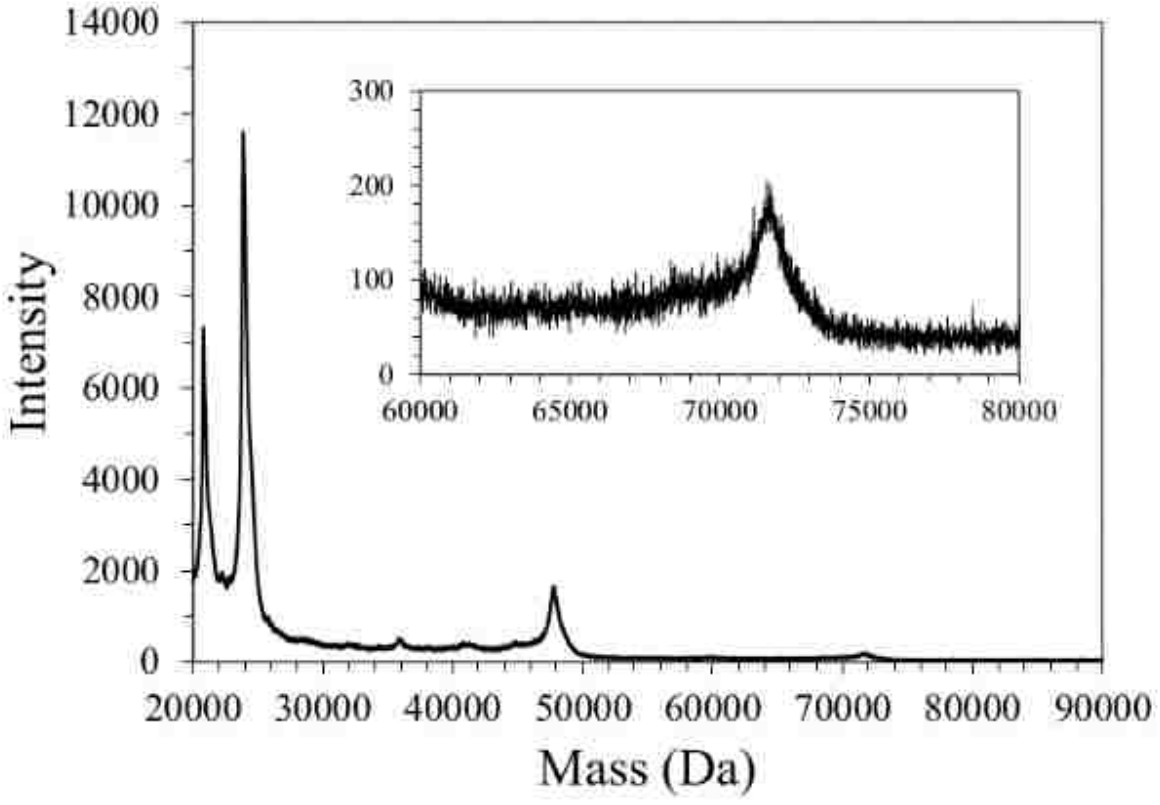

Figure 20. MALDI TOF analysis of *Re* NHase α-subunit and activator protein (ε) complex.

Previous spectroscopic and isothermal titration calorimetry data revealed that the *Re*NHase (**ε**) protein is capable of binding divalent cations such as Co(II) or Fe(II) with a 1:1 molar ratio [57]. However, metal analysis on the as-purified Fe-type α(**ε**) complex indicated that the complex only contained 0.1 equivalent of iron (Table 3). Combination of these data with those for Co-type (**ε**) proteins, which were shown to form an $\alpha(\boldsymbol{\varepsilon})_2$ complex that binds Co(II) and inserts it into apo-$\alpha_2\beta_2$ NHase *via* a "self-subunit swapping" mechanism [44], suggests a similar roll for the Fe-type (**ε**) protein.

Table 3. ICP-MS metal analysis data for the apo-α-subunit and apo-$\alpha(\varepsilon)_x$ complex.

Protein	**Protein: Fe Mole ratio**
apo-α-subunit	1: 0.06
apo-α(ε) complex	1: 0.12

Having in hand the apo-form of the *Re*NHase α(**ε**) complex, provides the unique opportunity to investigate if the α(**ε**) complex can bind Fe(II), which can in turn be inserted into an apo-$\alpha_2\beta_2$ *Re*NHase heterotetramer. It also provides the unique opportunity to determine if GTP hydrolysis plays a role in iron insertion and active site maturation. The as purified apo-α(**ε**) complex exhibits no detectable NHase activity under standard conditions (50 mM HEPES buffer at pH 7.5 and 25 ^{o}C) using 80 mM acrylonitrile as the substrate (Table 4; Figure 21). As expected, apo-NHases from *Pseudonocardia thermophila* (Co-type) and *Re*NHase (Fe-type) are inactive highlighting the importance of metal incorporation for NHase activity [31, 63].

Table 4. Kinetic data for the $\alpha(\varepsilon)_x$ complex in the absence and presence of TCEP at 25 °C.

Components	k_{cat} **(s^{-1})**	k_{cat} **(s^{-1}) +TCEP**
αε only	ND[a]	ND[a]
$\alpha\varepsilon + Fe^{2+}$	ND[a]	ND[a]
$\alpha\varepsilon + Fe^{2+}$ + GTP	ND[a]	ND[a]
$\alpha\varepsilon + \beta + Fe^{2+}$	0.7 ± 0.1	1.7 ± 0.2
$\alpha\varepsilon + \beta + Fe^{2+}$ + GTP	1.1 ± 0.2	2.1 ± 0.3

[a]None detected

Interestingly, purified α-subunit of the trimeric toyocamycin nitrile hydratase (TNHase) from *Streptomyces rimosus* exhibited ~0.3 % of wild type activity, suggesting that the α-subunit alone is capable of hydrating nitriles [61]. For TNHase, the as-purified α-subunit contained cobalt which is likely why detectable activity is observed. The step-wise addition of Fe(II), the reducing agent TCEP, GTP, and both TCEP and GTP to the apo-α(**ε**) complex followed by incubation under nitrogen for 12 hours, also produced no detectable NHase activity, suggesting that the *Re*NHase α-subunit on its own, unlike TNHase, is not capable of hydrating nitriles.

Several residues in the β-subunit are known to be important for the NHase activity. For example, βArg56, which is strictly conserved, forms hydrogen bonds with both active site oxidized axial Cys ligands and when replaced with lysine, the observed NHase activity is significantly decreased [64, 65]. Similarly, a strictly conserved active

site tyrosine (βTyr72) when mutated to Phe, significantly reduced the observed NHase activity [21].

As no β-subunit from any NHase has been independently expressed and purified, a plasmid was constructed that only expresses the His_6-tagged *Re*NHase β-subunit. Similar to the α(**ε**) complex, the *Re*NHase β-subunit also formed inclusion bodies but was solubilized in 4 M urea followed by its step-wise removal *via* dialysis and purification by IMAC (Figure 40) [62]. The as-purified β-subunit exhibited no detectable NHase activity, under standard assay conditions using acrylonitrile as the substrate, as expected.

With purified *Re*NHase apo-α(**ε**) complex and β-subunit in hand, the formation of a reconstituted form of the *Re*NHase $\alpha_2\beta_2$ enzyme was examined. The addition of the *Re*NHase β-subunit and Fe(II) to the *Re*NHase apo-α(**ε**) complex followed by incubation under nitrogen for 12 hours, provided an enzyme with a k_{cat} value of 0.7 ± 0.1 s^{-1} (Table 4; Figure 21). While this k_{cat} value is only ~0.1% of the value observed for WT *Re*NHase, it is highly reproducible across multiple purifications, is dependent on α(ε) complex and β-subunit concentrations, and the incubation time and the concentration of acrylonitrile. It is also greater than the k_{cat} value (0.44 ± 0.04 s^{-1}) reported for only the α-subunit of TNHase [61]. The addition of TCEP to this combination more than doubled the observed k_{cat} value to 1.7 ± 0.2 s^{-1} (Table 4; Figure 21). Reducing conditions likely enhance metal ion binding to the apo-α(ε) complex due to the reduction of disulfide bonds one of which was proposed to occur between the axial cysteine thiolate sulfur and the sulfenic acid sulfur atom of the NHase active site and/or in the proposed CXCC metal binding site of Fe-type (**ε**) proteins [31]. These data indicate that apo-α(**ε**) complex, in combination with β-subunit and Fe(II) can form an active NHase.

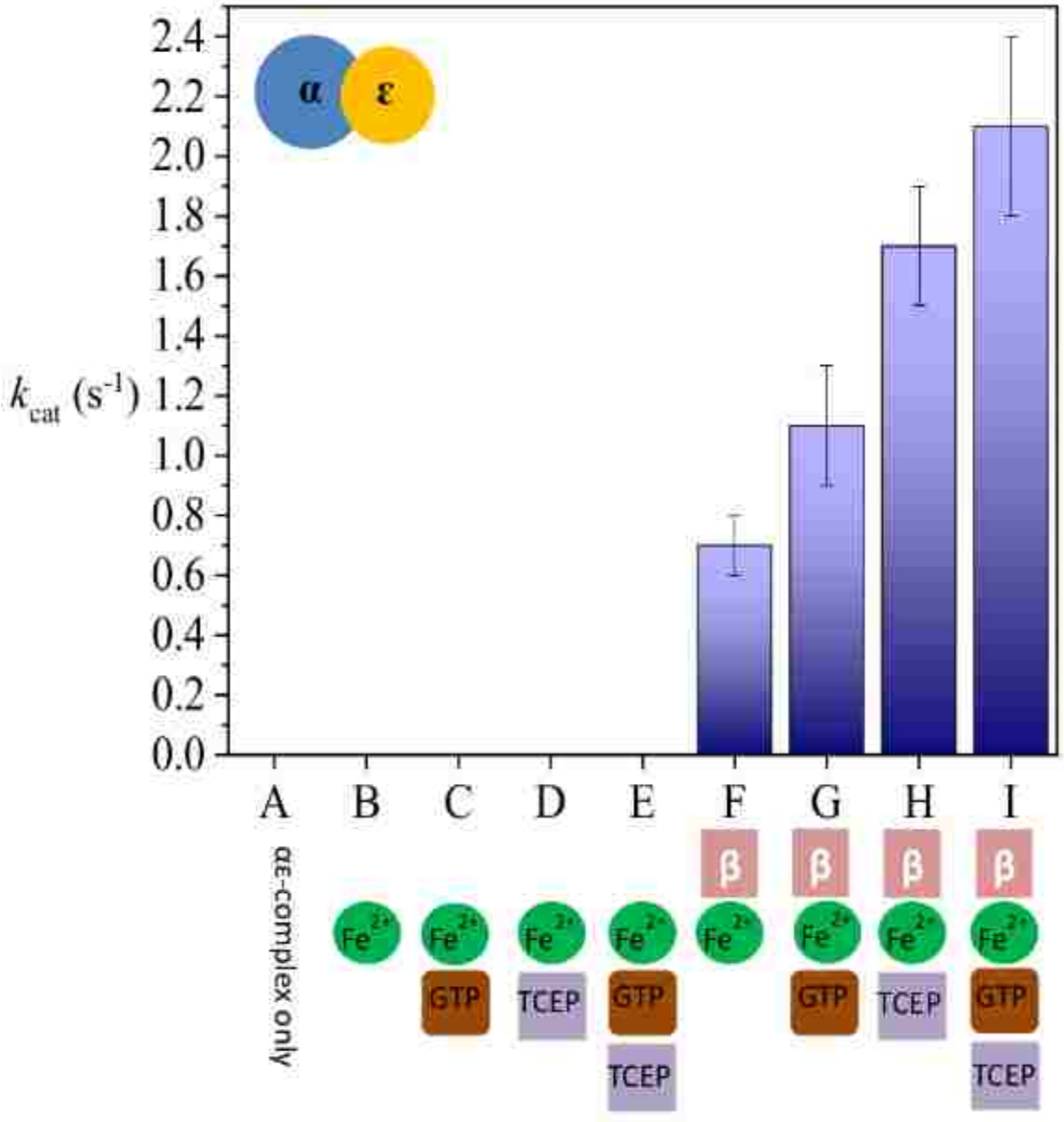

Figure 21. Observed k_{cat} (s^{-1}) values of the α(ε) complex combined with Fe(II), β-subunit, GTP, or TCEP in 50 mM HEPES, pH 7.5 at 25 ºC. All reactions were performed under nitrogen and incubated for 12 hours.

Having shown that an Fe-type NHase α(**ε**) complex can form and active NHase can be obtained by the addition of Fe(II) and β-subunit, under reducing conditions, the question of whether GTP hydrolysis is connected to iron insertion into the NHase α-subunit can be addressed. The addition of GTP to the as-purified α(**ε**) complex in 50 mM HEPES buffer at pH 7.5 and 25 ^{o}C using 80 mM acrylonitrile as the substrate, in the presence of Fe(II) and β-subunit followed by incubation under nitrogen for 12 hrs., resulted in active *Re*NHase enzyme with a k_{cat} value of 1.1 ± 0.2 s^{-1}. The addition of GTP enhances the observed activity by ~35% *vs.* the observed k_{cat} value for the same combination without GTP. As reducing conditions have been shown to enhance the resulting rate of acrylonitrile hydration, TCEP was added to this mixture, which indeed further enhances the observed NHase activity as a k_{cat} value of 2.1 ± 0.3 s^{-1} (Table 4; Figure 21) was observed. The addition of TCEP nearly doubles the observed k_{cat} value compared to the same combination of α(**ε**) complex, Fe(II), GTP, and β-subunit. These data indicate that while GTP enhances metal ion insertion and active site maturation in *Re*NHase, it is not essential.

Having established that the *Re*NHase α(**ε**) complex can be combined with Fe(II), GTP, and β-subunit under reducing conditions and provide active $\alpha_2\beta_2$ heterotetramer, the underlying question of can the α(**ε**) complex form in situ and provide observable NHase activity can be addressed. With the apo-forms of purified (**ε**), α- and β-subunit proteins in hand, these three components were mixed in a stepwise fashion with Fe(II), GTP, and TCEP. In the absence of TCEP, all combinations of (**ε**) protein in 50 mM HEPES buffer at pH 7.5 and 25 ^{o}C incubated with α- and β-subunits and Fe(II) and/or GTP under nitrogen for 12 hrs., resulted in no detectable activity (Table 5; Figure 22).

Table 5. Kinetic data for the α- and β-subunits in the absence and presence of TCEP at 25 °C.

Mixed components	k_{cat} **(s^{-1})**	k_{cat} **(s^{-1}) +TCEP**
α + β + ε + GTP	ND[a]	ND[a]
α + β + Fe^{2+}	ND[a]	0.7 ± 0.2
α + β + Fe^{2+} + ε	ND[a]	0.8 ± 0.2
α + β + Fe^{2+} + ε + GTP	ND[a]	1.0 ± 0.2

[a]None detected

The addition of TCEP to the α- and β-subunits plus Fe(II) provided a k_{cat} value of 0.7 ± 0.2 s^{-1}, a value identical to α(**ε**) complex combined with β-subunit and Fe(II). The addition of (**ε**) protein did not result in an increase in observed activity, however, the addition of both (**ε**) protein and GTP increased the observed rate of nitrile hydration by ~30%. These data further support the fact the GTP assists in metal ion insertion and NHase activation, but is not essential.

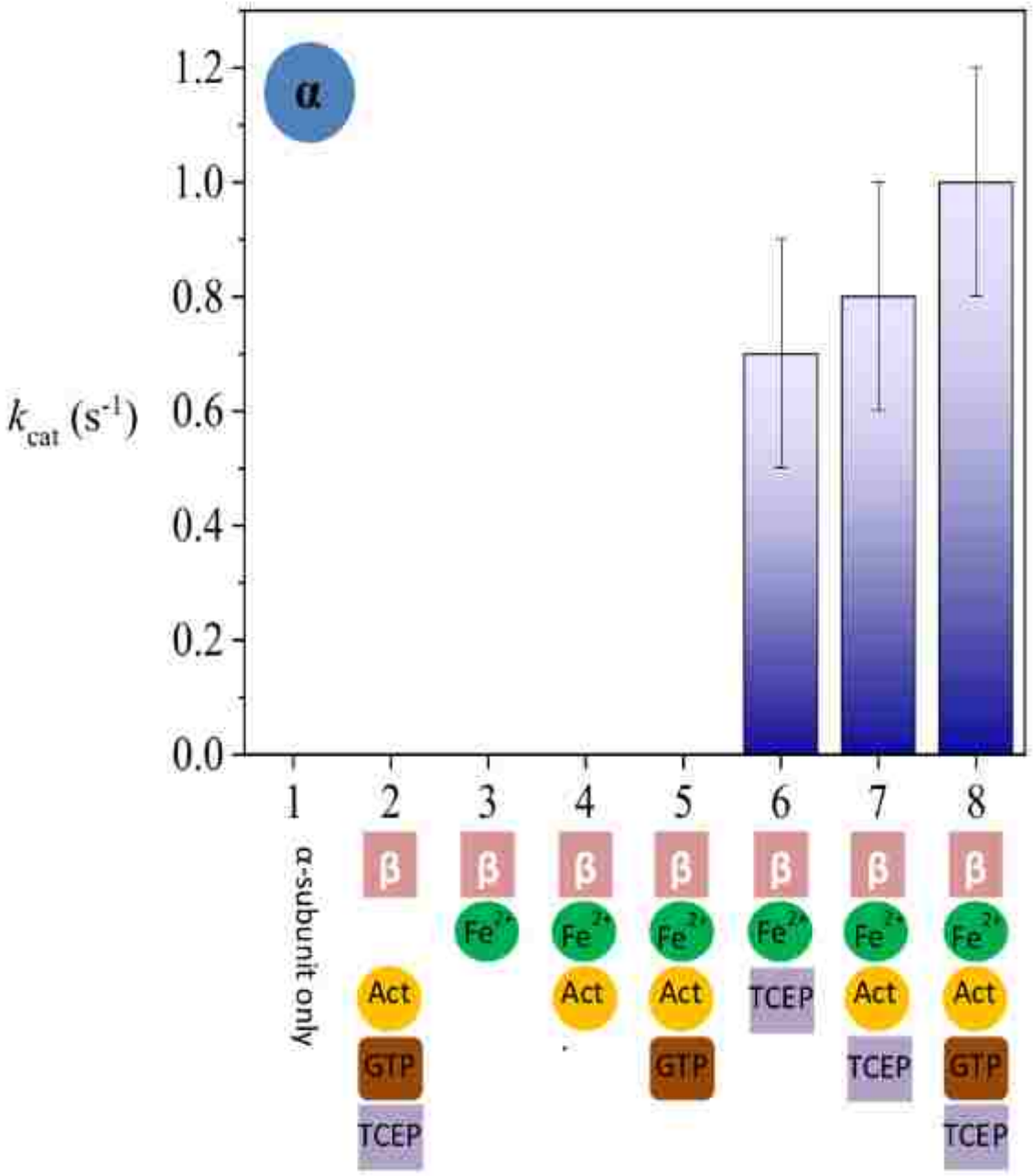

Figure 22. Observed k_{cat} (s^{-1}) values of the α-subunit combined with (**ε**) protein, Fe(II), β-subunit, GTP, or TCEP in 50 mM HEPES, pH 7.5 at 25 ºC. All reactions were performed under nitrogen and incubated for 12 hours.

2.4. Conclusion

In conclusion, the first known Fe-type α(**ε**) complex has been purified and shown to form a 1:1 mole ratio complex. This complex can be mixed *in vitro* with β-subunit and Fe(II), which results in NHase activity. The addition of GTP enhances the rate of acrylonitrile hydration indicating that GTP plays a role in Fe-type active site formation and activation but is not essential. The addition of TCEP markedly enhances the rate of nitrile hydration, likely due to the reduction of either a disulfide bond in the NHase active site and/or in the (**ε**) protein CXCC proposed metal binding site. The independent expression and purification of the *Re*NHase α- and β-subunits allowed purified α-subunit to be mixed with (**ε**) protein, in situ, to form the α(**ε**) complex, which could then be mixed with β-subunit, Fe(II), and/or GTP in the absence and presence of TCEP. These data also indicate that active *Re*NHase can be prepared under reducing conditions and that GTP assists in Fe-type active site formation and activation, but is not essential. Combination of these data along with those for Co-type NHase (**ε**) protein, which were suggested to insert Co(II) into apo-$\alpha_2\beta_2$ NHase *via* a "self-subunit swapping" mechanism [44], allows a similar mechanism to be proposed for Fe-type NHases (Figure 23). For Fe-type NHases, an α(**ε**) complex forms rather than an $\alpha(\boldsymbol{\varepsilon})_2$ complex for Co-type enzymes. This α(**ε**) complex is proposed to bind Fe(II) under reducing conditions and insert iron into the NHase active site in the α-subunit. This metal loaded α-subunit can "self-subunit swap" with apo α-subunit to form a metallated $\alpha_2\beta_2$ NHase enzyme.

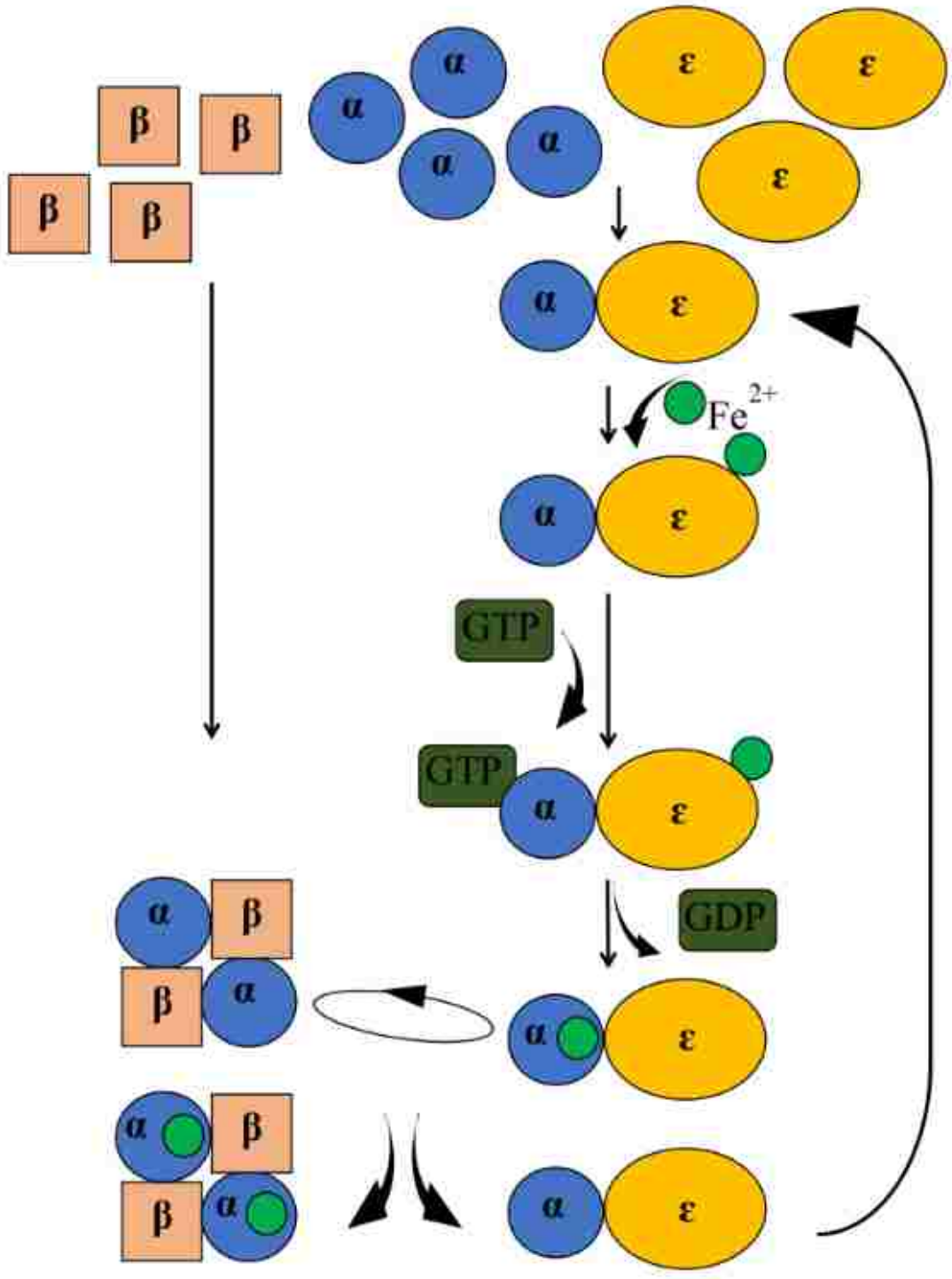

Figure 23. A proposed model iron incorporation into the Fe-type NHase α-subunit and activation to $\alpha_2\beta_2$ heterotetramer.

CHAPTER 3

CELLULAR MATURATION OF AN IRON-TYPE NITRILE HYDRATASE INTERROGATED USING EPR SPECTROSCOPY

3.1. Introduction

Nitrile hydratases (NHases, EC 4.2.1.84) are metalloenzymes capable of hydrating a wide range of synthetic nitriles, which has resulted in their intense biotechnological exploitation as biocatalysts in both preparative organic chemistry and several industrial applications, most notably the production of acrylamide and nicotinamide [4, 51, 66, 67]. A key advantage of NHases is their stereoselectivity, which is of particular importance in the pharmaceutical arena [68]. NHases have also proven useful in the bioremediation of chemical and wastewater runoff, specifically for the hydration of nitrile-based pesticides such as bromoxynil. NHases are thus becoming increasingly recognized as a new type of "green" catalyst [69] and an understanding of their reaction mechanism opens up the possibility for engineered analogs with tailored catalytic properties. However, despite the biological, industrial, and bioremediation importance of NHases, many details of their reaction mechanism and metallocenter assembly remain poorly defined.

NHases contain either a low-spin ($S = {}^1/_2$) Fe(III) (Fe-type) or a low-spin ($S = 0$) Co(III) (Co-type) ion in their active site [51]. X-ray crystallographic studies on NHases from prokaryotes indicate that they are $\alpha_2\beta_2$ heterotetramers with the active site metal ion coordinated by three cysteine residues, two amide nitrogens, and a water or hydroxy moiety [51, 52, 70]. Two of the active site cysteine residues are post-translationally modified to cysteine-sulfinic acid ($-SO_2H$) and cysteine-sulfenic acid (–SOH),

respectively, yielding a coordination geometry termed a “claw-setting”; oxidation of the equatorial Cys residues is essential for catalysis [47]. Structurally, Fe- and Co-type NHases are very similar, yet Fe-type NHases are specific for activation by Fe(III) while Co-type NHases are specific for Co(III) [51]. One of several open reading frames (ORFs) identified just downstream from the structural α- and β-subunit genes in NHases encodes a protein, termed the (ε) protein [54-56]. The prevailing dogma is that both Co- and Fe-type NHase enzymes require the co-expression of the (ε) protein to be fully metallated, post-translationally modified, and functional [54-56]. While Co- and Fe-type NHases have high α- and β-subunit sequence similarity, their respective (ε) proteins differ in size and share little to no sequence identity, suggesting that the mechanism of metallocenter assembly is different [42-44].

Recently, the myriad $S = {}^{1}/_{2}$ EPR signals arising from the active site Fe(III) ion in the Fe-type NHase from *Rhodococcus equi* TG328-2 (*Re*NHase-TG328-2) were deconvoluted by chemical and spectroscopic means and subsequently assigned to distinct chemical species with the aid of reference to X-ray crystallographic structures and with the assistance of DFT calculations [23]. The EPR signals constituting the spectra of as-prepared enzyme were assigned to: (i) active enzyme; (ii) enzyme complexes with inhibitory carboxylic acids (butyric acid is used during purification to prevent active site oxidation); (iii) inactive oxidized forms of (i) and (ii); and (iv) pH-dependent forms of these signals [23, 71]. An outstanding question is whether these multiple species arise as a consequence of how the enzyme is isolated or whether they are formed in intact cells during NHase expression and prior to enzyme isolation. The answer to this question has important consequences, (i) for the preparation of NHase samples for mechanistic

studies, particularly by advanced EPR methods that generally require non-overlapping EPR absorption envelopes (i.e. χ'' vs. B_0) in the region of the single-crystal-like orientations (g_1 and g_3 for rhombic EPR spectra), and (ii) for the design and management of protocols for the use of sustainable bacterial cultures that express NHase for reclamation and green chemistry applications. We have, therefore, utilized EPR spectroscopy to examine whole cells expressing *Re*NHase-TG328-2 to identify active site-species and their catalytic competencies both *in vitro* and *in vivo* [72]. In addition, we compared the spectroscopic properties of *Re*NHase-TG328-2 purified under anaerobic and aerobic conditions, and with different exposures to the inhibitory anti-oxidation prophylactic butyric acid.

Abbreviations. BuBA: butane boronic acid; ELNMR: electron-electron double resonance-detected nuclear magnetic resonance; ENDOR: electron-nuclear double resonance; EPR: electron paramagnetic resonance; NHase: nitrile hydratase; $NHase^{Aq}$: active nitrile hydratase and its EPR signal; $NHase^{BA}$: butyrate (carboxylate) complex of active nitrile hydratase and its EPR signal; $NHase^{Im}$: imidazole complex of active nitrile hydratase and its EPR signal; $NHase^{ACN}$: intermediate complex of active nitrile hydratase formed upon addition of acetonitrile, and its EPR signal; $NHase^{Acryl}$: intermediate complex of active nitrile hydratase formed upon addition of acrylonitrile, and its EPR signal; $NHase^{BuBA}$: butane boronic acid complex of active nitrile hydratase and its EPR signal; NHaseOx: inactive nitrile hydratase in which the cysteine sulfenic acid has been oxidized to sulfinic acid, and its EPR signal; $NHaseOx^{BA}$: butyrate (carboxylate) complex of inactive nitrile hydratase in which the cysteine sulfenic acid has been oxidized to sulfinic acid, and its EPR signal.

3.2. Materials and methods

3.2.1. Materials

Chemicals and reagents were obtained from ThermoFisher Scientific and were purchased at the highest quality available. NERL^{TM} 18 MΩ cm^{-1} high purity water (9805, ThermoFisher) was used throughout.

3.2.2. Expression of *Re*NHase-TG328-2 in *E. coli*

The α- and β-subunits of *Re*NHase-TG328-2 were expressed in *E. coli* BL21 DE3 cells co-transformed with a pET28a vector carrying an activator (ε) protein [72]. Cells were agitated at 300 r.p.m., at 37 °C, in 2 L baffled flasks that contained 1 L of LB Miller broth supplemented with 100 μg mL^{-1} of disodium ampicillin and 50 μg mL^{-1} kanamycin sulfate. Once the optical density at 600 nm (OD_{600}) reached 0.5 cm^{-1}, the temperature was lowered to 15 °C. After ~30 min (OD_{600} ≈ 0.8 to 1.0), 300 μM isopropyl β-D-1-thiogalactopyranoside (IPTG) was added and the cells were incubated for an additional 21 hours. Cells were collected by centrifugation for ~30 min at 2,000 × *g* and re-suspended in 50 mL of Buffer A (50 mM HEPES; 500 mM NaCl; 40 mM C_3H_7COONa; pH 7.5).

3.2.3. Aerobic isolation of *Re*NHase-TG328-2

Cells were lysed by sonication (Misonix 3000) for 10 minutes (10 s pulses of 21 W with 20 s intervals), with the temperature maintained at ≤ 5 °C by rotating the beaker continuously on ice. Insoluble cell debris was removed by centrifugation (13,000 × *g*, 40 min), and *Re*NHase-TG328-2 was subsequently isolated from the soluble fraction.

Buffer B (50 mM HEPES; 500 mM NaCl; 40 mM C_3H_7COONa; 500 mM imidazole; pH 7.5) was added to the cleared lysate to a final concentration of 30 mM imidazole. The solution was loaded at 1 mL min^{-1} onto a metal ion affinity chromatography column (5 mL HisTrap, GE Healthcare) that was pre-equilibrated with Buffer C (50 mM HEPES; 500 mM NaCl; 40 mM C_3H_7COONa; 30 mM imidazole; pH 7.5) and washed with 50 mL Buffer C. A 50 mL linear gradient of Buffer C to Buffer B was applied and 5 mL fractions were collected. Subsamples were collected for SDS-PAGE, kinetic analyses, and EPR spectroscopic studies. The remaining enzyme was diluted ten-fold with Buffer D (50 mM HEPES; 40 mM C_3H_7COONa; pH 7.5) loaded (5 mL min^{-1}) onto a pre-equilibrated (Buffer D) anion exchange column (5mL HiTrap Q HP, GE Healthcare), washed with 100 mL of Buffer D, and eluted with a 100 mL linear gradient of Buffer D to Buffer A.

3.2.4. Anaerobic isolation of *Re*NHase-TG328-2

Cleared lysate, from cells harvested and resuspended in Buffer D after sonication, was transferred to an anaerobic chamber maintained at 20 °C (Coy Laboratories) and applied to a 50 mL anion exchange column (Q-Sepharose Fast Flow, GE Healthcare), washed with 300 mL of Buffer D, and eluted with Buffer E (50 mM HEPES; 40 mM C_3H_7COONa; 400 mM NaCl; pH 7.5). NHase-containing fractions, that exhibited a blue-green color, were applied to a 5 mL HisTrap affinity column pre-equilibrated with Buffer F (50 mM HEPES; 40 mM C_3H_7COONa; 40 mM imidazole; pH 7.5). The column was washed with 50 mL of Buffer F and eluted with Buffer G (50 mM HEPES; 40 mM C_3H_7COONa; 300 mM imidazole; pH 7.5). The eluate was diluted ten-fold with Buffer H (50 mM HEPES; pH 7.5), applied to a 10 mL Q-Sepharose Fast Flow column and

washed with 100 mL of Buffer I (50 mM HEPES; 100 mM NaCl; pH 7.5). *Re*NHase-TG328-2 was eluted with Buffer J (50 mM HEPES; 400 mM NaCl; pH 7.5).

3.2.5. Kinetic analyses

The aerobic activity of *Re*NHase-TG328-2 enzymes was determined by following the hydration of acrylonitrile spectrophotometrically at 225 nm ($\Delta\varepsilon_{225}$ = 2.9 mM^{-1} cm^{-1}) in Buffer I at 25 °C, using a Shimadzu UV-2450 PC spectrophotometer in a 1 mL quartz cuvette and various substrate concentrations. The anaerobic hydration of acrylonitrile by *Re*NHase-TG328-2 in Buffer I at 25 °C, was determined spectrophotometrically at 231 nm ($\Delta\varepsilon_{231}$ = 1.57 mM^{-1} cm^{-1}) using an Ocean Optics Flame-S-UV-VIS spectrophotometer. The kinetic constants V_{max} and K_m were calculated by fitting the data to the Michaelis-Menten equation using OriginPro 9.0 (OriginLab, Northampton, MA).

3.2.6. Whole cell samples for EPR

Aliquots (20 mL) of *E. coli* expressing *Re*NHase-TG328-2 were pelleted by centrifugation for 30 min at 2,000 × *g* and re-suspended in either Buffer D (i.e. with butyric acid) or in deoxygenated Buffer J (i.e. without butyric acid) under anaerobic conditions. Aliquots were placed in EPR tubes under nitrogen and frozen in liquid nitrogen.

3.2.7. EPR spectra

EPR spectra were obtained at either 77 K, 5 mW microwave power or 50 K, 2 mW microwave power (non-saturating), and 5 G field modulation at 100 kHz, on an updated Bruker EMX-AA-TDU/L spectrometer equipped with an ER4112-SHQ

resonator (~ 9.45 GHz) and an HP 5350B microwave counter for precise frequency measurement. 77 K was maintained with liquid nitrogen, and 50 K was maintained with a ColdEdge/Bruker Stinger S5-L recirculating helium refrigerator, and an Oxford ESR900 cryostat and MercuryITC temperature controller. EPR simulations were carried out using EasySpin [73]. An integration standard of 1.7 mM Cu(II) in 50 mM HEPES buffer containing 15 % $^{v}/_{v}$ glycerol and 10 mM imidazole at pH 7.5 was prepared and EPR spectra were recorded at 77 K, 0.5 mW. These data were used to calibrate spin densities from *Re*NHase-TG328-2 EPR spectra with standard corrections for differences in $1/T$, $\sqrt{(\text{microwave power})}$, and $(\text{field range})^2$.

3.3. Results and discussion

Aerobically isolated ReNHase-TG328-2. *Re*NHase-TG328-2 was eluted from a HisTrap column with an approximate gaussian activity profile that correlated with the intensity of the SDS-PAGE bands at ~25 kDa (Figure 24). These bands correspond to the α-subunit (23.9 kDa) and the β-subunit (25.1 kDa) of *Re*NHase-TG328-2 (Figure 24A). Fractions containing *Re*NHase-TG328-2 activity were found to exhibit a blue-green color (Figure 24B), consistent with the broad electronic absorption band centered around 700 nm for *Re*NHase-TG328-2 [74], making localization of NHase activity straightforward. An additional band at ~47 kDa was observed on the SDS-PAGE gel that co-eluted with the *Re*NHase-TG328-2 α- and β-subunits, and has previously been assigned to the activator (ε) protein [47]. Kinetic analysis indicated a k_{cat} of 518 ± 8 s^{-1} for *Re*NHase-TG328-2 using acrylonitrile as the substrate, which is similar to previously reported values [72]. Further purification of *Re*NHase-TG328-2 using a HiTrap Q column resulted in a similar SDS-PAGE profile and k_{cat} values albeit with a somewhat less prominent band at ~47 kDa.

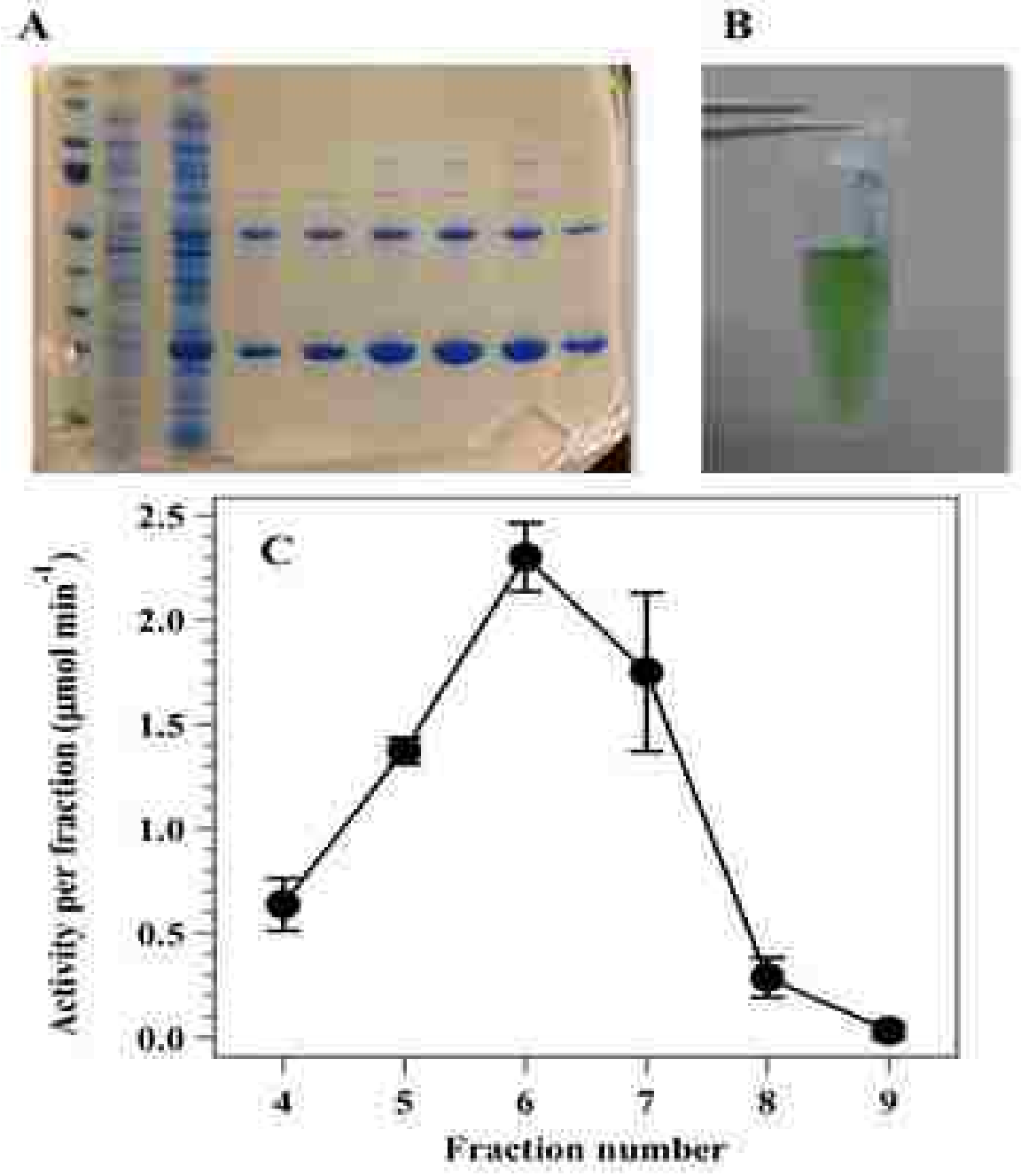

Figure 24. Expression and aerobic isolation of *Re*NHase. A) SDS-PAGE: Lane 1, markers; Lane 2, flow-through from the His-Trap column; Lane 3, cleared lysate prior to column loading; Lane 4 – 9, fractions 4 – 9 eluted from the His-Trap column. B) Vial of as-isolated *Re*NHase. C) Activities contained in fraction 4-9 (acrylonitrile).

EPR spectra of a 250 µM sample *Re*NHase-TG328-2 purified aerobically, were recorded before and after removal of the imidazole eluent used in metal affinity chromatography (Figure 25). Prior to imidazole removal, a complex signal (Figure 25A) was observed that could be reasonably simulated with three distinct species, all arising from low-spin Fe(III) ions. The observed *g*-values are indicative of: (i) active reversibly inhibited *Re*NHase-TG328-2 with butyric acid bound ($NHase^{BA}$: g = 2.28, 2.14, 1.97, labeled **a** in Figure 25), (ii) active *Re*NHase-TG328-2 with imidazole reversibly bound ($NHase^{Im}$: g = 2.21, 2.14, 1.98, labeled **i** in Figure 25), and (iii) active *Re*NHase-TG328-2 with a water molecule bound ($NHase^{Aq}$: g = 2.20 2.13 1.99, labeled **b** in Figure 25). The **g**-tensor for $NHase^{Aq}$ is essentially indistinguishable from that of the irreversibly inactivated oxidized (bis-sulfinated) butyric acid complex of *Re*NHase-TG328-2 ($NHaseOx^{BA}$) but the latter exhibits a well-resolved ^{1}H superhyprfine splitting on the g = 1.99 feature at 3440 G [23] that was not observed in the experimental spectra in Figure 25. The catalytic activity, however, was only around 75 % of that of the anaerobically-isolated enzyme (*vide infra*), suggesting an unresolved but nevertheless present 25 % contribution to the EPR spectrum from $NHaseOx^{BA}$ and NHaseOx. Upon removal of imidazole, via ion-exchange chromatography, the observed *Re*NHase-TG328-2 EPR signal was simplified with the loss of the $NHase^{Im}$ EPR signature, **i**, consistent with the replacement of bound imidazole with a water molecule (Figure 25B). The EPR spectrum was simulated as an equimolar mixture of $NHase^{BA}$ (**a**) and $NHase^{Aq}$ (**b**) (Figure 25B) but a small bump at 3300 G did betray the presence of trace amounts of NHaseOx.

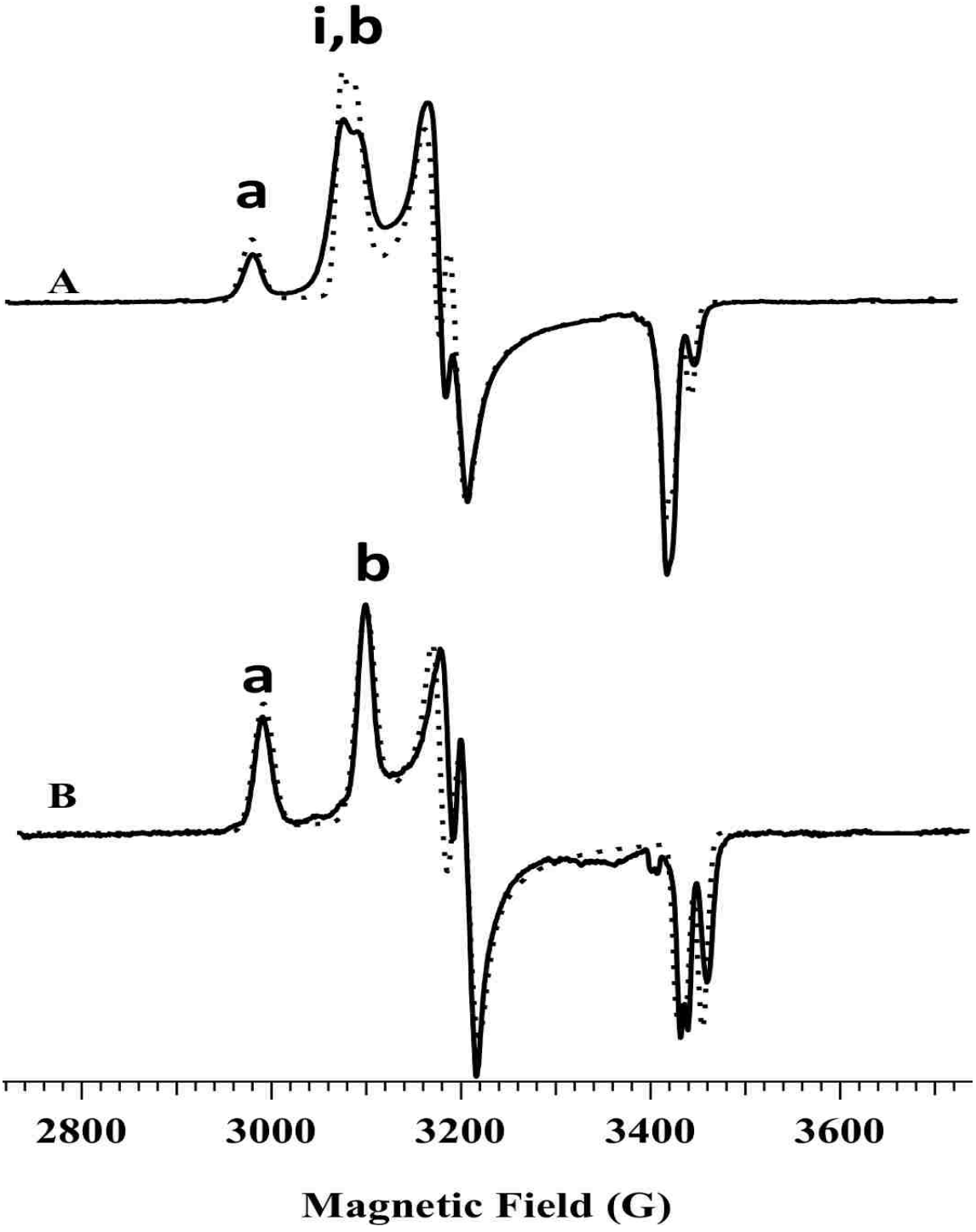

Figure 25. EPR spectra of aerobically prepared *Re*NHase after elution from the His-Trap column; A) prior to removal of imidazole; B) after removal of imidazole. The dashed lines are simulations assuming; A) 30 % $NHase^{BA}$ (a), 35 % $NHase^{Aq}$ (b), and 35 % $NHase^{im}$ (i); B, 50 % $NHase^{BA}$ (a), and 50% $NHase^{Aq}$ (b).

Anaerobically isolated ReNHase-TG328-2. Anaerobically-isolated *Re*NHase-TG328-2 (Figure 26) exhibited high purity by SDS-PAGE, a characteristic green color, and a k_{cat} value of 701 ± 11 s^{-1} with acrylonitrile as the substrate, i.e. 35 % higher than the corresponding aerobic preparation described herein and 25 % higher than the highest reported literature value [72]. The elevated k_{cat} suggested an enzyme sample containing little oxidized enzyme (*i.e.* the bis-sulfinic acid form), which would be expected from Fe-type NHase enzymes handled under anerobic conditions. The EPR signal from anaerobically-isolated NHase, during which butyric acid is eliminated from the sample, indicated 90 % $NHase^{Aq}$ (**b**) with < 10% of NHaseOx (**c**; g = 2.18, 2.11, 1.99).

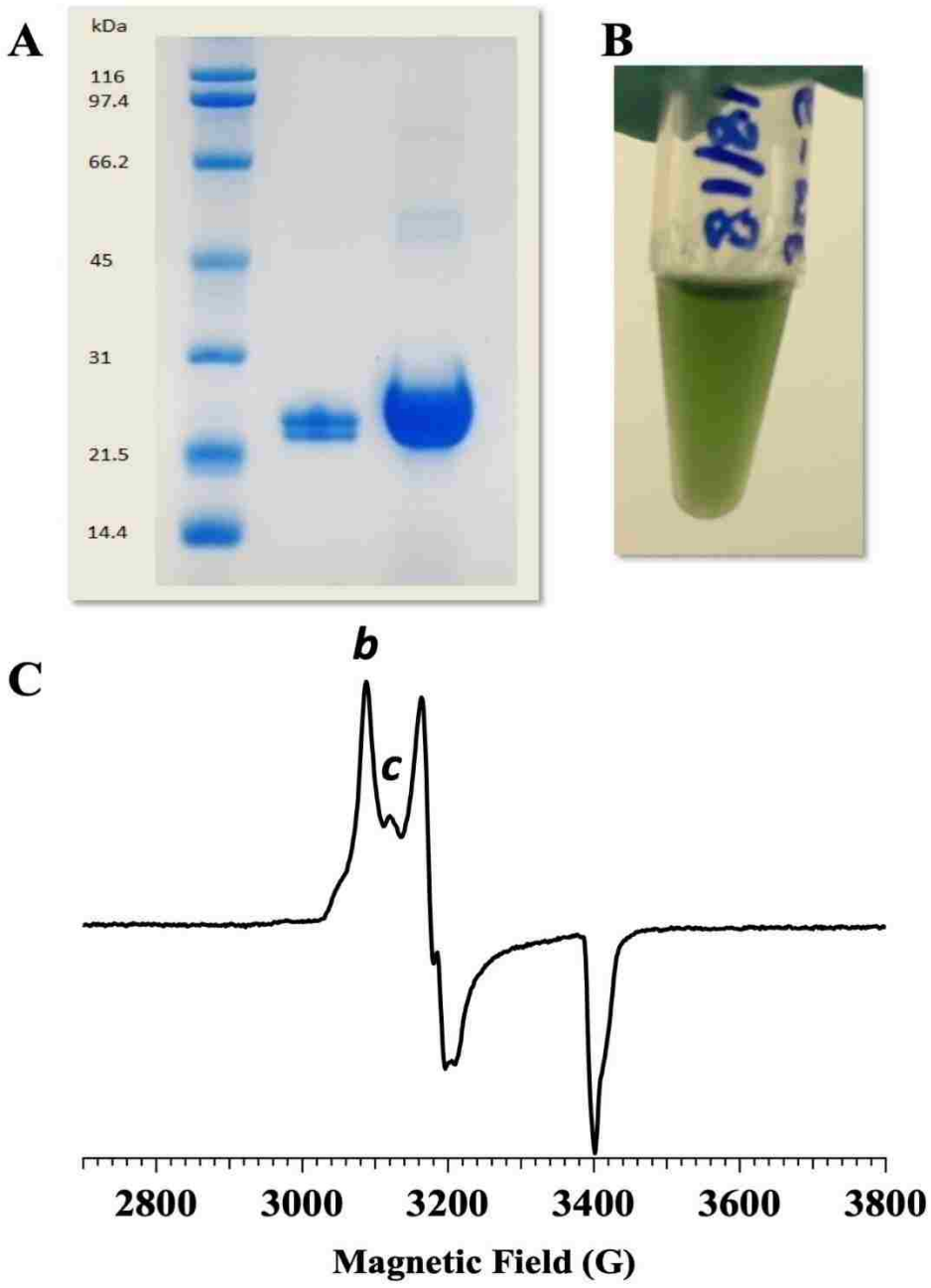

Figure 26. Anaerobic isolation of NHase. **A**. SDS-PAGE: Lane 1, markers; Lane 2, following HisTrap affinity chromatography; Lane 3, following Q-sepharose ion exchange chromatography. **B**. A vial of anaerobically-isolate NHase. **C**. EPR spectrum of NHase; ***b*** corresponds to g_1 of $NHase^{Aq}$, and ***c*** to g_1 of NHaseOx.

EPR Studies of ReNHase-TG328-2 in vivo. A goal of this study is to determine which species of *Re*NHase-TG328-2 are present within whole cells and to determine whether the oxidized species of *Re*NHase-TG328-2 originate solely during *ex vivo* handling, and may therefore be completely preventable in principle, or else arise post-expression *in vivo*. Aliquots of *E. coli* cells expressing *Re*NHase-TG328-2 were collected at the time of induction and periodically thereafter for 22 h. Each whole cell sample was pelleted, resuspended and equilibrated anaerobically in Buffer J (i.e. without butyric acid) and frozen in an EPR tube by immersion in liquid nitrogen. EPR spectra were recorded revealing several distinct species, with select resonances labeled **a** – **d** and **e** in Figure 27, corresponding to $NHase^{BA}$ (**a**), $NHase^{Aq}$ (**b**), NHaseOx (**c**), and $NHaseOx^{BA}$ (**d**), respectively. Not surprisingly, signals due to Mn(II) were observed (the labels **z** indicate the $M_I = |+^5/_2\rangle$ and $|-^5/_2\rangle$ resonances of the $M_S = |\pm^1/_2\rangle$ doublet of the Mn(II) $S = |^5/_2\rangle$ spin system), which is common for EPR spectra of bacterial and cultured mammalian cells, including *E. coli* [75]. Signals denoted **y** exhibited resonant fields indicative of $[3Fe4S]^+$ (3360 G; $g \sim 2.01$) and $[2Fe2S]^+/[4Fe4S]^+$ (3500 G; $g \sim 1.92$) clusters. These latter signals are likely due to *E. coli* bacterial aconitase [76] and respiratory chain components [77], respectively.

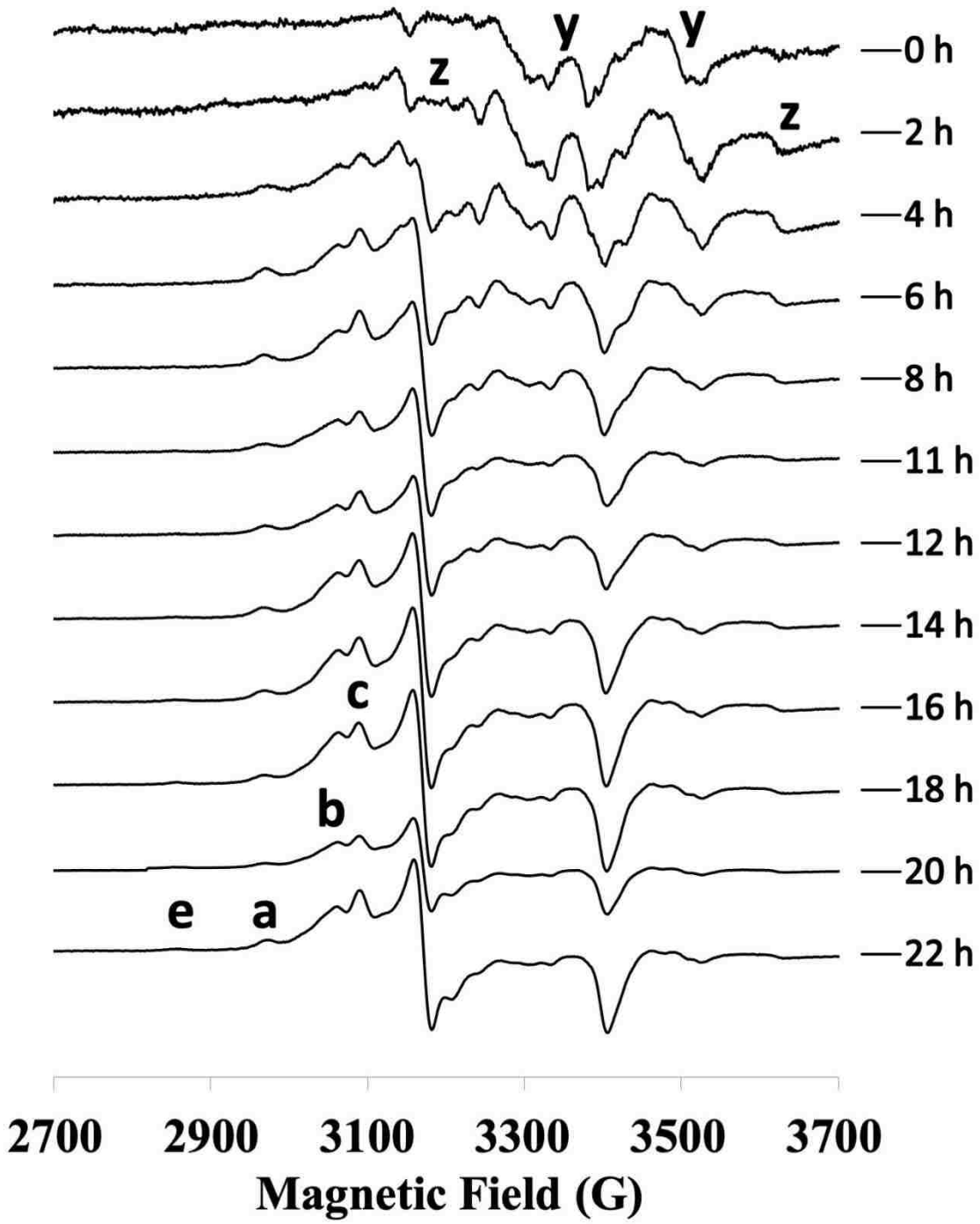

Figure 27. EPR spectra from anaerobically-prepared samples of whole cells expressing NHase in the absence of exogenous butyric acid as a function of time after induction. Labeled features correspond to $NHase^{BA}$ (**a**), $NHase^{Aq}$ (**b**), NHaseOx (**c**), native *E. coli* reduced $[2Fe2S]^{+}$ and/or $[4Fe4S]^{+}$ clusters and oxidized $[3Fe4S]^{+}$ clusters (**y**), and Mn(II) (**z**). The resonance (**e**) is unassigned.

EPR signals arising from NHase^{Aq} (**b**) were observed at 4 h post-induction and increased in relative intensity throughout the 22-hour induction period. Unexpectedly, however, additional signals due to NHase^{BA} (**a**) and NHaseOx (**c**) were also observed in cell samples 4 h post-induction and remained present for the entire experimental time frame of 22 h (signals from NHaseOx^{BA} may also be present but would not be distinguishable from NHase^{Aq}). As no butyric acid was added to either the bacterial media or the EPR samples themselves, an endogenous carboxylic acid must be responsible for the appearance of the NHase^{BA} signal. The origin of an additional low-amplitude resonance, **e**, whose intensity appears to correlate with other NHase signals, is unknown; DFT calculations have been unable to replicate features at such low fields using a variety of models for NHase active site species, and signal **e** remains unassigned. That NHaseOx (**c**) is present in *vivo,* and increases in intensity over the course of the entire induction period, establishes for the first time that the NHase active site is oxidized to the bis-sulfinic acid form *in vivo*. Importantly, by 22 h post-induction NHase^{Aq} (**b**) accounts for only ~30% of the total spins due to the low-spin Fe(III) ion in the *Re*NHase-TG328-2 active site.

To ascertain the effects of exogenous carboxylic acids on the species of NHase within intact cells, aliquots of *E. coli* cells expressing *Re*NHase-TG328-2 were collected at the time of induction and periodically for 22 h and equilibrated with Buffer E, which contained butyric acid, prior to EPR investigation. The equilibration was carried out in a sealed 15 mL vial without anaerobic precautions but without agitation. The observable EPR signals at the time of induction were primarily due to iron-sulfur cluster proteins (**y**; Figure 28), followed soon afterward by Mn(II) signals (**z**; the $M_I = |+^5/_2\rangle$, $|+^3/_2\rangle$, $|-^1/_2\rangle$, and

$|-^5/_2\rangle$ lines of $M_S = |\pm^1/_2\rangle$ are labeled; $M_I = |+^1/_2\rangle$ and $|-^3/_2\rangle$ are obscured by the iron-sulfur signals). EPR spectra recorded by 2 h post-induction revealed signals due to $NHase^{BA}$ (**a**) indicating that the exogenous butyric acid was taken up by *E. coli* and completely converted $NHase^{Aq}$ to $NHase^{BA}$. From 4 h post-induction, signals arising from NHaseOx (**c**) were evident and increased steadily in relative intensity from 2 % to 10 % of NHase spin density between 4 and 22 h post-induction.

From 16 h onwards, signals due to $NHaseOx^{BA}$ (**d**) were observed. The late onset of the appearance of the $NHaseOx^{BA}$ signal clearly indicates that the oxidation of $NHase^{BA}$, which is the mechanism of generation of $NHaseOx^{BA}$ [16], is not a consequence of the aerobic equilibration of cells with exogenous butyric acid but, rather, must be occurring within the cell and is therefore due to oxidation of a complex of NHase with endogenous carboxylate. The catalytic activities of the aliquots, measured after sonication, corresponded well with the $NHase^{BA}$ EPR signal intensities as a function of time post-induction (Figure 29). It is noteworthy that, at the very low concentrations used in the *in vitro* assay, the equilibrium constant for $NHase^{Aq} \leftrightarrow NHase^{BA}$ is firmly in favor of $NHase^{Aq}$ and that, therefore, the intensity of the $NHase^{BA}$ EPR signal effectively measures the amount of recoverable active $NHase^{Aq}$; in contrast, NHaseOx and $NHaseOx^{BA}$ are irreversibly inactivated via oxidation of the catalytically-necessary cysteine-sulfenic acid to sulfenic [16,25]. The rapid and total conversion of intracellular $NHase^{Aq}$ to $NHase^{BA}$ upon butyric acid exposure suggests that microbial nitrile-hydrating activity, in catalytic or remediation applications, would be severely compromised in an environment containing carboxylic acids.

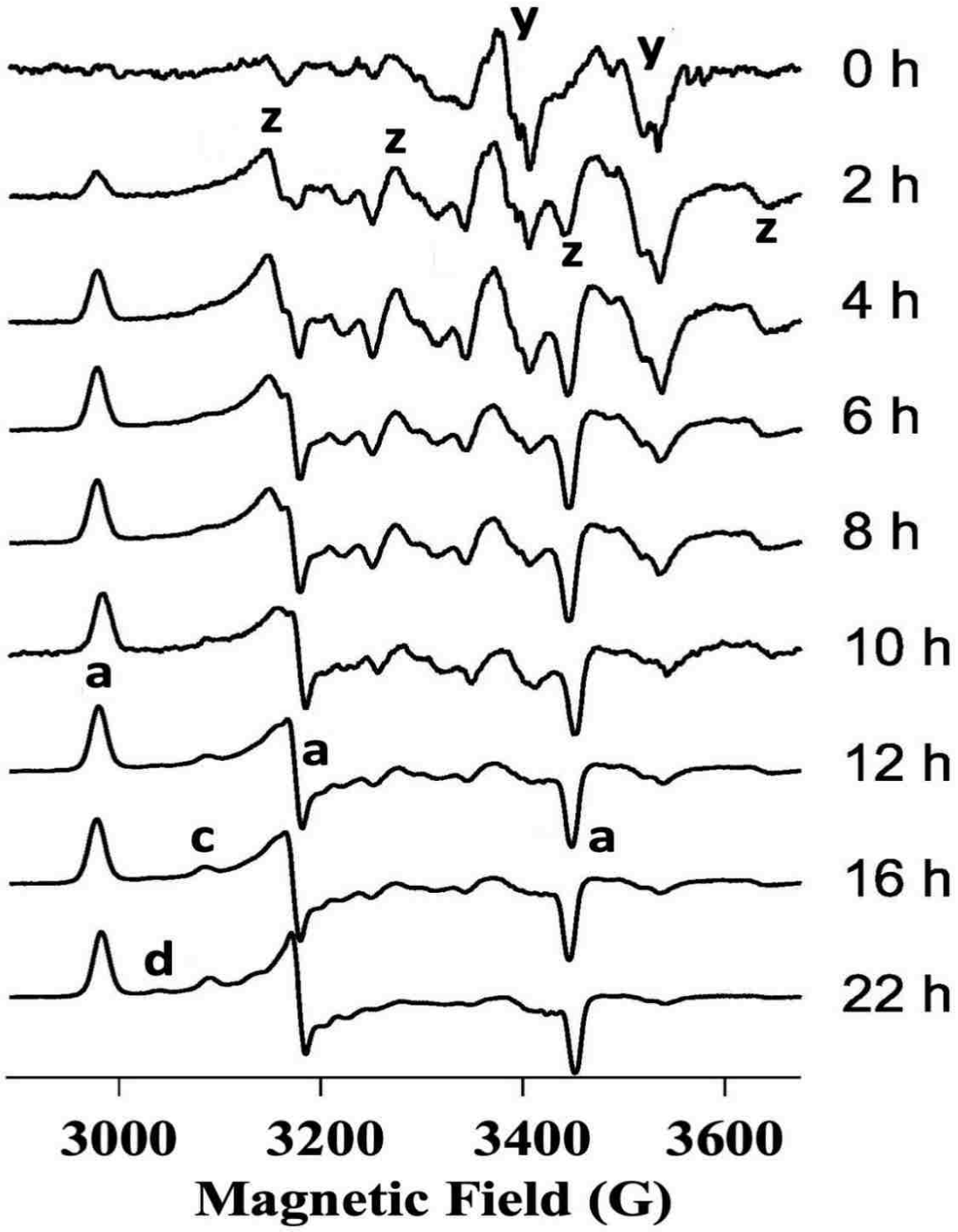

Figure 28. EPR spectra from aerobically-prepared samples of whole cells expressing NHase equilibrated with butyric acid as a function of time after induction. Labeled features correspond to $NHase^{BA}$ (**a**), NHaseOx (**c**), $NHaseOx^{BA}$ (**d**) native *E. coli* reduced $[2Fe2S]^{+}$ and/or $[4Fe4S]^{+}$ clusters and oxidized $[3Fe4S]^{+}$ clusters (**y**), and Mn(II) (**z**).

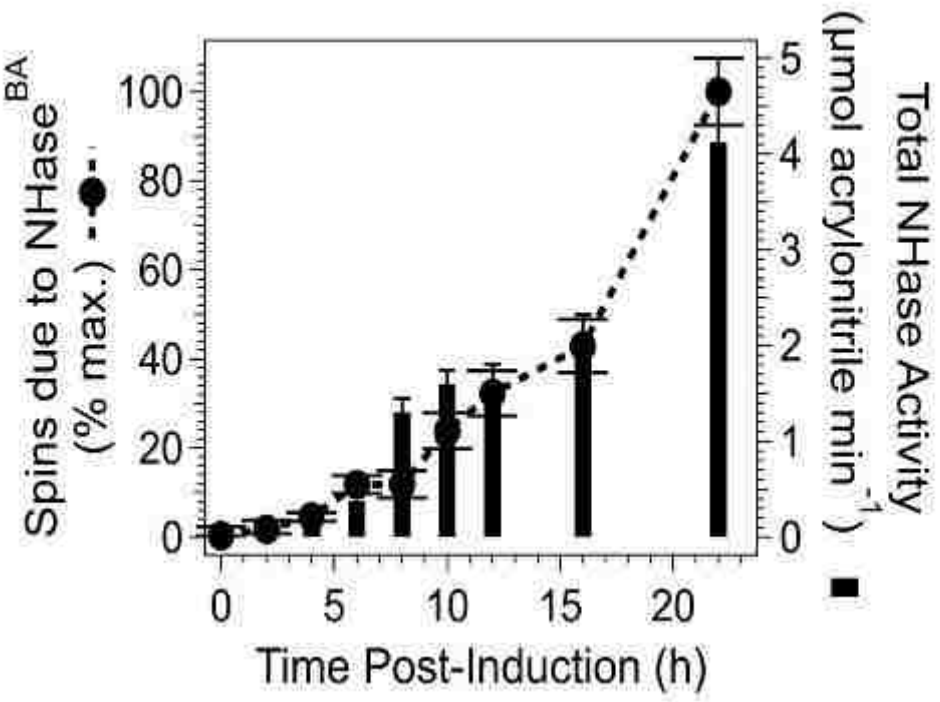

Figure 29. Correlation of catalytic activity of NHase with the intensity of the NHase^{BA} signal observed after equilibration of *E. coli* with butyric acid buffer.

The observation that butyric acid can rapidly and completely, if reversibly, negate NHase activity in cell cultures, such as are used in acrylamide production and remediation of contaminated land, suggested further investigations into the effects of NHase substrates and inhibitors on viable cells expressing the enzyme. The addition of the inhibitor butaneboronic acid (BuBA) to *E.coli* 22 h post-induction of *Re*NHase-TG328-2 elicited an EPR signal (NHase^{BuBA}; Figure 30) that was previously observed upon addition of BuBA to the pure enzyme, and whose **g** tensor (g = 2.20, 2.10, 1.98) was returned from Taylor/DFT calculations of a structural model for the BuBA-bound complex based on the crystal structure of the BuBA complex with Co-Type *Pt*NHase [23]. The crystal structure revealed that BuBA was not only bound to the metal ion, but

was additionally bound by the sulfenic acid ligand following nucleophilic attack, forming a five-membered cyclic intermediate [16].

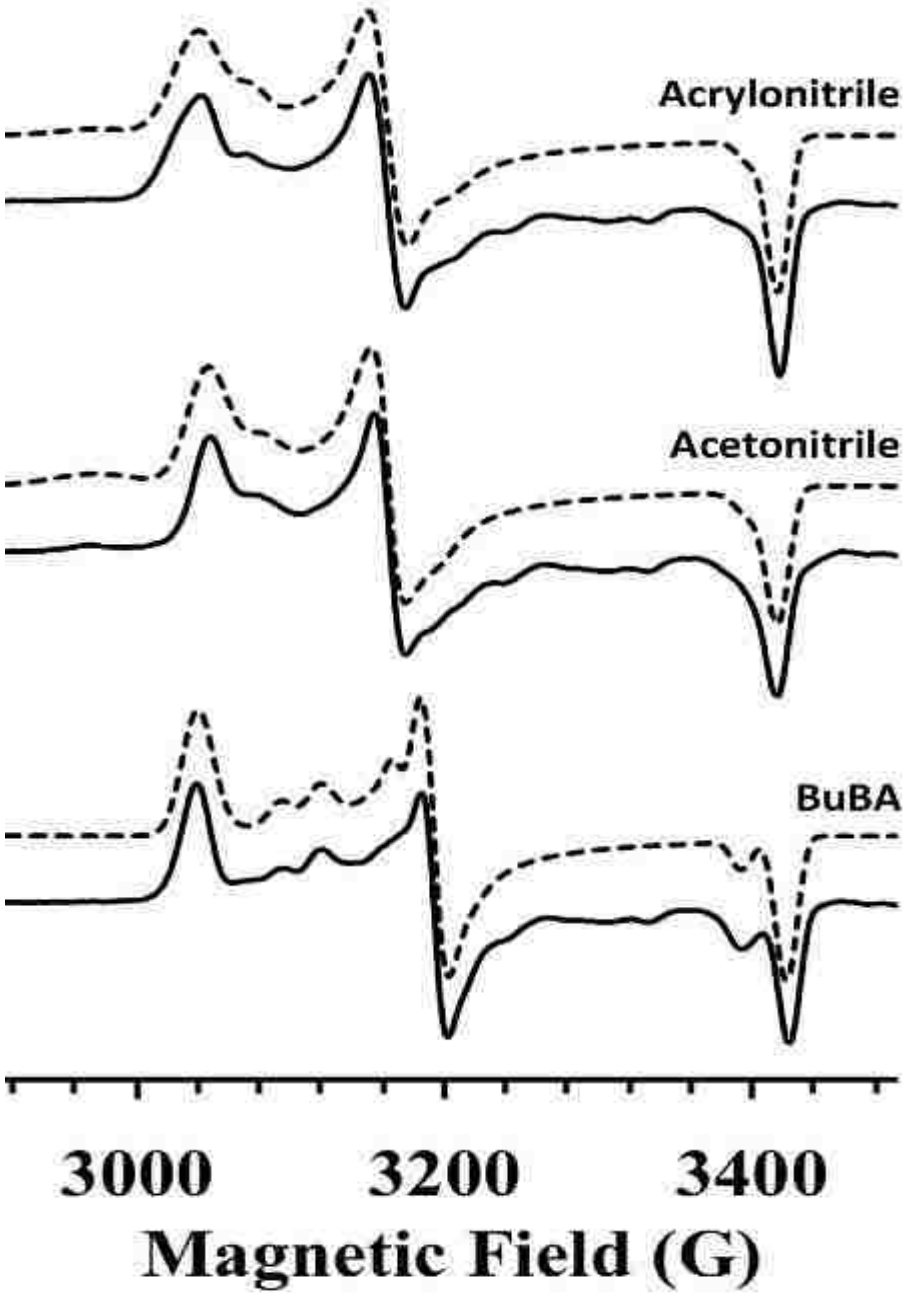

Figure 30. EPR signals from *E. coli* incubated with acrylonitrile, acetonitrile, and BuBA, 22 h following induction of NHase. The dashed lines are computer simulations that include minor species.

E. coli cells were also incubated with the substrates acetonitrile and acrylonitrile and, again, novel EPR signals were observed, NHase^{ACN} and NHase^{Acryl}, respectively. Simulations of the EPR signals returned g = 2.22, 2.14, 1.98 for NHase^{ACN} and g = 2.23, 2.14, 1.98 for NHase^{Acryl}, identifying them as the same signals obtained upon incubation of the isolated enzyme with these substrates [16]. The signals are very similar to those from the crystallographically-characterized NHase^{BuBA} species and suggest, therefore, that a five-membered cyclic intermediate complex forms *in vivo* due to the nucleophilic attack by the active site sulfenic acid ligand on an Fe(III)-bound nitrile substrate. These data, showing uptake of substrates and *in vivo* catalysis, provide the first insight into the mechanism of nitrile hydration by intact cells that express NHase.

3.4. Conclusion

*Re*NHase-TG328-2 is available in high yield and with high activity from an *E.coli* expression system in which recombinant variants can be readily generated. However, mechanistic study of *Re*NHase-TG328-2 has been hampered because of the presence of multiple overlapping EPR signals that are exhibited in proportions that vary from preparation to preparation. This has hindered investigation of proton trafficking during the reaction and investigation of substrate orientation by ^{1}H, ^{13}C, and ^{15}N ENDOR and ELDOR-NMR, for example, which require uncontaminated EPR absorption at the extrema of the absorption envelope. Some of these complicating signals are, despite precautions against oxidation during preparation, due to irreversibly oxidized species and, therefore, 100 % functional enzyme can never be recovered. Recently, the individual EPR signals were assigned to species that were additionally characterized by DFT calculations [16,17]. In the present study, we have characterized the origins of the various species with a view to obtaining less heterogeneous samples for study, and to explore whether environmental conditions may act to compromise the nitrile hydrating potential of bacteria in applications such as microbial reclamation of bromoxynil-contaminated land and production of important chemicals such as nicotinamide and acrylamide. For this purpose, the presence of the multiple EPR-detectable species, now assigned to chemical species, was essential. EPR spectroscopy of whole cells as a function of post-induction time, and of *Re*NHase-TG328-2 subsequently prepared either aerobically or anaerobically provided some striking findings.

First, EPR revealed that inactive forms of the enzyme were generated *in vivo*. Perhaps the less surprising of two distinct findings was that the enzyme formed a stable

complex with intracellular carboxylic acids in the absence of any added exogenous carboxylates. The indistinguishability of the signal **a** exhibited by NHase-expressing *E. coli* cells from the signal of purified NHase incubated with butyric acid indicates that the complex formed in cells is entirely analogous to the reversibly inhibited $NHase^{BA}$ species. Further, the effect of addition of exogenous butyric acid to cells on the EPR spectrum shows that it is rapidly taken up by cells and results in complete conversion of active $NHase^{Aq}$ to inactive $NHase^{BA}$. Both of these processes provide a mechanism for compromising the potential of overexpression systems of NHase, and perhaps of natively-expressing systems, for microbially-assisted chemical synthesis and land reclamation.

The other finding in this category was not anticipated. EPR quite clearly demonstrated that NHase is subject to *irreversible* inactivation *in vivo,* through oxidation of a cysteine-sulfenic acid ligand of the active iron ion to sulfinic acid. This process occurs with an approximately exponential dependence on the time post-induction up to at least 24 h. Because of this *in vivo* oxidation, NHase harvested for purification at the time of optimum yield contains a substantial fraction of permanently inactivated NHaseOx and $NHaseOx^{BA}$. NHase intended for mechanistic and spectroscopic study must therefore be harvested significantly earlier, when yield is only around 10 % of optimal, in order to limit the contamination by oxidized forms to a few percent. Additional studies will be required to characterize the effect this oxidative inactivation has on the useful nitrile-hydrating lifetime of a bacterial inoculation. An additional finding was the demonstration that the substrates acrylonitrile and acetonitrile were taken up by NHase-expressing *E.coli* and formed complexes with *Re*$NHase^{Aq}$ that exhibited distinct EPR signals that are

characteristic of the respective catalytic intermediates previously observed with the isolated enzyme. This indicates that the mechanism of nitrile hydration by NHase-expressing bacteria occurs via uptake of the substrate by the cell and *in vivo* catalysis. The signals with substrates closely resembled that from cells incubated with the inhibitor BuBA, which is known from X-ray diffraction to form a cyclic species with the active site of NHase that is proposed to mimic a catalytic cycle intermediate. These studies indicate the potential utility of the *E. coli* overexpression system in "green" chemical reaction systems. The amenability of the expression system to producing recombinant variants with different catalytic properties opens up a wealth of possibilities for new applications.

CHAPTER 4

IDENTIFICATION OF AN INTERMEDIATE SPECIES ALONG THE NITRILE HYDRATASE REACTION PATHWAY BY EPR

4.1. Introduction

Industrially important nitrile hydratases (NHases) are mononuclear metalloenzymes that catalyze the hydration of nitriles to their corresponding higher-value amides [4, 49, 50]. NHases typically exists as $\alpha_2\beta_2$ heterotetramers with an unusual active site located in the α-subunit at the interface of the α and β-subunits within each αβ heterodimer [1, 3, 6]. The active site contains either a low-spin, non-heme Fe(III) ion (Fe-type) or a low-spin, non-corrin Co(III) ion (Co-type) residing in an octahedral coordination geometry and ligated by two deprotonated backbone amides, a cysteine thiolate, two post-translationally oxidized cysteine sulfenic (αCys-SOH) and sulfinic (αCys-SO_2H) groups, and a water molecule [5, 51, 52, 78]. The protonation states of the axial αCys and the equatorial post-translationally modified cysteine-sulfenic and cysteine-sulfinic acids were suggested to be αCys-S^-, αCysSOH, and a αCysSO2$^-$ based on sulfur K-edge EXAFS and geometry-optimized density functional theory (DFT) calculations [79]. These uncommon post-translational oxidized sulfenic and sulfinic groups are essential for the nitrile hydratase activity [79].

As the low spin Fe(III) is paramagnetic, EPR spectroscopic methods have been used in the analysis of Fe-type nitrile hydratases [23, 51, 78, 80, 81]. EPR spectra of the resting Fe-type nitrile hydratases from *Brevibacterium* R 312 (*Br*NHase) and *Pseudomonas chloraphis* 23 (*Pc*NHase) and in the presence of substrates (propionitrile or isobutyronitrile) and mercury, which is an inhibitor, have been reported [81]. The

resting-state EPR spectrum of *Br*NHase exhibits a rhombic low-spin Fe(III) signal (g_1= 2.284, g_2 = 2.140, and g_3 = 1.971) and clear changes upon the addition of nitrile substrates [81]. Similarly, the observed EPR signals for the Fe-type NHase from *Rhodococcus erythropolis* N771 (*Rh*Nase) resulted from a rhombic low-spin Fe(III) ion bound by water (*Rh*NHase^{Aq}, g_1= 2.20, g_2 = 2.13, g_3 = 1.99) [78]. The EPR spectrum of the butyric acid complex of *Rh*Nase (*Rh*Nase^{BA}) revealed a single EPR signal with significantly closer g values (g_1= 2.28, g_2 = 2.14, g_3 = 1.97) to the resting form of *Br*NHase. Changes in the EPR signals of *Rh*Nase upon altering the pH was interpreted to be due to the deprotonation of two active site residues, which were proposed to be the sulfinic (p$K_a \approx 8.5$) and sulfenic (p$K_a \approx 6.5$) acid groups [78]. Recently, EPR studies on the Fe-type NHase from *Rhodococcus equi* TG328-2 (*Re*NHase) revealed a complex EPR spectrum made up of multiple species, which was deconvoluted into *Re*NHase^{Aq} (g_1= 2.206, g_2 = 2.131, g_3 = 1.987) , *Re*NHase^{BA} (g_1= 2.281, g_2 = 2.150, g_3 = 1.974), *Re*NHaseOx (double sulfinated form of *Re*NHase ; g_1= 2.180, g_2 = 2.114, g_3 = 1.998), and *Re*NHaseOx^{BA} (butyric acid complex of the double sulfinated form of *Re*NHase ; g_1= 2.201, g_2 = 2.125, g_3 = 1.982) and supported by the DFT calculations [23].

Recently, a catalytic mechanism for NHase enzymes was proposed with a novel role for the αCys-OH sulfenic acid ligand (Figure 14) [23]. Within this mechanism, the nitrile substrate coordinates directly to the active site metal center activating the CN bond towards nucleophilic attack by the αCys-OH sulfenic acid ligand [23]. Once nucleophilic attack of the nitrile carbon occurs, two protons are transferred in the rate-limiting step allowing the covalently bound imidate to tautomerize to an amide upon nucleophilic attack by a water molecule on the S atom of the αCys-OH sulfenic acid ligand [23].

Finally, the amide product is displaced by a water molecule thus regenerating the catalyst. However, several theoretical studies suggest the formation of an intermediate species where a disulfide bond forms between the axial αCys residue and the S atom of the αCys-OH sulfenic acid ligand [25, 82]. In an effort to identify intermediate species along the proposed reaction pathway, a cryoenzymological approach was employed using a 23% (w/w) $NaCl/H_2O$ eutectic mixture at -20 °C with *Re*NHase and the slow substrate acetonitrile. A new catalytically competent EPR signal was observed for the first time, providing new insight into the proposed catalytic mechanism of NHase enzymes.

4.2. Material and methods

4.2.1. Materials

Ampicillin, kanamycin, N-2-hydroxyethylpiperazine-N-2-ethane sulfonic acid (HEPES**)**, 2-(N-morpholino) ethanesulfonic acid (MES), N-Cyclohexyl-2-aminoethanesulfonic acid (CHES), Isopropyl-β-D-1- thiogalactopyranoside (IPTG), acrylonitrile, acetonitrile, benzonitrile, 3-hydroxybenzonitrile, 3,4-dihydroxybenzonitrile, 2-Methyl Butane, 2-Methyl Pentane, and Pentane were purchased from Sigma-Aldrich or Fisher scientific as the highest purity available. All other reagents were purchased commercially and were the highest purity available.

4.2.2. Expression and isolation of *Re*NHase

The plasmid expressing *Re*NHase was kindly provided by Professor Uwe Bornscheuer [58]. The original plasmid had the NHase α, β, and ε (activator) genes in tandem. Isolated α and β genes were inserted into a pET-28a$^+$ plasmid, and activator gene was inserted into a pET-21a$^+$ plasmid [2]. *E-coli* BL21(DE3) cells containing both

pET-28a$^+$ plasmids hosting the *Re*NHase α and β structural genes, and pET-21a$^+$ plasmid containing the **ε** gene, were used for the expression of functional *Re*NHase. A single colony was used to inoculate 50 mL of LB Miller culture medium containing kanamycin (50 μg/mL) and ampicillin (100 μg/mL). Cultures were incubated at 37 °C with constant agitation for 16 h. These cultures were used to inoculate 6 × 1 L of LB Miller medium containing kanamycin (50 μg/mL) and ampicillin (100 μg/mL). Cells were grown at 37 °C in 2 L baffled flasks with constant agitation at 300 r.p.m. until an optical density of ~0.8 at 600 nm was reached. Then, the culture was cooled to 18 °C in the incubating shaker, induced with 0.3 mM Isopropyl-β-D-1- thiogalactopyranoside (IPTG), and shaken for an additional 16 hrs at 18 °C. Cells were pelleted by centrifugation at 5000 × *g* for 10 minutes and resuspended in 50 mM HEPES buffer, pH 7.5 containing 40 mM butyric acid. Cell paste was stored at -80 ºC until needed.

4.2.3. Anaerobic purification of *Re*NHase

A series of buffers were prepared for the anaerobic purification: **A**, 50 mM HEPES, 40 mM butyric acid, pH 7.5; **B**, 50 mM HEPES, 40 mM butyric acid, 1 M NaCl, pH 7.5; **C**, 50 mM HEPES, 40 mM butyric acid, 50 mM imidazole, pH 7.5; **D**, 50 mM HEPES, 40 mM butyric acid, 500 mM imidazole, pH 7.5; **E**, 50 mM HEPES, pH 7.5; and **F**, 50 mM HEPES, 1 M NaCl, pH 7.5. Deoxygenated buffers were prepared by bubbling nitrogen through them with stirring for 30 minutes. Two 20 mL, manually packed anion exchange columns (Q fast flow resin), and one 15 mL manually packed immobilized-metal affinity chromatography (IMAC) nickel-nitrilotriacetic acid (Ni-NTA) column were placed in a Coy anaerobic chamber, maintained at 20 °C, for 24 hours prior to the purification. The two Q columns, designated here 'QA' and 'QE' were subsequently

equilibrated with buffers **A** and **E**, respectively, and the Ni-NTA column was equilibrated with buffer **C**. Cells were lysed by ultrasonication (Misonix Sonicator 3000) on ice in 30 second increments at 21 W for a total of 4 min. The cell lysate was separated from cell debris by centrifugation for 40 min. at 10,000 × *g*. The supernatant was loaded onto the QA column and washed with 20 column volumes of buffer **A**. Buffers **A** and **B** were mixed to make a series of buffers that contained 100 mM ('AB100'), 150 mM ('AB150'), and 400 mM ('AB400') NaCl. The QA column was washed with 5 column volumes of AB100 followed by five column volumes of AB150, and NHase, identified by its green color, was collected upon subsequent application of AB400. The NHase-containing eluate was applied to the Ni-NTA column and the column was washed with 10 column volumes of buffer **C**, followed by 10 column volumes of a mixture of buffers **C** and **D** (4 % buffer **D** by volume). NHase was eluted from the Ni-NTA column with a mixture of buffers **C** and **D** (40 % buffer **D**). The green-colored eluate was applied to column QE, washed with 20 column volumes of buffer **E**, and eluted with AB400 (400 mM NaCl). The pooled eluate from column QE was removed from the anaerobic chamber in sealed vials (Eppendorf), frozen on dry ice, and stored at -80 °C. Purity of the *Re*NHase enzyme was assessed by SDS-PAGE.

4.2.4. Steady-state kinetic assays

The enzymatic activity of *Re*NHase towards the substrates benzonitrile (benzamide; $\Delta\varepsilon_{244} = 3.49\ mM^{-1}\ cm^{-1}$), 3-hydroxybenzonitrile (3-hydroxybenzamide; $\Delta\varepsilon_{247} = 2.19\ mM^{-1}\ cm^{-1}$), 3,4-dihydroxybenzonitrile controller (3,4-dihydroxybenzamide; $\Delta\varepsilon_{264} = 4.04\ mM^{-1}\ cm^{-1}$), acrylonitrile (acrylamide; $\Delta\varepsilon_{225} = 2.9\ mM^{-1}\ cm^{-1}$), and acetonitrile (acetamide; $\Delta\varepsilon_{220} = 4.96\times10^{-2}\ mM^{-1}\ cm^{-1}$) were measured by following product formation

using a Shimadzu UV-2450 spectrophotometer with a TCC temperature. A 1 mL reaction mixture was prepared in 2.5 mM HEPES buffer, pH 7.5 at 25 °C. Assay concentrations of benzonitrile, 3-hydroxybenzonitrile, and 3,4-dihydroxybenzonitrile were 1 µM – 400 µM and 1 mM – 100 mM for acrylonitrile and acetonitrile. Concentrations of *Re*NHase in assays were 20 nM – 200 nM. Temperature-dependent activities with acetonitrile were determined by pre-equilibration of the reaction mixture in a cuvette between 5 – 35 °C prior to the addition of substrate, followed by activity measurements. Kinetic data were analyzed using OriginPro 9.0 (OriginLab, Northampton, MA). The kinetic constants V_{max} and K_m were calculated by fitting these data to the Michalis-Menten equation. Temperature-dependent data were compared to those predicted by the Arrhenius equation from the activity observed at 25 °C.

4.2.5. Trapping reaction intermediates for *Re*NHase

Three approaches for pre-steady-state EPR spectrokinetics were considered. One was the use of rapid-freeze-quench (RFQ), in which the reaction mixture is squirted as a fine spray into an immiscible organic cryogen maintained at around –100 °C, allowing for the trapping of intermediates after about 9 ms and beyond [83]. RFQ employed a model 715 Update Instruments ram controller that was used to drive a PMI-Kollmorgen stepping motor (model 00D12F-02001-1) connected to a ram that in turn drove either one or two Update Instrument syringes, and the syringes, mixer, and tubing were all contained in a water bath that was maintained at 2 °C with ice [84, 85]. Samples were collected in a quartz funnel connected to a quartz EPR tube by silicone tubing with 2-methylbutane (2MeBu; isopentane, Fischer) at –95 °C.

The second approach was so-called cryoenzymology, in which the very low-temperature at which the eutectic mixtures of aqueous solutions and dimethylsulfoxide (DMSO) remain liquid, < –80 °C. Under certain conditions, such a mixture can exploited to significantly slow the reaction and allow trapping of intermediates by manual techniques [86].

A third approach to EPR spectrokinetics was envisioned, in which high salt concentration replaced DMSO in a cryoenzymological approach. The eutectic (cryohydratic) point of the NaCl-H_2O binary system occurs at 23% NaCl by weight, with a melting temperature $T°_{23\,\%}$ = –21 °C. It was found that a solution ('CSS 7.5' for cryogenic salt solution, pH 7.5) made by adding 23 g NaCl to 77 mL of 32.5 mM HEPES buffer at pH 7.5 remained liquid indefinitely in a commercial –20 °C freezer (measured temperature –18 to –20 °C; Fluke 2165A Digital Thermometer). Solutions of NHase in CSS 7.5 were prepared and the activity and EPR spectra measured. Analogous samples were similarly prepared with the HEPES buffer pH 7.5 being replaced with MES pH 5.0, CHES pH 9.0, CHES pH 9.5, and CHES pH 10.0 (CSS 5.0, CSS 9.0, CSS 9.5, and CSS 10.0, respectively). Separate aliquots of 100 µM *Re*NHase and 250 µM acetonitrile in CSS at each pH were prepared. For studies with benzonitrile, a saturated solution of benzonitrile in buffer was prepared and then the appropriate amount of NaCl added to make CSS. A 150 µL slug of the substrate solution was placed in the lower half of a 3 mm I.D. EPR tube (707-SQ-250M, Wilmad) and the NHase solution was placed in the upper half of the EPR tube. The ~ 1.5 cm slugs were quite stable in position, unless significantly agitated, due to capillary attraction to the tube walls. The EPR tube was allowed to thermally equilibrate in the –20 °C freezer for 30 min. The reaction was then

initiated by holding the EPR tube by the neck and violently flicking the tube to propel the contents to the bottom of the tube; this method has been observed to provide surprisingly efficient mixing [87]. For the shortest reaction times, the tube was immediately plunged into a bath of methanol on solid CO_2. For incubation times of > 5 s, the mixing was carried out in the freezer compartment and the door immediately closed afterwards, with the remainder of the incubation (up to 30 s) carried out with the tube lying directly on the cold freezer floor. Following freezing, samples were stored either under liquid N_2 or at –80 °C prior to EPR examination. When possible, samples were examined as soon as possible after generation as sample tubes had a tendency to shatter upon transfer from one temperature to another, presumably due to a high thermal coefficient of expansion that is likely associated with low-temperature phase changes. Even the use of home-blown 2 mm wall-thickness quartz EPR tubes did not alleviate this problem. The use of a liquid nitrogen finger dewar for EPR, which contains no salt-corrodible parts and is easy to clean in the event of a tube shattering, was therefore preferred for EPR studies over a variable-temperature cryostat.

4.2.6. EPR spectroscopy

EPR spectra were obtained on an updated Bruker EMX-AA-TDU/L spectrometer equipped with an ER4112-SHQ resonator and an HP 5350B microwave counter for precise frequency measurement. Spectra were recorded with 5 G magnetic field modulation at 100 kHz at either 77 K (~ 9.45 GHz) with 5 mW microwave power, 50 K with 2 mW microwave power, or either 25 K or 35 K (~ 9.49 GHz) with 0.5 – 5 mW microwave power; the conditions at 50 K and 77 K were non-saturating for low-spin Fe(III), and 0.5 mW at 25 K was only slightly saturating, whereas putative high-spin

Fe(III) signals could be much better observed with 5 mW at 25 K. 77 K was maintained with liquid nitrogen, and temperatures of 25 - 50 K were maintained with a ColdEdge/Bruker Stinger S5-L recirculating helium refrigerator, and an Oxford ESR900 cryostat and MercuryITC temperature controller. EPR simulations were carried out using EasySpin [73] and all spectra are presented here on a field scale corresponding to a resonant frequency of 9.49 GHz. An integration standard of 1.7 mM Cu(II) in 50 mM HEPES buffer containing 15 % $^{v}/_{v}$ glycerol and 10 mM imidazole at pH 7.5 was prepared and EPR spectra were recorded at 77 K, 0.5 mW. These data were used to calibrate spin densities from *Re*NHase EPR spectra with standard corrections for differences in $1/T$, $\sqrt{(\text{microwave power})}$, and $(\text{field range})^2$.

4.2.7. In silico characterization of the dimer-dimer interface of NHase

The crystal structure of *Re*NHase was analyzed using the Swiss PDB viewer to assess the hydrophobicity of the dimer-dimer interface. The number of hydrophobic residues and the total number of residues at the dimer-dimer interface were determined and the percent hydrophobicity was calculated.

4.3. Results and discussion

Steady-state kinetic analyses. Steady-state kinetic parameters for *Re*NHase in 50 mM HEPES buffer at pH 7.5 and 25 ^{o}C with various substrates are given in Table 6. Kinetic characterization of *Re*NHase using acrylonitrile as the substrate provided a k_{cat} of 620 ± 5 s^{-1} and a K_m of 25 ± 11 mM. In an attempt to identify slower substrates that would be useful for cryoenzymology EPR studies, acetonitrile was examined and provided a k_{cat} of 200 ± 11 s^{-1} and a K_m of 25 ± 2 mM. The remaining benzonitrile substrates tested exhibited decreasing k_{cat} values (30.9 to 1.5 s^{-1}) based on increasing hydroxy substitution of the benzyl ring (Benzonitrile>3-Hydroxybenzonitrile>3,4-Dihydroxybenzonitrile). With this series of NHase substrates in hand, RFQ and cryoenzymology methods could be employed to trap catalytic intermediates.

Table 6. Steady-state kinetic analysis of *Re*NHase at pH 7.5, 25 °C with different substrates.

Substrate[a]	k_{cat} **(s^{-1})**	K_m
Benzonitrile	30.9 ± 1.5	13.2 ± 1.4 μM
3-Hydroxybenzonitrile	15.9 ± 1.6	77 ± 17 μM
3,4-Dihydroxybenzonitrile	1.5 ± 0.2	168 ± 21 μM
Acrylonitrile	620 ± 140	25 ± 11 mM
Acetonitrile	200 ± 11	25 ± 2 mM
Acetonitrile[b]	92 ± 7	

Footnote: [a] In 50 mM HEPES pH 7.5. [b] In CSS 7.5.

RFQ and cryoenzymology with DMSO. Earlier attempts to employ RFQ with *Re*NHase produced anomalous results and, therefore, it was considered prudent to assess the compatibility of *Re*NHase with the proposed cryogens for RFQ and cryoenzymology. *Re*NHase that was exposed to solutions containing 50 % to 66 % DMSO was found to be completely inactive, even after dilution to negligible concentrations of DMSO. Therefore, that strategy for cryoenzymology was hastily abandoned

EPR of *Re*NHase that had been thoroughly agitated with 2-MeBu initially appeared promising (Figure 31). A two-component signal was observed that exhibited g_1- and g_3-values indistinguishable from those of the active *Re*NHase^{Aq} form, though the middle g_2-value had shifted upfield. Furthermore, signals due to inactivated *Re*NHase^{Ox} (at 3120 G) and another uncharacterized *Re*NHase species apparently arising *in vivo* during expression (at 3044 G) were no longer observed. The same behavior was exhibited with 2-methylpentane and *n*-pentane. However, activities of the *Re*NHase after exposure to 2-MeBu, 2-methylpentane, and *n*-pentane were less than 0.5%, 1%, and 0.3% respectively, compared to the pre-exposed activity, and the enzyme preparations adopted a brown color, distinct from the green starting solution. When *Re*NHase was sprayed into 2-MeBu at –95 °C, in the absence of substrate, significant and unexpected changes in the EPR spectrum were observed. The observed form of the low-spin Fe(III) signal was identical to that obtained from *Re*NHase manually agitated with 2-MeBu. However, its intensity now accounted for only 50 % of the known iron complement of the sample (the volumetric dilution of frozen aqueous microbeads in the 2-MeBu matrix was accounted for, calibrated with a myoglobin standard).

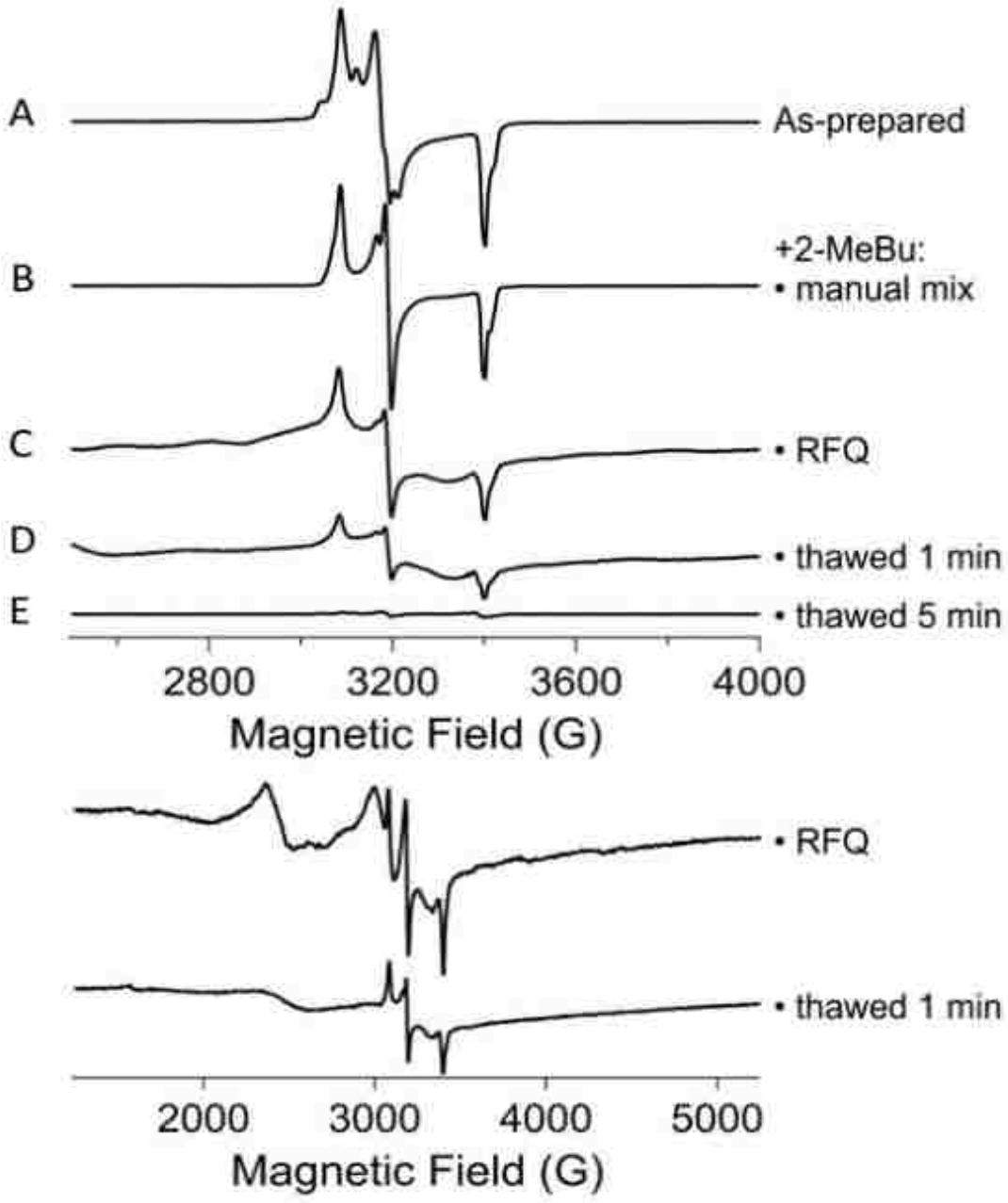

Figure 31. EPR spectra of, upper half (A) as-prepared *Re*NHase, (B) 2-MeBu mixed *Re*NHase, (C) rapidly frozen *Re*NHase in 2-MeBu, (D) thowed sample C - after 1 min, (E) thowed sample C – after 5 min, lower half – full range of C and D, recorded at 25 K.

In addition, new but ill-defined signals were observed at 3000 G ($g' \sim 2.26$) and around 2400 G ($g' \sim 2.8$), under conditions at which fast relaxing species would be observable (25 K, 5 mW; lower panel of Figure 31), and small features arose at 2800 G ($g' \sim 2.42$) and 2600 ($g' \sim 2.61$) in the spectrum recorded at lower power (0.5 mW; upper panel of Figure 31). Resonances similar to these latter features had been observed in earlier unpublished RFQ studies and attributed to genuine catalytic intermediates; however, DFT calculations on a wide variety of both likely and unlikely chemical models were entirely unable to yield such high values for g_1 of a low-spin *Re*NHase Fe(III) species. Upon thawing and re-freezing of the RFQ sample with 2-MeBu alone, the overall spin density diminished further by a factor of 2 –3, the sharp, fast-relaxing $g' \sim 2.8$ signal was replaced by a broad derivative at $g' \sim 2.47$ (2745 G) and the line shape changed (lower panel, Figure 31). The two smaller, slower relaxing features at $g' \sim 2.42$ and 2.61 were replaced with a single peak at $g' \sim 2.47$ (2745 G) (upper panel, Figure 31). After three freeze-thaw cycles, with an estimated 5 min total in the thawed state, the EPR signals had almost completely vanished. These observations prompted a re-examination of earlier RFQ samples, which exhibited entirely analogous behavior, despite having arisen from a different batch of *Re*NHase, prepared in a different manner (aerobically, with butyric acid stabilizer throughout), and using different components (syringes, hoses) for the RFQ experiment. This remarkable behavior is entirely unprecedented for metalloenzymes using the current instrumentation. For the purposes of the present study, RFQ was clearly not a suitable approach for trapping intermediates.

Hydrophobicity of the dimer-dimer interface of ReNHase. The most successful spectrokinetic method for EPR, RFQ, was found to be completely unsuitable for *Re*NHase when using immiscible alkanes at cryogenic temperatures as the cooling medium. Limited effects on the EPR spectrum were observed upon vortex-agitation of *Re*NHase with e.g. 2-MeBu, possibly due to the limited surface area for interaction of *Re*NHase with 2-MeBu at the interface of the immiscible phases ($k_{cat} < 3.5\ s^{-1}$). However, in the RFQ experiment itself, the aqueous phase is projected at high velocity as a spray with very high surface area into the cold 2-MeBu and, even though freezing occurs in ~ 4 ms, irreversible damage to the integrity of *Re*NHase is initiated during this contact that continues even after thawing and re-freezing the sample, during which time the phases rapidly separate. The interacting face of the *Re*NHase dimer at the dimer-dimer interface is characterized by 27 hydrophobic residues among a total of 45, (Figure 32, Table 7) and we hypothesized that the effects of 2-MeBu etc. are due to disruption of this interface followed very rapidly by conformational change that prevents subsequent reassociation of the dimers to form the active and structurally stable tetramer.

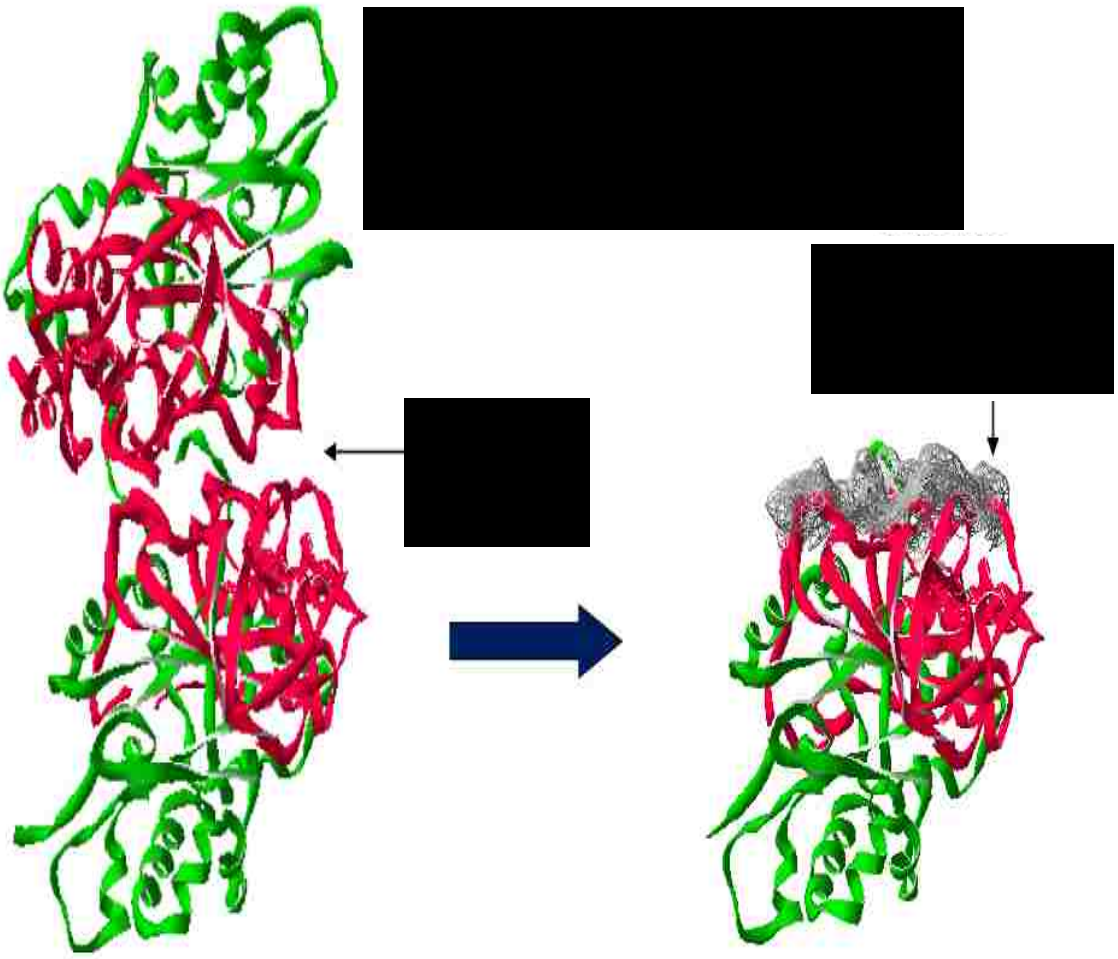

Figure 32. Hydrophobicity at the dimer-dimer interface of *Re*NHase analyzed by the Swiss PDB viewer.

Table 7. Interface residues of *Re*NHase α and β subunits

Interface residues belong to the α – subunit	**Interface residues belong to the β – subunit**
Arg138	Met 1, Asp 2, Gly 3, Val 4, His 5, Asp 6, Leu 7, Ala 8, Gly 9, Val 10, Gln 11, Gly 12, Phe 13, Gly 14, Met 67, Glu 68, Pro 69, Agr 70, His 71, Tyr 72, Leu 73, Ala 111, Leu 112, Pro 113, Ala 114, Ala 115, Ser 116, Asp 138, Glu 139, Phe 140, Phe 141, Ala 142, Gly 143, Ala 149, Tyr 150, Cys 151, Arg 152, Gly 153, Arg 154, Leu 194, Phe 195, Gly 196, Asp 197, Asp 198

Hydrophobic residues are highlighted

Residues at the interface = 45, hydrophobic residues = 27, % of hydrophobicity = 60 %

The appearance of ill-defined but fast-relaxing Fe(III) signals suggests disassembly of the active site. However, the ultimate total loss of Fe(III) EPR signals is not understood as, at the very least, one may expect to see a rhombic $S = {}^{5}/_{2}$ signal due to liberated Fe(III), and the presence of another redox active component must be considered. This phenomenon with *Re*NHase is unique for RFQ of metalloenzymes and, yet, was entirely reproducible.

The utilization of solutions that remain liquid at very low temperatures was considered, with a DMSO-water eutectic having been used successfully for EPR spectrokinetics of molybdenum enzymes at temperatures as low as –80 °C [86]. DMSO

proved to be incompatible with *Re*NHase, probably for the same reason that RFQ with cold immiscible solvents could not be used.

Kinetics at low temperatures using a salt-water eutectic system. Experiments with the 23% NaCl-H_2O eutectic mixture, that in contrast to the other two approaches, resulted in *Re*NHase maintaining its integrity. The steady-state k_{cat} values for *Re*NHase with acetonitrile in the eutectic CSS solutions varied from about 2 % of that in the corresponding unsalted buffer at pH 10, to almost 50 % at pH 7.5, and down to 6 % at pH 5.0 (Table 8). Analysis of the temperature dependence for the activity towards acetonitrile (Figure 33) yielded a linear relationship, $\ln k_{\mathrm{cat}}(\mathrm{s}^{-1}) = \frac{3810}{T(\mathrm{K})} + 17.6$, predicting a k_{cat} value at –20 °C of 12 s^{-1}, i.e. a turnover time of about 80 ms.

Table 8. Comparison of k_{cat} for *Re*NHase with acetonitrile at 25 °C in NaCl-free buffer and in 23% (W/W) NaCl:H_2O eutectic CSS solutions.

pH	$\boldsymbol{k}_{\mathrm{cat}}$ **no NaCl**	$\boldsymbol{k}_{\mathrm{cat}}$ **in CSS**
5.0	160 ± 15	10 ± 5
7.5	198 ± 11	111 ± 4
9.0	170 ± 7	21 ± 1
9.5	110 ± 6	5 ± 1
10.0	64 ± 3	1.0 ± 0.1

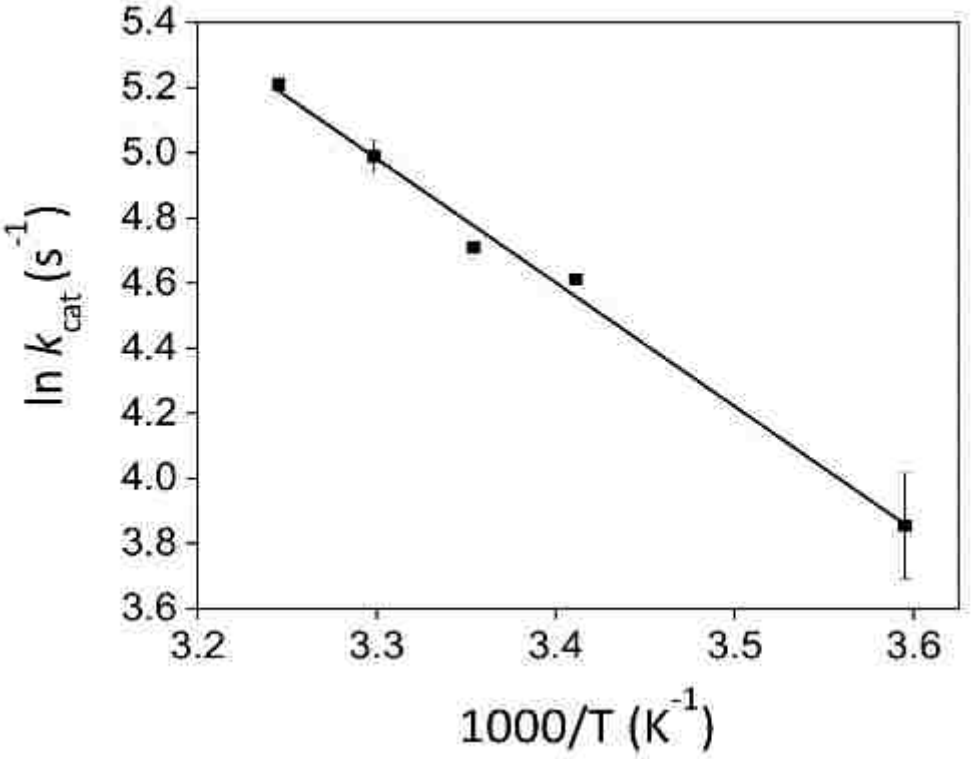

Figure 33. Temperature dependence *Re*NHase activity (ln k_{cat}) towards acetonitrile in 2.5 mM HEPES prepared in 23% (w/w) NaCl/H_2O, pH 7.5 at 25 °C.

EPR spectrokinetic studies with acetonitrile at pH 7.5 using the salt-water eutectic system. At pH 7.5, the EPR spectrum of as-prepared *Re*NHase in high-salt CSS 7.5 (top trace, Figure 34) was almost indistinguishable from that obtained in unsalted HEPES buffer (top trace, Figure 31). In both cases, the spectrum could be simulated as a mixture containing predominantly the active $NHase^{Aq}$ (~63%) with *g*-values 2.197, 2.136, and 1.994 (the *g*-values for the *Re*NHase EPR species reported here differ slightly, though unimportantly, from the previously reported ones; the present values, obtained from simultaneous simulation of each of the contributory species and from experimental spectra uncontaminated with large amounts of $NHase^{BA}$, are likely more reliable), a

smaller amount of NHaseOx (~22%) with *g*-values 2.175, 2.124, and 1.986, and an uncharacterized trace signal (~15%) with a low-field shoulder at $g \sim 2.2$ and an inflection at $g = 2.115$ (*g*-values of 2.218, 2.115 and 1.981 provided the best overall simulation but the latter value, especially, should be treated with caution).

The temperature-dependence of the kinetics with acetonitrile indicated that the pre-steady state would be inaccessible at pH 7.5 using the eutectic system and, with 2.5 eq acetonitrile, the substrate would be expected to be exhausted after only 0.2 s. Reaction of *Re*NHase with acetonitrile for 2 s at –20 °C yielded an EPR spectrum that was indistinguishable from the product complex obtained by the direct addition of 2.5 eq of acetamide, as expected. Each of these spectra consisted of at least four distinct signals, as evidenced by four distinct g_1 resonances that are clearly observable at 2975, 3050, 3080, and 3100 G (Figure 34).

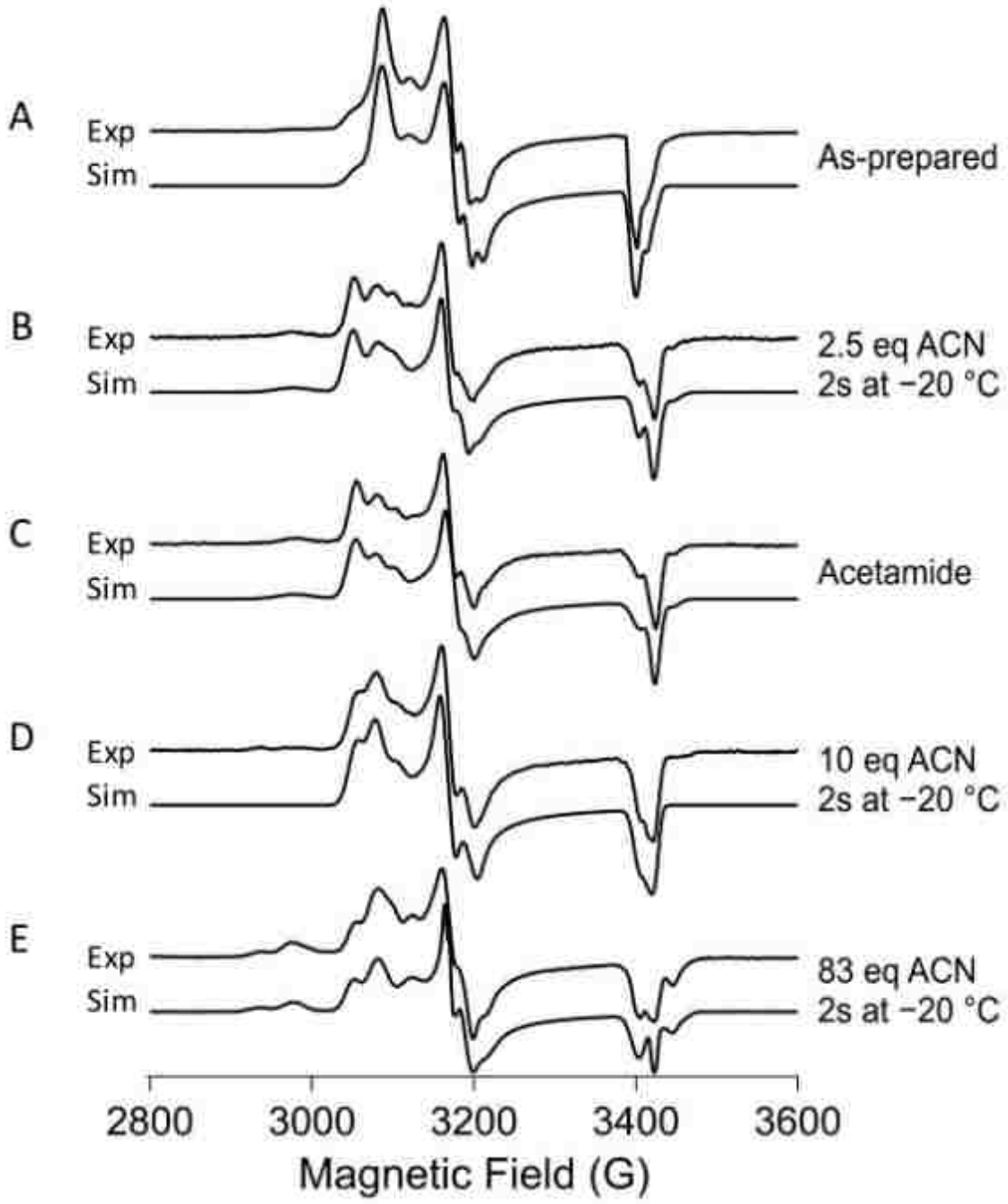

Figure 34. EPR spectra of (A) as-prepared *Re*NHase, (B) 2.5 eq of ACN added *Re*NHase, (C) 2.5 eq acetamide added *Re*NHase, (D) 10 eq of ACN added *Re*NHase, and (E) 83 eq of ACN mixed *Re*NHase, recorded at 25 K. Samples prepared in 12 mM HEPES, 23% (w/w) NaCl/H_2O, pH 7.5. (Exp; experimental EPR spectrum, Sim; computer simulation of experimental EPR spectrum)

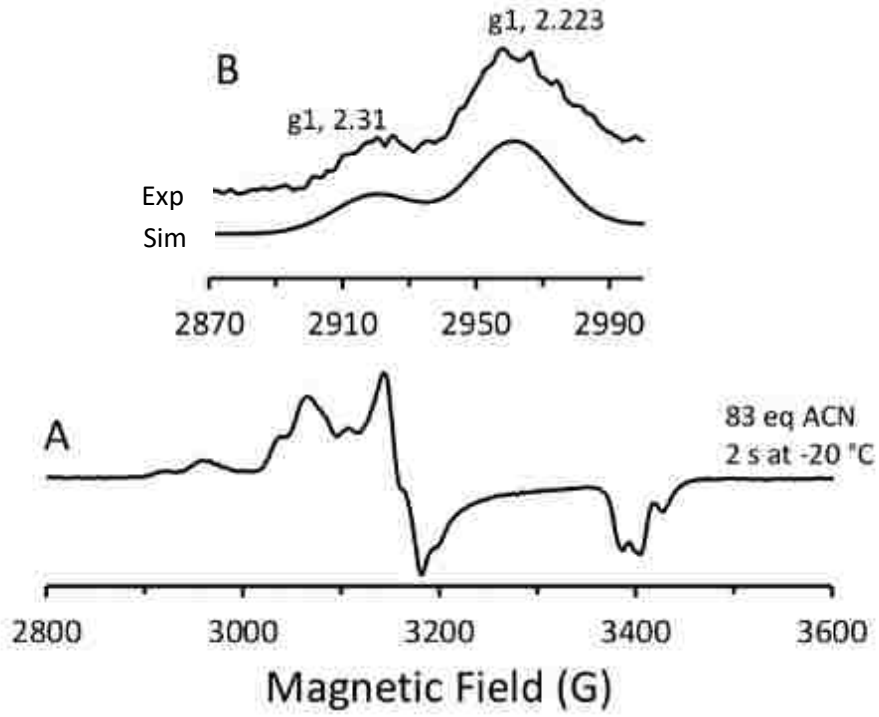

Figure 35. Expanded EPR spectrum of trace E of Figure 34 in the 2800 to 3600 G region, (A) 83 eq of ACN mixed with *Re*NHase, (B) Low-field portion of spectrum A.

The most anisotropic signal is a weak signal (~6% to 9%) with g_1 = 2.276 (other *g*-values of 2.128 ± 0.004 and 1.973 ± 0.003 were used in simulations; the range includes the values for simulations of both the acetonitrile and acetamide spectra), that is reminiscent of NHase^{BA} (g_1 = 2.281) and is thus tentatively assigned to binding of acetamide in a substrate binding site without direct coordination to the metal ion. The predominant signal, with g_1 at 3050 G, was simulated with *g*-values 2.223 ± 0.002, 2.139 ± 0.003, and 1.971 ± 0.001. This signal is very similar to one of the species observed in earlier work [23] upon the addition of acetonitrile to *Re*NHase, and to the signal observed upon the addition of acetonitrile to intact *Re*NHase-expressing in *E. coli* [88]. The generation of this signal upon treatment with acetamide effectively precludes it being a catalytic intermediate on the reaction coordinate prior to the product-bound state. Of the

other two smaller signals, that with g_1 at 3080 G (g = 2.201) is likely due to uncomplexed NHase^{Aq} (g_1 = 2.197 in the absence of acetonitrile or acetamide), and the other, smallest signal, was simulated with g-values of 2.185 ± 0.002, 2.118 ± 0.004, and 1.973 ± 0.005.

Upon reaction with a higher concentration of acetonitrile, 10 eq, an EPR spectrum was observed that very closely resembled that observed upon the addition of acetonitrile to *Re*NHase in earlier work [23]. Although kinetic analysis predicted that the reaction would have terminated in 800 ms with 10 eq acetonitrile, comparison of this EPR spectrum with those from reaction with 2.5 eq, or from direct addition of product, indicates that the reaction did not go to completion (it is unclear why the reaction with lower concentrations of acetonitrile apparently did not go to completion in the earlier study [23], although the temperature dependence of K_m, or a 'micro-K_m' within the reaction coordinate, has not yet been explored and the earlier reactions were carried out at ambient temperature. No new species were observed in the high-amplitude central part of the spectrum – that region of the spectrum is fully accounted for by the product complex, the naked active *Re*NHase^{Aq} species, and the new small g_1 = 2.185 signal observed with acetamide – but additional, broad, low-amplitude features were observed at 2938 G (g ~ 2.31), 2977 G (g ~ 2.28) and 3446 G (g ~ 1.97), while the g_1 = 2.201 signal was not observed at all. The g ~ 2.31 and 2.28 features were too weak to justify inclusion in the simulation of the 10 eq spectrum, but were much better developed in an EPR spectrum obtained after reaction with 5 M (83 eq) of acetonitrile (Figure 35), in which the reaction mixture was frozen well within the expected reaction duration of 6.6 s, i.e. in the steady state, and simulations suggested two species with g-values (i) 2.310, 2.136, and 1.960, and (ii) 2.278, 2.136, and 1.976. The central region of the 83 eq

spectrum was again simulated using known species: the product complex, $NHase^{Aq}$, the $g_1 = 2.185$ signal, and a set of parameters indicative of NHaseOx, although the product complex signal was much diminished compared to those in the spectra obtained well after the steady state had expired (2.5 eq), at the presumed near-end of the steady state (10 eq), or upon direct addition of acetamide.

EPR spectrokinetic characterization of NHase with benzonitrile at pH 7.5 using the salt-water eutectic system. The kinetic data in Table 6 suggests that benzonitrile would be a much preferable substrate to acetonitrile for pre-steady-state kinetics because of its slower reaction rate, allowing the pre-steady-state or steady-state to be trapped more readily using the salt-water eutectic system, along with its comparatively stronger binding affinity. The drawback was that the final concentration of benzonitrile available for reaction was unknown due to the already limited solubility in water at ambient temperature and the additional antagonists of low temperature and high salt concentration, although it was hoped that a supersaturated solution that was metastable over the course of the experiment may arise from the sample preparation method.

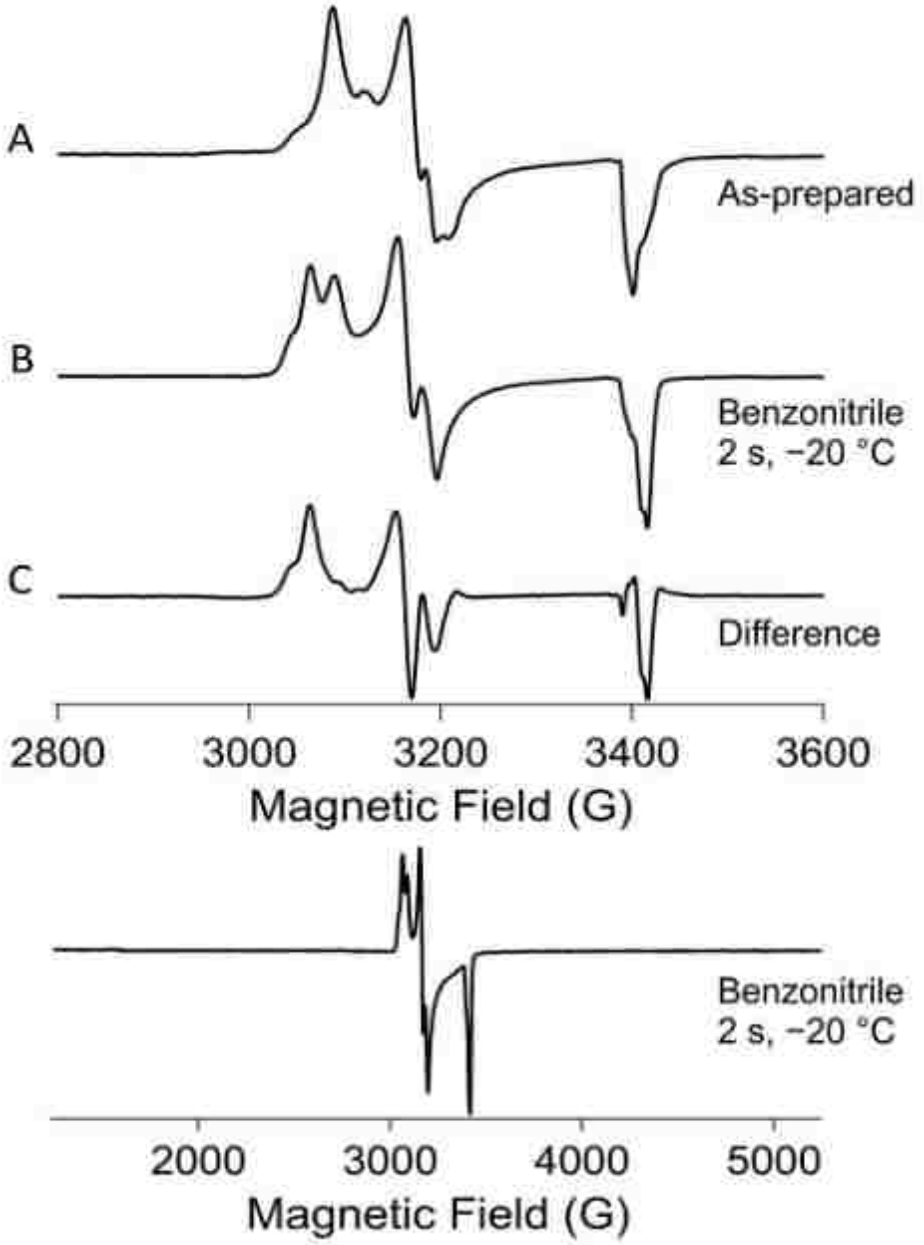

Figure 36. EPR spectra of, upper half (A) as-prepared *Re*NHase, (B) benzonitrile added Re NHase, (C) difference of the spectra A and B, lower half – full range of spectra B, recorded at 35 K. Samples prepared in 2.5 mM HEPES, 23% (w/w) NaCl/H_2O, pH 7.5.

The EPR spectrum obtained upon reaction of benzonitrile for 2 s at –20 °C is shown in Figure 36. Subtraction of the as-isolated signal from that with benzonitrile yielded a difference spectrum that was dominated by a signal with *g*-values of 2.214, 2.144, and 1.985. These *g*-values do not correspond directly to any other previously observed NHase species but are closest to those observed upon adding acetonitrile to *Re*NHase-expressing in *E.coli* cells (*g*-values of 2.22, 2.14 and 1.98), which in turn are similar to those of the dominant species of the acetonitrile-product complex with *g*-values 2.223 ± 0.002, 2.139 ± 0.003, and 1.971 ± 0.001. No signals comparable to the low-field acetonitrile *g* ~ 2.31 and 2.28 signals were observed, and the benzonitrile signal is therefore likely due to a product complex. Notwithstanding the approximations involved in extrapolating a turnover time for benzonitrile in the salt-water eutectic system at –20 °C from a single determination at 25 °C in unsalted buffer, these data suggest that the chemical activity of benzonitrile under the reaction conditions corresponded to a concentration in solution of < 1 mM.

EPR spectrokinetic studies with acetonitrile at pH 5 and pH 10 using the salt-water eutectic system. In another attempt to capture intermediates by exploiting a slower reaction, *Re*NHase was reacted with 2.5 eq of acetonitrile at pH 5 and pH 10 at –20 °C. Under these conditions the steady-state would be expected to persist for 3.3 s and 12.8 s, respectively. The resting signal at pH 5 (Figure 37) was unusual in that a reasonably strong resonance at 2976 G (*g* ~ 2.278) was observed, reminiscent of the *Re*NHase^{BA} butyric acid complex, that was barely detectable at pH 7.5.

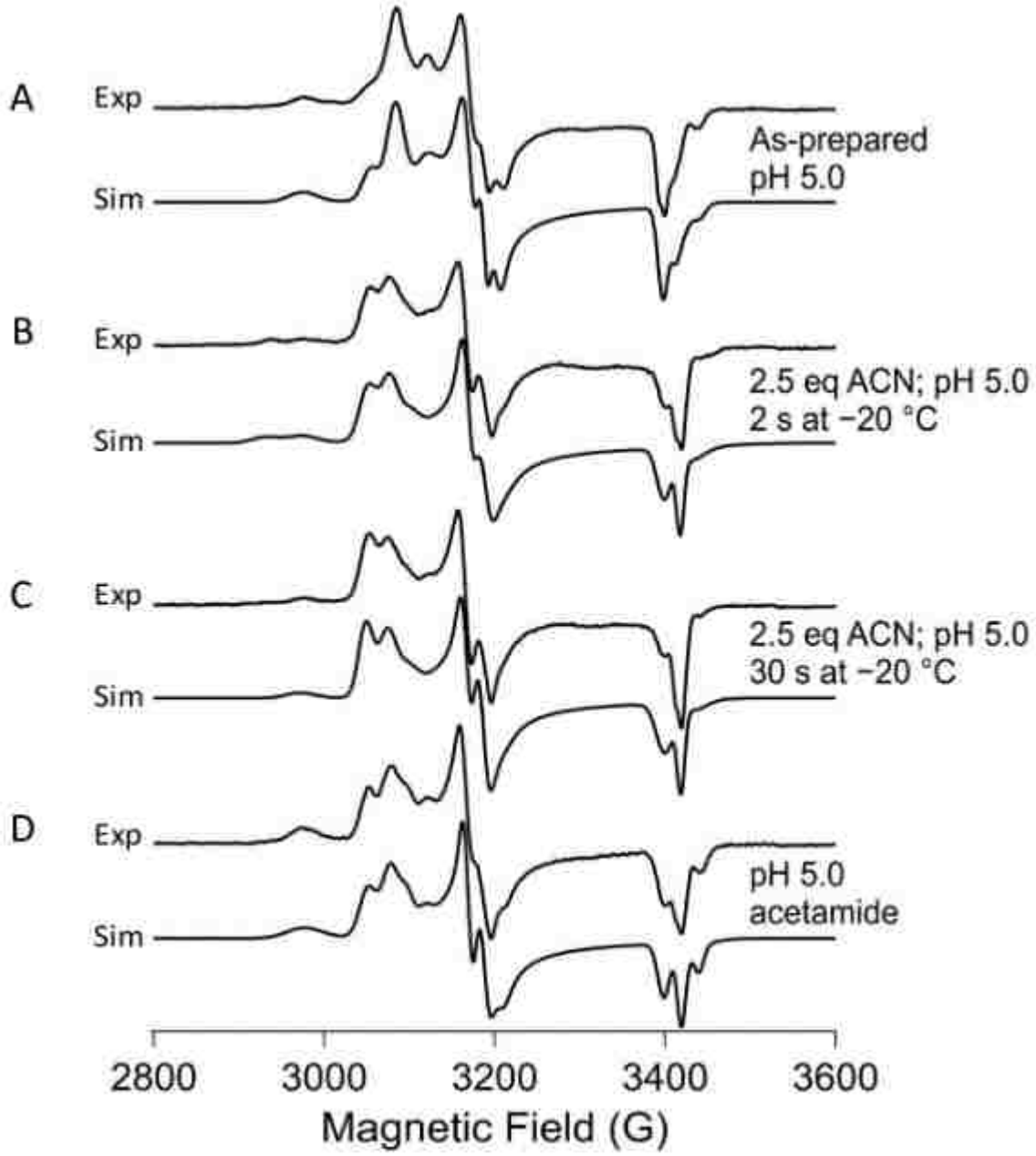

Figure 37. EPR spectra of (A) as-prepared *Re*NHase, (B) 2.5 eq of ACN added *Re*NHase, frozen after 2 s, (C) 2.5 eq ACN added *Re*NHase, frozen after 30 s, and (D) 2.5 eq acetamide added *Re*NHase, recorded at 25 K. Samples prepared in 12 mM HEPES, 23% (w/w) NaCl/H_2O, pH 5.0. (Exp; experimental EPR spectrum, Sim; computer simulation of experimental EPR spectrum)

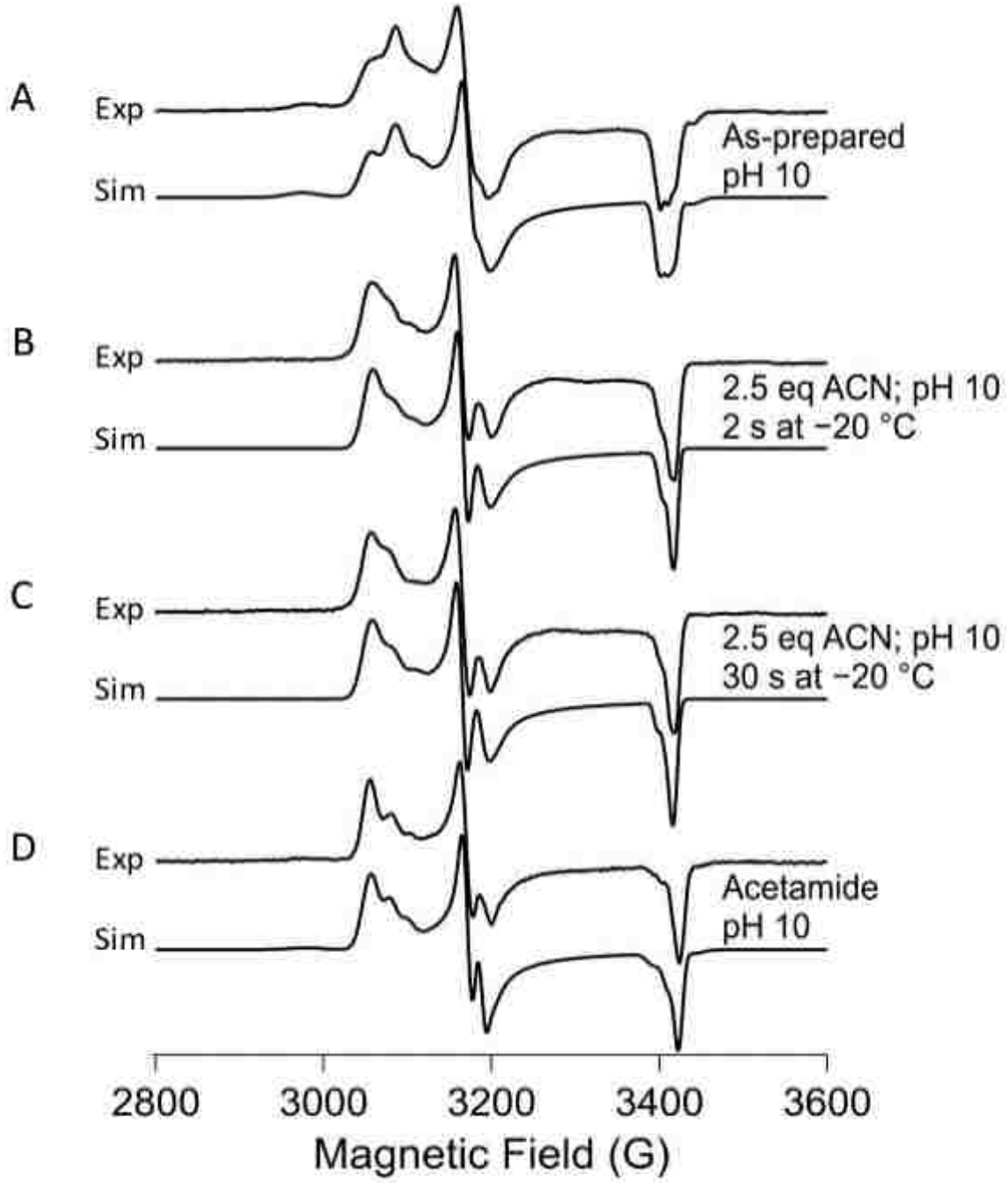

Figure 38. EPR spectra of (A) as-prepared *Re*NHase, (B) 2.5 eq of ACN added *Re*NHase, frozen after 2 s, (C) 2.5 eq ACN added *Re*NHase, frozen after 30 s, and (D) 2.5 eq acetamide added *Re*NHase, recorded at 25 K. Samples prepared in 12 mM HEPES, 23% (w/w) NaCl/H_2O, pH 5.0. (Exp; experimental EPR spectrum, Sim; computer simulation of experimental EPR spectrum)

After a reaction time of 2 s at pH 5, two signals with low-field weak resonances were observed, one perhaps corresponding to the resting signal and simulated with *g*-values of 2.278, 2.134, and 1.977, and another with *g*-values of 2.310, 2.136, and 1.960. These latter parameters are indistinguishable from those obtained with the faster reaction at pH 7.5 using higher acetonitrile concentrations. After 30 s, the $g = 2.310$ had all but disappeared, consistent with the predicted lifetime of the steady state. Interestingly, the signal elicited with direct addition of acetamide at pH 5.0 strongly resembled that obtained with a very high concentration of acetonitrile at pH 7.5, except for the complete lack of a $g = 2.31$ signal in the former.

At pH 10, the overall behavior of the central part of the spectrum was similar to that at pH 7.5, despite the expected lengthy lifetime of the steady-state, and no signals indicative of reaction intermediates other than the product complex were observed (Figure 38). It may be that the rate limiting step, product release, is the only significantly slowed step and that the instantaneous concentration of other intermediates in the steady state is therefore very low.

Studies at pH 5.0, 7.5, and 10.0 with acetonitrile and its reaction product acetamide showed that EPR signals previously obtained upon incubation of *Re*NHase with acetonitrile, and assigned to a proposed cyclic catalytic intermediate by virtue of their similarity with the EPR signal of a crystallographically-characterized complex with butaneboronic acid (*Re*NHase^{BuBA}), could be equally elicited by direct addition of acetamide. This signal, with $g_1 \sim 2.223$ and termed the *Re*NHase^{ACN} signal must, therefore, be due to a complex with product acetamide. The unique g_1-value still suggests direct interaction of the ligand molecule with the metal ion and, the similarity to

the *Re*NHase^{BuBA} species, supported by DFT calculations, perhaps indicates additional interactions with the catalytically-essential cysteine-sulfenic acid moiety. As such, this species may represent the penultimate step on the reaction coordinate. An additional signal obtainable with either acetonitrile or acetamide was reminiscent of the butyric acid complex, *Re*NHase^{BA}, and likely represents acetamide bound to the enzyme adjacent to the active site but not interacting directly with it, i.e. the last step on the reaction coordinate. These EPR data with acetamide would indicate that these steps are in equilibrium; titration of *Re*NHase with acetamide may further prove enlightening.

In the search for genuine catalytic intermediates, one signal was observed that fulfilled the criteria. A signal with g_1 = 2.31 was observed at pH 7.5 and at pH 5 under conditions predicted by kinetic analyses to represent the steady-state. The relative concentration of this signal was low, ~5 - 6 % of total spin density, as would be expected for a non-rate limiting step in the steady-state. Furthermore, this signal was catalytically competent – it was only observed under steady-state conditions and was extinguished upon the exhaustion of substrate and formation of the terminal product complexes. The g_1-value is the highest ever observed in an NHase, suggesting considerable disruption to the Fe(III) electronic structure as, again, might be expected in a catalytic intermediate, and the g_1-value of *Re*NHase^{BA} returned by Taylor/DFT of 2.248 (experimentally, 2.281) suggests that a plausible structural model will be obtainable for the g_1 = 2.31 species.

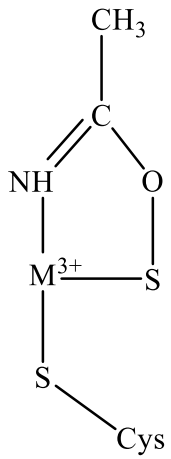

Figure 39. Proposed catalytic cyclic intermediate (*Re*NHase vs. aceronitrile) for the newly observed EPR signal with g_1= 2.31

Comparison of the product complex spectra obtained with acetonitrile and benzonitrile suggests that the perturbation of the electronic structure of the Fe(III) ion is dependent on the precise nature of the molecule. This is an important observation that will inform future tailoring of catalytic properties of *Re*NHase variants and biomimetics. Acetonitrile and benzonitrile exhibit very different catalytic rates and binding affinities, and a demonstration of a general correlation of catalytic properties and EPR parameters would provide a useful screening tool for potential substrates among NHases and engineered NHase variants.

4.4. Conclusion

In conclusion, two methods, (i) the RFQ of intermediates in 2-MeBu, 2-methylpantane, *n*-pentane, and DMSO at -95 °C, (ii) use of a 23 % (w/w) NaCl/H_2O eutectic mixture as the reaction medium for obtaining lower activities by keeping the reaction mixture in the liquid state at -20 °C, were investigated. In method (i), distorted EPR species were observed with organic solvents used, and sharp decrements of 2-MeBu, 2-methylpantane, n-pentane, and DMSO treated *Re*NHase (k_{cat} remains < 1%) were observed showing that the RFQ is inappropriate for trapping intermediates in the catalytic cycle of *Re*NHase. In method (ii), *Re*NHase was found to be compatible with the salt-water system providing similar signals for as-prepared *Re*NHase, compared to the EPR spectra of as-prepared *Re*NHase under normal buffer conditions. Further, salt-water eutectic solution provided several distinguishable signals, including a completely new signal with g_1 of 2.31, indicative of a catalytic intermediate. Therefore, here we have developed a new method of trapping intermediates in the *Re*NHase vs. acetonitrile catalytic cycle, while discovering a new intermediate EPR signal, which is promising in that this technique will be worthy in enzyme mechanistic studies. Next steps should be performed under controlled conditions (mixing and freezing times) for trapping new species, which will then provide insight to the complete catalytic cycle.

CHAPTER 5

CONCLUSION

NHases have become one of the most important industrial enzymes due to their catalytic properties and low environmental impact. They are also able to produce extraordinary high concentrations of amides from nitriles quickly. Since NHase was first discovered more than 40 years ago, there remains great interest in using NHases in industrial applications despite the lack of information about their biological assembly and the catalytic cycle. Hence, research on the enzymatic reaction including the bio-assembly of the metallocentre, post-translational oxidations, reaction intermediates, and the involvement of the activator protein in the enzyme maturation process will provide insight into how to improve biocatalyst design that is more efficient, stable, and selective. In this dissertation, several important, unanswered questions have been addressed.

The co-expression of a corresponding NHase activator (ε) protein is required for the fully functional expression of both Co-type and the Fe-type NHases. Studying the factors that control metallocentre assembly is important to understand the structure and the function of NHases. Such studies will elucidate the redox events that occur during the active site maturation process including the generation of the low-spin iron/cobalt center as well as the post-translational oxidations of the active site equatorial Cys ligands. Recently, an expression system and a purification method for the soluble expression of the Fe-type (ε) protein from *Rhodococcus equi* TG328-2 was reported [41]. These studies revealed that the *Re*NHase (ε) protein is a G3E P-loop GTPase within the COG0523 subfamily. Further, ITC data has shown that the *Re*NHase (**ε**) protein binds

Co(II) with ~1: 1 molar ratio and a K_d value of ~3 μM. Reported herein, the first known Fe-type α(**ε**) complex has been purified and shown to form a 1:1 mole ratio complex. The resulting α**ε** complex was an apo-protein complex and as expected, no activity was detected. The apo α(**ε**) complex could be combined *in vitro* with β-subunit and Fe(II) to produce an active NHase enzyme. Activity studies revealed that the addition of β-subunit was essential for the reconstitution of NHase enzyme. The addition of GTP enhances the rate of acrylonitrile hydration, indicating that GTP plays a role in Fe-type active site formation and activation, but is not essential for catalysis. The addition of TCEP markedly enhances the rate of nitrile hydration, likely due to the reduction of either a disulfide bond in the NHase active site and/or in the (**ε**) protein CXCC proposed metal binding site. The independently expressed and purified *Re*NHase α- and β-subunits were also mixed with (**ε**) protein to form the α(**ε**) complex in situ, and then mixed with Fe(II), and/or GTP in the absence and presence of TCEP. Activity data indicated that TCEP and GTP play a role in iron insertion and active site maturation of Fe-type NHases.

However, even with these advances, the mechanism of biological assembly for Fe-type NHases is not fully understood. Therefore, factors that control metallocenter assembly in Fe-type NHases, the importance of the 72CXCC75 motif of the ReNHase (ε) protein for iron transportation, and the role of GTP for iron insertion requires additional investigation. In order to investigate the importance of CXCC motif and, which cysteine residues are essential for Fe(II) binding, new expression systems with MBP-tagged C72A, C74A, and C75A mutants need to be prepared. Obtaining soluble, pure, mutant (ε) proteins will allow Fe(II) binding to be investigated by ITC under anaerobic conditions (to prevent Fe(II) from oxidations), the ability of these mutant (ε) proteins to

hydrolyze GTPase, and if the mutant (ε) proteins can transfer Fe(II) to the NHase α-subunit and provide an active NHase enzyme. Such studies will provide insight into the role of the proposed CXCC metal binding site.

In an attempt to understand the observed EPR signals for *Re*NHase, studies aimed at preparing a homogeneous enzyme sample for EPR studies were undertaken. While several of the observed individual EPR signals have recently been assigned to distinct chemical species with the assistance of DFT calculations, further inventions into the origins and evolution of the observed EPR signals from cells overexpressing the enzyme provided important insight into the various NHase species and if they evolve duing the expression process. Interestingly, these studies revealed that NHase forms two inactive complexes *in vivo* over time. One is due to the reversible complexation with an endogenous carboxylic acid, while the second is due to the oxidation of the active site cysteine-sulfenic acid. It was also shown that the homogeneity of preparations can be improved by employing an anaerobic purification protocol. Further, the ability of the substrate acetonitrile and the competitive inhibitor butyric acid, to be taken up by *E. coli* and to form NHase complexes *in vivo*, suggests that care must be taken with environmental variables when attempting microbially-assisted amide synthesis and reclamation.

Having in hand relatively homogeneous *Re*NHase enzyme, which was purified under anaerobic conditions, EPR studies of catalytic intermediate species was initiated. An EPR time course study was undertaken after the addition of substrate. The RFQ method was initially applied for trapping intermediates and found to be inappropriate due to the loss of NHase EPR species upon mixing with cryogenic solvents such as 2-

methylbutane (2-MeBu), 2-methylpantane, *n*-pentane, and dimethyl sulfoxide (DMSO). Exposure to those solvents largely inactivated *Re*NHase (k_{cat} < 1%), while DMSO treated *Re*NHase exhibited the complete and irreversible inactivation of the enzyme, suggesting the enzyme active site integrity is destroyed by organic solvents (the 60% hydrophobicity at the dimer-dimer interface may be the cause this observation).

Interestingly, a 23 % (w/w) NaCl/H_2O eutectic mixture has no effect on the EPR-spectra of *Re*NHase, and this solution could be cooled to -20 °C while retaining the liquid state. EPR experiments performed in the salt-water eutectic solution provided several distinguishable signals. Studies with acetonitrile and its reaction product acetamide showed that EPR signals previously obtained upon incubation of NHase with acetonitrile, and assigned to a proposed cyclic catalytic intermediate by virtue of their similarity with the EPR signal of a crystallographically-characterized complex with butaneboronic acid ($NHase^{BuBA}$), could be equally elicited by direct addition of acetamide. This signal, with g_1 ~ 2.223 and termed the $NHase^{ACN}$ signal must, therefore, be due to a complex with the product acetamide. A new signal observed with g_1 of 2.31, was proposed to be due to the suggested cyclic intermediate. This signal was catalytically competent as it is only observed under steady-state conditions. Therefore, a new method of trapping intermediates in NHase systems was discovered allowing the discovery of a heretofore unobserved catalytic intermediate. The next step in these studies will be to perform experiments under tightly controlled conditions (mixing and freezing times), in order to trap additional new intermediate species.

EPR studies on the *Re*NHase enzyme is complicated due to the multiple overlapping signals. Thesefore, a mutant *Re*NHase enzyme was prepared where a Thr

(αT162) residue that forms a hydrogen bond to the S atom of the axial Cys residue was converted into an Ala residue (αT162A), which is catalytically active. Interestingly, the EPR spectrum of αT162A exhibits primarily the active form, *Re*NHase^{Aq}, signal suggesting that this mutant is a good candidate for future cryoenzymatic EPR studies. EPR studies of intermediates generated from the addition of various substrates and comparison of those data with EPR spectra obtained from inhibitors and product bound forms of *Re*NHase αT162A, will possibly allow for the observation of new intermediate species. Further, the *Re*NHase αT162A enzyme will be a good candidate for ENDOR experiments with ^{13}C and ^{15}N labeled nitrile substrates and products for understanding structural aspects of any observed intermediates. ^{1}H-ENDOR data will also provide insight into the protonation states of active site residues.

REFERENCES

1. Song, L.; Wang, M.; Shi, J.; Xue, Z.; Wang, M.-X.; Qian, S., High resolution x-ray molecular structure of the nitrile hydratase from rhodococcus erythropolis aj270 reveals posttranslational oxidation of two cysteines into sulfinic acids and a novel biocatalytic nitrile hydration mechanism. *Biochem. Biophys. Res. Commun.* **2007,** *362*, 319-324.

2. Gumataotao, N.; Kuhn, M. L.; Hajnas, N.; Holz, R. C., Identification of an active site-bound nitrile hydratase intermediate through single turnover stopped-flow spectroscopy. *J. Biol. Chem.* **2013,** *288*, 15532-15536.

3. Huang, W.; Jia, J.; Cummings, J.; Nelson, M.; Schneider, G.; Lindqvist, Y., Crystal structure of nitrile hydratase reveals a novel iron centre in a novel fold. *Structure* **1997,** *5*, 691-699.

4. Prasad, S.; Bhalla, T. C., Nitrile hydratases (nhases): At the interface of academia and industry. *Biotechnol. Adv.* **2010,** *28*, 725-741.

5. Murakami, T.; Nojiri, M.; Nakayama, H.; Odaka, M.; Yohda, M.; Dohmae, N.; Takio, K.; Nagamune, T.; Endo, I., Post-translational modification is essential for catalytic activity of nitrile hydratase. *Protein Sci. : A Publication of the Protein Society* **2000,** *9*, 1024-1030.

6. Lu, J.; Zheng, Y.; Yamagishi, H.; Odaka, M.; Tsujimura, M.; Maeda, M.; Endo, I., Motif cxcc in nitrile hydratase activator is critical for nhase biogenesis in vivo. *FEBS Lett.* **2003,** *553*, 391-396.

7. Zhou, Z.; Hashimoto Y Fau - Shiraki, K.; Shiraki K Fau - Kobayashi, M.; Kobayashi, M., Discovery of posttranslational maturation by self-subunit swapping. *Proc. Natl. Acad. Sci.* **2008,** *105*, 14849-14854.

8. Yano, T.; Ozawa, T.; Masuda, H., Structural and functional model systems for analysis of the active center of nitrile hydratase. *Chem. Lett.* **2008,** *37*, 672-677.

9. Zhou, S.; Junge, K.; Addis, D.; Das, S.; Beller, M., A general and convenient catalytic synthesis of nitriles from amides and silanes. *Org. Lett.* **2009,** *11*, 2461-2464.

10. Legras, J. L.; Chuzel, G.; Arnaud, A.; Galzy, P., Natural nitriles and their metabolism. *World J. Microbiol. Biotechnol.* **1990,** *6*, 83-108.

11. McNaught, A. D.; Wilkinson, A., *I{upac}. Compendium of chemical terminology, 2nd ed. (the "gold book")*. WileyBlackwell; 2nd Revised edition edition.

12. Mowry, D. T., The preparation of nitriles. *Chem. Rev.* **1948,** *42*, 189-283.

13. Daniele, C. F., P.; Fabrizio, C.; Esmeralda, N.; Ivano, V.,, Comparison of different chemical processes from a life cycle perspective. *Chem. Eng. Trans.* **2014,** *36*, 169-174.

14. Telvekar, V. N.; Rane, R. A., A novel system for the synthesis of nitriles from carboxylic acids. *Tetrahedron Lett.* **2007,** *48*, 6051-6053.

15. OECD, *The application of biotechnology to industrial sustainability*. OECD Publishing.

16. Martinez, S.; Wu, R.; Sanishvili, R.; Liu, D.; Holz, R., The active site sulfenic acid ligand in nitrile hydratases can function as a nucleophile. *J. Am. Chem. Soc.* **2014,** *136*, 1186-1189.

17. Yamada, H.; Kobayashi, M., Nitrile hydratase and its application to industrial production of acrylamide. *Biosci. Biotechnol. Biochem.* **1996,** *60*, 1391-1400.

18. Van Pelt, S. The application of nitrile hydratases in organic synthesis Dissertation, Technical University of Delft, 2010.

19. Yamanaka, Y.; Kato, Y.; Hashimoto, K.; Iida, K.; Nagasawa, K.; Nakayama, H.; Dohmae, N.; Noguchi, K.; Noguchi, T.; Yohda, M.; Odaka, M., Time-resolved crystallography of the reaction intermediate of nitrile hydratase: Revealing a role for the cysteinesulfenic acid ligand as a catalytic nucleophile. *Angew. Chem.* **2015,** *127*, 10913-10917.

20. Hopmann, K. H.; Guo, J.-D.; Himo, F., Theoretical investigation of the first-shell mechanism of nitrile hydratase. *Inorg. Chem.* **2007,** *46*, 4850-4856.

21. Yamanaka, Y.; Hashimoto, K.; Ohtaki, A.; Noguchi, K.; Yohda, M.; Odaka, M., Kinetic and structural studies on roles of the serine ligand and a strictly conserved tyrosine residue in nitrile hydratase. *J. Biol. Inorg. Chem.* **2010,** *15*, 655-665.

22. Heinrich, L.; Mary-Verla, A.; Li, Y.; Vaissermann, J.; Chottard, J.-C., Cobalt(iii) complexes with carboxamido-n and sulfenato-s or sulfinato-s ligands suggest that a coordinated sulfenate-s is essential for the catalytic activity of nitrile hydratases. *Eur. J. Inorg. Chem.* **2001,** *2001*, 2203-2206.

23. Stein, N.; Gumataotao, N.; Hajnas, N.; Wu, R.; Lankathilaka, K. P. W.; Bornscheuer, U. T.; Liu, D.; Fiedler, A. T.; Holz, R. C.; Bennett, B., Multiple states of nitrile hydratase from rhodococcus equi tg328-2: Structural and mechanistic insights from electron paramagnetic resonance and density functional theory studies. *Biochemistry* **2017,** *56*, 3068-3077.

24. Mitra, S.; Holz, R. C., Unraveling the catalytic mechanism of nitrile hydratases. *J. Biol. Chem.* **2007,** *282*, 7397-7404.

25. Hopmann, K. H., Full reaction mechanism of nitrile hydratase: A cyclic intermediate and an unexpected disulfide switch. *Inorg. Chem.* **2014,** *53*, 2760-2762.

26. Waldron, K. J.; Rutherford, J. C.; Ford, D.; Robinson, N. J., Metalloproteins and metal sensing. *Nature* **2009,** *460*, 823-830.

27. Shoshan, M. S.; Tshuva, E. Y., The mxcxxc class of metallochaperone proteins: Model studies. *Chem. Soc. Rev.* **2011,** *40*, 5282-5292.

28. O'Halloran, T. V.; Culotta, V. C., Metallochaperones, an intracellular shuttle service for metal ions. *J. Biol. Chem.* **2000,** *275*, 25057-25060.

29. Giedroc, D. P.; Arunkumar, A. I., Metal sensor proteins: Nature's metalloregulated allosteric switches. *Dalton Trans* **2007**, 3107-3120.

30. Nojiri, M.; Nakayama, H.; Odaka, M.; Yohda, M.; Takio, K.; Endo, I., Cobalt-substituted fe-type nitrile hydratase of rhodococcus sp. N-771. *FEBS Lett.* **2000,** *465*, 173-177.

31. Miyanaga, A.; Fushinobu, S.; Ito, K.; Shoun, H.; Wakagi, T., Mutational and structural analysis of cobalt-containing nitrile hydratase on substrate and metal binding. *Eur. J. Biochem.* **2004,** *271*, 429-438.

32. Kuhn, M. L.; Martinez, S.; Gumataotao, N.; Bornscheuer, U.; Liu, D.; Holz, R. C., The fe-type nitrile hydratase from comamonas testosteroni ni1 does not require an activator accessory protein for expression in escherichia coli. *Biochem. Biophys. Res. Commun.* **2012,** *424*, 365-370.

33. Haas, C.; Rodionov, D.; Kropat, J.; Malasarn, D.; Merchant, S.; de Crécy-Lagard, V., A subset of the diverse cog0523 family of putative metal chaperones is linked to zinc homeostasis in all kingdoms of life. *BMC Genomics* **2009,** *10*, 1-21.

34. Cameron, R. A.; Sayed, M.; Cowan, D. A., Molecular analysis of the nitrile catabolism operon of the thermophile bacillus pallidus rapc8. *Biochim. Biophys. Acta* **2005,** *1725*, 35-46.

35. Nojiri, M.; Yohda, M.; Odaka, M.; Matsushita, Y.; Tsujimura, M.; Yoshida, T.; Dohmae, N.; Takio, K.; Endo, I., Functional expression of nitrile hydratase in escherichia coli: Requirement of a nitrile hydratase activator and post-translational modification of a ligand cysteine. *J. Biochem.* **1999,** *125*, 696-704.

36. Liu, Y.; Cui, W.; Xia, Y.; Cui, Y.; Kobayashi, M.; Zhou, Z., Self-subunit swapping occurs in another gene type of cobalt nitrile hydratase. *PLoS One* **2012,** *7*, e50829.

37. Sydor, A. M.; Jost, M.; Ryan, K. S.; Turo, K. E.; Douglas, C. D.; Drennan, C. L.; Zamble, D. B., Metal binding properties of escherichia coli yjia, a member of the

metal homeostasis-associated cog0523 family of gtpases. *Biochemistry* **2013,** *52*, 1788-1801.

38. Leipe, D. D.; Wolf, Y. I.; Koonin, E. V.; Aravind, L., Classification and evolution of p-loop gtpases and related atpases. *J. Mol. Biol.* **2002,** *317*, 41-72.

39. Rossbach, M.; Daumke, O.; Klinger, C.; Wittinghofer, A.; Kaufmann, M., Crystal structure of thep1 from the hyperthermophile aquifex aeolicus: A variation of the reca fold. *BMC Struct. Biol.* **2005,** *5*, 7.

40. Huffman, D. L.; O'Halloran, T. V., Energetics of copper trafficking between the atx1 metallochaperone and the intracellular copper transporter, ccc2. *J. Biol. Chem.* **2000,** *275*, 18611-18614.

41. Gumataotao, N.; Lankathilaka, K. P.; Bennett, B.; Holz, R. C., The iron-type nitrile hydratase activator protein is a gtpase. *Biochem. J* **2017,** *474*, 247-258.

42. Haas, C.; Rodionov, D.; Kropat, J.; Malasarn, D.; Merchant, S.; de Crecy-Lagard, V., A subset of the diverse cog0523 family of putative metal chaperones is linked to zinc homeostasis in all kingdoms of life. *BMC Genomics* **2009,** *10*, 470.

43. Cameron, R. A.; Sayed, M.; Cowan, D. A., Molecular analysis of the nitrile catabolism operon of the thermophile bacillus pallidus rapc8. *Biochim. Biophys. Acta - General Subjects* **2005,** *1725*, 35-46.

44. Zhou, Z.; Hashimoto, Y.; Cui, T.; Washizawa, Y.; Mino, H.; Kobayashi, M., Unique biogenesis of high-molecular mass multimeric metalloenzyme nitrile hydratase: Intermediates and a proposed mechanism for self-subunit swapping maturation. *Biochemistry* **2010,** *49*, 9638-9648.

45. Zhou, Z.; Hashimoto, Y.; Shiraki, K.; Kobayashi, M., Discovery of posttranslational maturation by self-subunit swapping. *Proc. Natl. Acad. Sci.* **2008,** *105*, 14849-14854.

46. Cheng, T.; Li, H.; Yang, X.; Xia, W.; Sun, H., Interaction of slyd with hypb of helicobacter pylori facilitates nickel trafficking. *Metallomics* **2013,** *5*, 804-807.

47. Lu, J.; Zheng, Y.; Yamagishi, H.; Odaka, M.; Tsujimura, M.; Maeda, M.; Endo, I., Motif cxcc in nitrile hydratase activator is critical for nhase biogenesis in vivo. *FEBS Lett.* **2003,** *553*, 391-396.

48. Tsujimura, M.; Odaka, M.; Nakayama, H.; Dohmae, N.; Koshino, H.; Asami, T.; Hoshino, M.; Takio, K.; Yoshida, S.; Maeda, M.; Endo, I., A novel inhibitor for fe-type nitrile hydratase: 2-cyano-2-propyl hydroperoxide. *J. Am. Chem. Soc.* **2003,** *125*, 11532-11538.

49. Yamada, H.; Kobayashi, M., Hydratases involved in nitrile conversion: Screening, characterization and application. *Biosci. Biotech. Biochem.* **1996,** *60*, 1391-1400.

50. Brady, D.; Beeton, A.; Zeevaart, J.; Kgaje, C.; van Rantwijk, F.; Sheldon, R. A., Characterisation of nitrilase and nitrile hydratase biocatalytic systems. *Appl. Microbiol. Biotechnol.* **2004,** *64*, 76-85.

51. Kovacs, J. A., Synthetic analogues of cysteinate-ligated non-heme iron and non-corrinoid cobalt enzymes. *Chem. Rev.* **2004,** *104*, 825-848.

52. Harrop, T. C.; Mascharak, P. K., Fe(iii) and co(iii) centers with carboxamido nitrogen and modified sulfur coordination: Lessons learned from nitrile hydratase. *Acc. Chem. Res.* **2004,** *37*, 253-260.

53. Dey, A.; Chow, M.; Taniguchi, K.; Lugo-Mas, P.; Davin, S.; Maeda, M.; Kovacs, J. A.; Odaka, M.; Hodgson, K. O.; Hedman, B.; Solomon, E. I., Sulfur k-edge xas and dft calculations on nitrile hydratase: Geometric and electronic structure of the non-heme iron active site. *J. Am. Chem. Soc.* **2006,** *128*, 533 - 541.

54. Nishiyama, M.; Horinouchi, S.; Kobayashi, M.; Nagasawa, T.; Yamada, H.; Beppu, T., Cloning and characterization of genes responsible for metabolism of nitrile compounds from pseudomonas chlororaphis b23. *J. Bacteriol.* **1991,** *173*, 2465-2472.

55. Hashimoto Y., N., M., Horinouchi S., Beppu T., Nitrile hydratase gene from rhodococcus sp. N-774 requirement for its downstream region for efficient expression *Biosci. Biotechnol. Biochem.* **1994,** *58*, 1859-1869.

56. Nojiri, M.; Yohda, M.; Odaka, M.; Matsushita, Y.; Tsujimura, M.; Yoshida, T.; Dohmae, N.; Takio, K.; Endo, I., Functional expression of nitrile hydratase in escherichia coli: Requirement of a nitrile hydratase activator and post-translational modification of a ligand cysteine. *J. Biochem.* **1999,** *125*, 696-704.

57. Gumataotao, N.; Lankathilaka, K. P. W.; Bennett, B.; Holz, R. C., The iron-type nitrile hydratase activator protein is a gtpase. *Biochem. J* **2017,** *474*, 247-258.

58. Rzeznicka, K.; Schatzle, S.; Bottcher, D.; Klein, J.; Bornscheuer, U. T., Cloning and functional expression of a nitrile hydratase (nhase) from rhodococcus equi tg328-2 in escherichia coli, its purification and biochemical characterisation. *Appl. Microbiol. Biotechnol.* **2010,** *85*, 1417-1425.

59. Blaby-Haas, C. E.; Flood, J. A.; Crécy-Lagard, V. d.; Zamble, D. B., Yeir: A metal-binding gtpase from escherichia coli involved in metal homeostasis. *Metallomics.* **2012,** *4*, 488-497.

60. Song, B. D.; Schmid, S. L., A molecular motor or a regulator? Dynamin's in a class of its own. *Biochemistry* **2003,** *42*, 1369-1376.

61. Nelp, M. T.; Astashkin, A. V.; Breci, L. A.; McCarty, R. M.; Bandarian, V., The alpha subunit of nitrile hydratase is sufficient for catalytic activity and post-translational modification. *Biochemistry* **2014,** *53*, 3990-3994.

62. Yamaguchi, H.; Miyazaki, M., Refolding techniques for recovering biologically active recombinant proteins from inclusion bodies. *Biomolecules* **2014**, *4*, 235-251.

63. Kuhn, M. L.; Martinez, S.; Gumataotao, N.; Bornscheuer, U.; Liu, D.; Holz, R. C., The fe-type nitrile hydratase from comamonas testosteroni ni1 does not require an activator accessory protein for expression in escherichia coli. *Biochem. Biophys. Res. Commun.* **2012,** *424*, 365-370.

64. Piersma, S. R.; Nojiri, M.; Tsujimura, M.; Noguchi, T.; Odaka, M.; Yohda, M.; Inoue, Y.; Endo, I., Arginine 56 mutation in the beta subunit of nitrile hydratase: Importance of hydrogen bonding to the non-heme iron center. *J. Inorg. Biochem.* **2000,** *80*, 283-288.

65. Yamanaka, Y.; Kato, Y.; Hashimoto, K.; Iida, K.; Nagasawa, K.; Nakayama, H.; Dohmae, N.; Noguchi, K.; Noguchi, T.; Yohda, M.; Odaka, M., Time-resolved crystallography of the reaction intermediate of nitrile hydratase: Revealing a role for the cysteinesulfenic acid ligand as a catalytic nucleophile. *Angew. Chem. Int. Ed. Engl.* **2015,** *54*, 10763-10767.

66. Mathew, C.; Nagasawa, T.; Kobayashi, M.; Yamada, H., Nitrilase catalyzed production of nicotinic acid from 3-cyanopyridine in rhodococcus rhodochrous j1. *Appl. Environ. Microbiol.* **1988,** *54*, 1030–1032.

67. Banerjee, A.; Sharma, R.; Banerjee, U., The nitrile-degrading enzymes: Current status and future prospects. *Appl. Microbiol. Biotechnol.* **2002,** *60*, 33-44.

68. Mylerova, V.; Martinkova, L., Synthetic applications of nitrile-converting enzymes. *Cur. Org. Chem.* **2003,** *7*, 1-17.

69. Baxter, J.; Cummings, S. P., The current and future applications of microorganism in the bioremediation of cyanide contamination. *Antonie Van Leeuwenhoek* **2006,** *90*, 1-17.

70. Jin, H.; Turner, J., I.M.; Nelson, M. J.; Gurbiel, R. J.; Doan, P. E.; Hoffman, B. M., Coordination sphere of the ferric ion in nitrile hydratase'. *J. Am. Chem. Soc.* **1993,** *115*, 5290-5291.

71. Light, K. M.; Yamanaka, Y.; Odaka, M.; Solomon, E. I., Spectroscopic and computational studies of nitrile hydratase: Insights into geometric and electronic structure and the mechanism of amide synthesis. *Chem. sci.* **2015,** *6*, 6280-6294.

72. Rzeznicka, K.; Schätzle, S.; Böttcher, D.; Klein, J.; Bornscheuer, U. T., Cloning and functional expression of a nitrile hydratase (nhase) from rhodococcus equi tg328-2 in escherichia coli, its purification and biochemical characterisation. *Appl. Microbiol. Biotechnol.* **2010,** *85*, 1417-1425.

73. Stoll, S.; Schweiger, A., Easyspin, a comprehensive software package for spectral simulation and analysis in epr. *J. Magn. Reson.* **2006,** *178*, 42-55.

74. Gumataotao, N.; Kuhn, M. L.; Hajnas, N.; Holz, R. C., Identification of an active site-bound nitrile hydratase intermediate through single turnover stopped-flow spectroscopy. *J. Biol. Chem.* **2013,** *288*, 15532-15536.

75. Sharma, A.; Gaidamakova, E. K.; Matrosova, V. Y.; Bennett, B.; Daly, M. J.; Hoffman, B. M., Responses of Mn^{2+} speciation in deinococcus radiodurans and escherichia coli to γ-radiation by advanced paramagnetic resonance methods. *Proc. Natl. Acad. Sci.* **2013,** *110*, 5945-5950.

76. Bennett, B.; Gruer, M. J.; Guest, J. R.; Thomson, A. J., Spectroscopic characterisation of an aconitase (acna) of escherichia coli. *Eur. J. Biochem.* **1995,** *233*, 317-326.

77. Friedrich, T., The nadh:Ubiquinone oxidoreductase (complex i) from escherichia coli. *Biochim. Biophys. Acta* **1998,** *1364*, 134-146.

78. Light, K. M.; Yamanaka, Y.; Odaka, M.; Solomon, E. I., Spectroscopic and computational studies of nitrile hydratase: Insights into geometric and electronic structure and the mechanism of amide synthesis. *Chem. sci.* **2015,** *6*, 6280-6294.

79. Dey, A.; Chow, M.; Taniguchi, K.; Lugo-Mas, P.; Davin, S.; Maeda, M.; Kovacs, J. A.; Odaka, M.; Hodgson, K. O.; Hedman, B.; Solomon, E. I., Sulfur k-edge xas and dft calculations on nitrile hydratase: Geometric and electronic structure of the non-heme iron active site. *J. Am. Chem. Soc.* **2006,** *128*, 533-541.

80. Popescu, V.-C.; Münck, E.; Fox, B. G.; Sanakis, Y.; Cummings, J. G.; Turner, I. M.; Nelson, M. J., Mössbauer and epr studies of the photoactivation of nitrile hydratase. *Biochemistry* **2001,** *40*, 7984-7991.

81. Sugiura, Y.; Kuwahara, J.; Nagasawa, T.; Yamada, H., Nitrile hydratase. The first non-heme iron enzyme with a typical low-spin iron(iii)-active center. *J. Am. Chem. Soc.* **1987,** *109*, 5848-5850.

82. Light, K. M.; Yamanaka, Y.; Odaka, M.; Solomon, E. I., Spectroscopic and computational studies of nitrile hydratase: Insights into geometric and electronic structure and the mechanism of amide synthesis. *Chem. Sci.* **2015**.

83. Bray, R. C., Sudden freezing as a technique for the study of rapid reactions. *Biochem. J.* **1961,** *81*, 189-193.

84. Kumar, A.; Periyannan, G. R.; Narayanan, B.; Kittell, A. W.; Kim, J.-J.; Bennett, B., Experimental evidence for a metallohydrolase mechanism in which the nucleophile is not delivered by a metal ion: Epr spectrokinetic and structural studies of aminopeptidase from vibrio proteolyticus. *Biochem. J.* **2007,** *403*, 527-536.

85. Sharma, N.; Hu, Z.; Crowder, M. W.; Bennett, B., Conformational changes in the metallo-β-lactamase imis during the catalytic reaction: An epr spectrokinetic study of co(ii)-spin label interactions. *J. Am. Chem. Soc.* **2008,** *130*, 8215-8222.

86. Tsopanakis, A. D.; Tanner, S. J.; Bray, R. C., Ph-jump studies at subzero temperatures on an intermediate in the reaction of xanthine oxidase with xanthine. *Biochem. J.* **1978,** *175*, 879-885.

87. Bennett, B.; Benson, N.; McEwan, A. G.; Bray, R. C., Multiple states of the molybdenum centre of dimethylsulphoxide reductase from rhodobacter capsulatus revealed by epr spectroscopy. *Eur. J. Biochem.* **1994,** *225*, 321-331.

88. Wasantha Lankathilaka, K. P., Stein, N., Holz, R.C., and Bennett, B., Cellular maturation of an iron-type nitrile hydratase interrogated using epr spectroscopy *J. Biol. Inorg. Chem.* **2019**.

APPENDIX

Chapter 1 Appendix

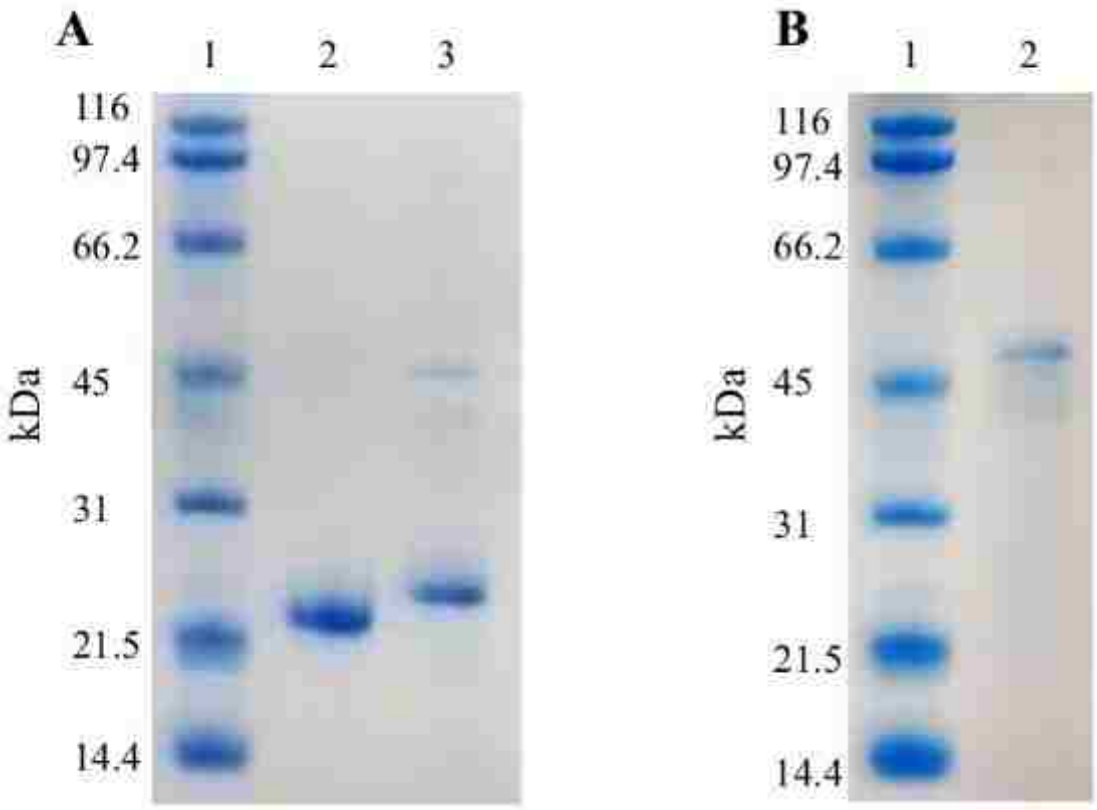

Figure 40. SDS-PAGE analysis of (A) purified *Re*NHase TG328-2 alpha subunit and *Re*NHase TG328-2 beta subunit (Lane 1-Protein marker, Lane 2- Purified *Re*NHase TG328-2 alpha subunit (~23.9 kDa), Lane 3- purified *Re*NHase TG328-2 beta subunit (~25.1 kDa)), (B) purified *Re*NHase TG328-2 activator protein (Lane 1-Protein marker, Lane 2-*Re*NHase TG328-2 activator (~47.8 kDa).

Chapter 4 Appendix

Table 9. Simulated g values of signals in EPR spectra of *Re*NHase at different pH values

pH	Signal	g_1	g_2	g_3	% Magnetic Spin
5.0	a	2.277	2.124	1.968	11
	b	2.196	2.135	1.992	20
	c	2.171	2.115	1.984	18
	d	2.217	2.124	1.979	50
7.5	b	2.197	2.136	1.994	63
	c	2.175	2.124	1.986	22
	d	2.218	2.115	1.981	15
10.0	a	2.277	2.132	1.97	7
	b	2.195	2.135	1.992	42
	c	2.177	2.117	1.98	15
	d	2.216	2.126	1.985	36

Table 10. Simulated g values of signals in EPR spectra of *Re*NHase, acetonitrile mixed *Re*NHase, and acetamide mixed *Re*NHase at pH 7.5

Description	Signal	g_1	g_2	g_3	% Magnetic Spin
***Re*NHase in pH 7.5**	b	2.197	2.136	1.994	63
	c	2.175	2.124	1.986	22
	d	2.218	2.115	1.981	15
***Re*NHase +125 mM AcetoN**	1	2.276	2.124	1.97	6
	2	2.223	2.141	1.982	47
	3	2.202	2.13	1.992	30
	4	2.187	2.121	1.978	17
***Re*NHase + 600 mM AcetoN**	1	2.219	2.127	1.991	38
	2	2.202	2.14	1.983	47
	3	2.184	2.12	1.979	15
***Re*NHase Acetamide**	1	2.276	2.131	1.976	9
	2	2.22	2.136	1.98	48
	3	2.201	2.124	1.99	33
	4	2.184	2.114	1.968	10
***Re*NHase +125 mM AcetoN (Further slowered)**	1	2.31	2.136	1.96	5
	2	2.278	2.136	1.976	12
	3	2.223	2.14	1.981	23
	4	2.201	2.127	1.992	45
	5	2.173	2.115	1.968	15

Table 11. Simulated g values of signals in EPR spectra of *Re*NHase, acetonitrile mixed *Re*NHase, and acetamide mixed *Re*NHase at different pH 5.0

Description	Signal	g_1	g_2	g_3	% Magnetic Spin
***Re*NHase in pH 5.0**	a	2.277	2.124	1.968	11
	b	2.196	2.135	1.992	20
	c	2.171	2.115	1.984	18
	d	2.217	2.124	1.979	50
***Re*NHase +125 mM AcetoN_2 s**	1	2.31	2.136	1.96	6
	2	2.278	2.134	1.977	9
	3	2.22	2.125	1.993	38
	4	2.202	2.138	1.982	36
	5	2.185	2.116	1.97	11
***Re*NHase + 125 mM AcetoN_30 s**	1	2.277	2.134	1.977	6
	2	2.22	2.125	1.993	44
	3	2.202	2.138	1.982	39
	4	2.185	2.117	1.973	11
***Re*NHase Acetamide**	1	2.276	2.131	1.973	12
	2	2.22	2.124	1.992	31
	3	2.201	2.137	1.98	38
	4	2.187	2.114	1.968	14
	5	2.172	2.127	1.976	5

Table 12. Simulated g values of signals in EPR spectra of *Re*NHase, acetonitrile mixed *Re*NHase, and acetamide mixed *Re*NHase at different pH 10.0

Description	Signal	g_1	g_2	g_3	% Magnetic spin
***Re*NHase in pH 10.0**	a	2.277	2.132	1.97	7
	b	2.195	2.135	1.992	42
	c	2.177	2.117	1.98	15
	d	2.216	2.126	1.985	36
***Re*NHase +125 mM AcetoN_2 s**	1	2.216	2.140	1.983	63
	2	2.198	2.125	1.990	30
	3	2.181	2.117	1.980	7
***Re*NHase + 125 mM AcetoN_30 s**	1	2.216	2.140	1.982	61
	2	2.198	2.125	1.987	31
	3	2.179	2.117	1.994	8
***Re*NHase Acetamide**	1	2.277	2.121	1.969	3
	2	2.218	2.137	1.980	59
	3	2.201	2.126	1.987	27
	4	2.187	2.121	1.997	11

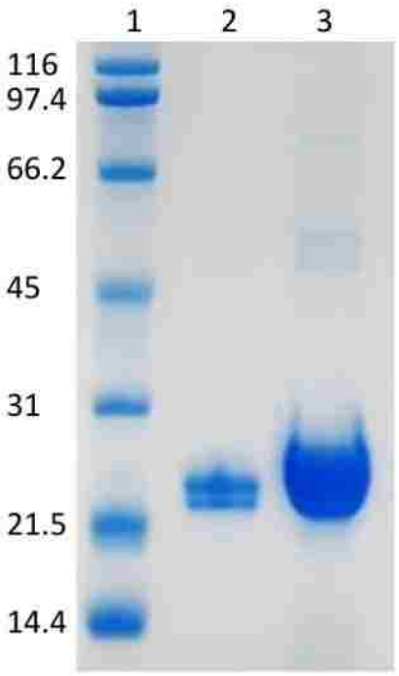

Figure 41. SDS-PAGE analysis of purified *Re*NHase TG328-2. (Lane 1-Protein marker, Lane 2- Diluted purified *Re*NHase TG328-2, Lane 3- Overloaded purified *Re*NHase TG328-2)